IAEA-TECDOC-1486

Small angle neutron scattering

Report of a coordinated research project
2000–2003

IAEA
International Atomic Energy Agency

March 2006

IAEA-TECDOC-1486

Small angle neutron scattering

Report of a coordinated research project
2000–2003

IAEA
International Atomic Energy Agency

March 2006

The originating Section of this publication in the IAEA was:

Physics Section
International Atomic Energy Agency
Wagramer Strasse 5
P.O. Box 100
A-1400 Vienna, Austria

SMALL ANGLE NEUTRON SCATTERING
IAEA, VIENNA, 2006
IAEA-TECDOC-1486
ISBN 92–0–102806–7
ISSN 1011–4289

Printed by the IAEA in Austria
March 2006

FOREWORD

Small angle neutron scattering (SANS) is a powerful technique for studying macro structures like polymers, precipitates in metallurgical specimens, biological molecules, micelles and magnetic systems like ferrofluids. Neutron scattering has an advantage over X ray scattering (XSAXS) due to selective absorption and scattering cross section of neutrons across the periodic table. It is possible to develop and use a SANS instrument even with a medium flux reactor. The present CRP was aimed at the development of components like collimators, monochromators, position sensitive detectors (PSD) etc. for improving the throughput of the instrument and foster the effective utilization of research reactors, as well as to provide a link between developing and developed facilities.

The CRP was launched with the first research coordination meeting (RCM) in 2000 to refine the project proposals and define the action plans and partnerships. There were eight research contracts and four research agreements. Good partnerships were established between various participants with collaborations among participants from various countries including those from developing and developed countries. The progress of the individual projects and team work under the CRP was evaluated and discussed during the second RCM and the action plan for the final phase was formulated. The results of the work done under the CRP were then reviewed in the final RCM held in Vienna, December 2003.

This publication presents the results of the work carried out by the participants under the CRP at their respective institutions. The information will be useful for the users and operators of research reactors in developing an instrument and building collaborations for capacity building. The development of collimators, detector assemblies, utilization of the SANS for microstructural characterization of advanced materials , development and design of a ultra small angle neutron scattering (USANS) and proposals for a new SANS facility can be cited as some of the achievements of the CRP. The details of the work done by the participants and the results obtained are included in this publication.

The IAEA officer responsible for this publication is S.K. Paranjpe of the Division of Physical and Chemical Sciences.

EDITORIAL NOTE

The papers in these proceedings are reproduced as submitted by the authors and have not undergone rigorous editorial review by the IAEA.

The views expressed do not necessarily reflect those of the IAEA, the governments of the nominating Member States or the nominating organizations.

The use of particular designations of countries or territories does not imply any judgement by the publisher, the IAEA, as to the legal status of such countries or territories, of their authorities and institutions or of the delimitation of their boundaries.

The mention of names of specific companies or products (whether or not indicated as registered) does not imply any intention to infringe proprietary rights, nor should it be construed as an endorsement or recommendation on the part of the IAEA.

The authors are responsible for having obtained the necessary permission for the IAEA to reproduce, translate or use material from sources already protected by copyrights.

CONTENTS

SUMMARY

1. BACKGROUND OF THE CRP

1.1. Introduction

Neutron scattering is an important technique that provides essential information about the fundamental properties of materials. An ever growing scientific community uses neutrons for research in various branches of science like physics, chemistry, biology and for applications in materials science, engineering and earth sciences.

A recent review [1] of neutron scattering facilities indicated that the presently installed capacity of neutron sources for beam research would decrease to a level below one third of that today. The authors have analyzed the future evolution both of sources and instruments and based on the available pattern of utilization, projections for individual classes of instruments were made for various regions of the world. For example, the study concluded that in the year 2017, in the absence of new sources, the number of available small angle neutron scattering (SANS) instruments in Europe would decrease to less than one quarter of the present level. Similarly, considering the low initial utilization profile almost all the current installations in the Pacific region will have shut down by 2017.

On the other hand, there are still many smaller SANS facilities that are under-utilized. Bringing these facilities up to their full potential is an important part of the overall solution to the upcoming shortage. Such facilities can easily act as feeders and test beds for experiments, which may later be performed on the larger, more sophisticated reactors, thereby relieving some pressure on the major facilities. In a discussion about the beam instruments, the review states “In general, to fully exploit the potential of existing and planned sources, new innovative experimental devices and techniques are needed”.

The basic understanding of physical materials and biological systems requires a detailed knowledge of the arrangement and dynamics of their atoms and molecules. Small angle neutron scattering enables the deduction of information from the fraction of a nanometer to the micrometer level. SANS finds its applications in classical metallurgy, soft matter, chemistry and industry. The use of large samples without any special preparation and of a non-destructive character gives it an edge over other techniques like transmission electron microscopy (TEM), Ffield ion microscopy (FIM), etc.

The application of SANS is possible and useful at low-power reactors:

(1) In well-selected topics where only a restricted Q range is required,

(2) When the scattering power is expected to be sufficiently high,

(3) When the sample size can be increased at the expense of resolution.

Examples of this type of application are:

(1) Phase separation and precipitates in materials science,

(2) Ultrafine grained materials (nanocrystals) and ceramics,

(3) Porous materials such as concretes and filter materials,

(4) Conformation and entanglements of polymer-chains,

(5) Aggregates of micelles in micro-emulsions, gels and colloids,

(6) Radiation damage in steels and other alloys.

There are well-developed facilities with highly utilized instruments, having high-technology facilities like cold neutron sources, neutron guides and two-dimensional position-sensitive detectors, and infrastructure to maintain them. For convenience such facilities have been defined as type-A.

On the other hand, there are many facilities which are under-utilized, have simple non-optimized instruments and lack necessary infrastructure. The scientists in these laboratories have a desire to work in solving specific problems with the assistance / cooperation of other centres. Such facilities have been defined as type-B facilities.

The purpose of this CRP was to discuss and try to solve problems hindering the increased use of SANS in under-utilized facilities, help to develop / upgrade existing facilities and related accessories, and to provide a link between developed and developing facilities..

1.2. The problem

There are several SANS facilities at low-power reactors, as well as reactor facilities in developing countries that are under-utilized (Type B facilities). Two major causes for this have been identified; one is people-related and the other is hardware related.

A major obstacle has been the absence of links between the reactor centres and the scientific community. In some countries the focus has been on the commissioning and operation of the reactor itself, rather than on any beam applications such as the design and installation of scattering instruments. The staff were fully involved with the reactor operation proper and not particularly concerned with instrumentation or reactor users.

The absence of links prevented a SANS research programme being defined which was suitable and reasonable for that specific reactor facility. As a consequence, SANS machines were crude copies of the instruments installed at high-flux reactors. Since the infrastructure necessary to support such sophisticated equipment (such as specialized service personnel) was missing, problems arose as soon as components failed. Typically, they cost a lot to repair or replace and had to be sent back to the manufacturer. During the long repair time the whole installation was out of operation, with the consequential loss of momentum and enthusiasm.

1.3. Purpose of the CRP

(a) A solution to many of the hardware-related problems of SANS at lower power reactors and in developing countries would be to use lower-technology equipment which is locally maintainable. The development and efficient usage of SANS equipment appropriate for the special requirements of developing countries' facilities were the first aims of this CRP.

The technical requirements of such SANS instruments include:

(1) Simple mechanical velocity selectors or crystal monochromators.

(2) Simple scattering geometries, i.e., one optimized collimation length, and fixed detector positions, thereby allowing for simple mechanics.

(3) Robust detector systems assembled from commercially available linear position sensitive detectors.

(4) Black-box type detector electronics with automatic adjustment procedure, using interchangeable modules.

In particular, great care has to be taken to improve the signal-to-noise ratio by effective shielding of the beam port and the improvement of filters for fast and epithermal neutrons (for example, Si, Ge, Be).

(b) The second major purpose of this CRP was to help overcome the isolation of the reactor centre in a developing country. It attempts to do this by:

(1) Establishing scientific and technical links between industrialized and developing countries.

(2) Forging bi-lateral cooperation between Type A and Type B groups. This cooperation would include training at SANS facilities and advice on the research programmes to be set up and on the design of the instrument. Scientific links to the SANS community should be mediated via conferences, workshops and private discussions with the host institute. The cooperation should be considered as a long term partnership.

(3) Cooperation in the solution of a practical technical problem. The individual project being worked on by the A-B country pair should lead to a solution of one of the topics listed above.

(4) Exchange of information among the participating scientists on the solutions of problems faced by individual facilities. Many of these problems are common to all reactor centres in developing countries, and solutions can be transferred.

1.4. Specific objectives

The specific purpose of this CRP was to solve current problems hindering the greater use of SANS in under-utilized facilities. The plan to achieve this objective was:

- Developing SANS-related equipment which is useful for many applications but easily maintainable in developing countries,
- Forging long term supportive relationships between Type A and B pairs of institutions and the scientists working there,
- Transferring solutions developed from the pair relationship research to other facilities involved in the CRP.

1.5. Expected outputs (results)

1.5.1. *Personnel-related outcomes*

(1) Formation of highly qualified local SANS specialists who are able to carry out SANS experiments, and maintain their instruments in operational shape.

(2) Establishment of bilateral and multilateral cooperation between the SANS centres of developing countries and/or the SANS laboratories of the industrially developed and developing countries.

(3) Inclusion of type B facilities in the worldwide SANS community to harmonize the efforts in the field of SANS instrumentation and SANS research programmes.

1.5.2. *Hardware-related outcomes*

(1) Development of a new generation of SANS instruments with enhanced capabilities, which are easy to handle, repair and maintain. This equipment should be robust and able to function in extreme climatic conditions.

(2) The improvements may include:

(a) Design of shielding for improved signal-to-noise ratio (filters, shutters),

(b) Devices increasing the incident beam intensity (simple monochromators),

(c) Simple and cheap detector systems for a large useful area, using commercially available linear detectors and modular electronics,

(d) Optimization of SANS devices according to the physical layout of the facilities,

(e) Sample environments including temperature, pressure, and magnetic field.

2. RESULTS AND OUTCOME OF THE CRP

2.1. Realization of a 2-D detection system using 1-D PSDs

The realization of a 2-D detector system from an array of 1-D detectors has been viewed as the most favourable option, as high count rates (>1Mcps) and easy maintenance are achievable. An array of such detectors (stacked or star-like) is especially feasible for SANS, where a position resolution between 5-15mm is adequate.

1-D detectors based on the charge division or RC encoding technique are suited for array configurations because the detector can be designed for minimal dead space. At NECSA, a prototype 1-D detector has been fabricated having a position resolution of less than 3mm and an efficiency of >81% for 6Å neutrons. Using commercially available 8 PSD electronics, count rates in excess of 40 kcps per detector have been recorded.

The realization of a star-like SANS detection system using 5 to 8 detectors is currently in progress by acquiring detectors based on the RUDETEC prototype. Thereafter, the next step would be to fabricate about 50 1-D PSDs with a width of 10 mm and a length 600 mm, so that they could be used in a stacked arrangement for the SANS facility. However, some design aspects remain to be resolved.

2.2. Study and design of a new generation SANS instrument

A variable geometry 100-channel CMC prototype was designed and its construction started. The collimator walls were formed by thin strips of a highly neutron absorbing composite material. Cross-talk between channels was studied by Monte Carlo Simulation. A process for fabricating the absorbing strips was developed. On the theoretical side, consideration was given to the development of the concept of converging multi-channel collimation applied to SANS instruments. Guidelines for the implementation of the concept in a specific SANS facility were established. Monte Carlo Simulation determined the contribution of the individual channels to the operation of a CMC device in terms of intensity and resolution of the transmitted neutrons. The feasibility of installing a set of neutron guide sections in the beam line of the ITN SANS facility was investigated. Results indicated that an association of guide sections with a CMC would improve the signal-to-noise ratio of the instrument. (details in [2])

2.3. Optimization of velocity monochromator

One of the main problems of SANS at low-power research reactors is the intensity of useful neutrons. Part of the solution for this problem is the use of a high-transmission mechanical velocity monochromator (VM). In this context it is very important to optimize the ratio of intensity to resolution by means of the geometrical parameters and the construction of the VM.

The main goal of the Russian work was the formulation of general recommendations for the creation of a simple and reliable VM of high transmission, variable resolution, and wide neutron wavelength range. To achieve this goal the following research has been carried out:

(1) Choosing the type of monochromator for low-power reactors;

(2) Optimizing the monochromator design;

(3) Choosing the type of neutron-absorbing (high absorption cross-section) materials;

(4) Avoiding problems like big weight and size by using modern designs and a judicious choice of materials.

The estimates and experimental study within the framework of CRP gave real parameters for the VM design and the improvment of the VM rotor.

A cylindrical-type VM for SANS installations has been designed. The rotor looks like a cylinder, rotating around its horizontal axis. It is constructed as a set of aluminium cylindrical sections, pivoted on a common aluminium tube of a diameter ~100 mm with steel butt ends. Thin adsorbing plates (δ = 0.5 mm), made of Gd (8 %) – Al alloy, are fastened on the periphery of these sections. The plates are inclined relative to the axis and their set forms a common helical slit along the cylindrical surface. The light and convenient aluminium alloys are good materials for designing the mechanical monochromator, as a part of the SANS, if the speed of rotation of the rotor monochromator is not too high (up to 6000-10000 rpm for the typical diameter of the rotor). Only a few percent of rare earth elements, for example gadolinium, are enough to get an excellent material for the absorbing plates of the monochromator. These lamellas are absolutely "dark" for the neutrons after the beryllium filter. One of the important advantages of the metal monochromator, in comparison with the plastic one, is its high radiation resistance. The effective transmission of the rotor is ≈0.88.

This variant of the VM can be recommended as an inexpensive, reliable and simple variant for the SANS at low-power research reactors. (details in [3])

2.4. Use of SANS for microstructural studies of advanced materials / installation of high-resolution SANS

A double crystal-based small angle scattering instrument has been installed at Trombay, Mumbai. The instrument is equipped with a single-bounce flat crystal serving both as monochromator and analyzer. This instrument is useful to access large inhomogeneities, which are commonly encountered in materials like cements, ceramics, magnetic materials, etc. With an available q range ~ 0.003-0.173 nm^{-1}, various technologically relevant materials like ceramics, alloys, rocks, etc., have been successfully characterized. However, to increase the resolution and also to enhance the signal-to-background ratio, a triple-bounce channel-cut crystal-based ultrasmall angle neutron scattering (USANS) instrument is under development. The proposed facility will consist of a non-dispersive (3, -3) setting of a pair of channel-cut perfect Si (111) crystals with a sample platform between them. Neutrons scattered from the sample are analyzed by angular displacement of the analyzer crystal in ultrafine steps (angular step size < 0.0001^{o}). The stability of the angular settings is maintained by mounting the double-crystal diffractometer (DCD) on a vibration-free platform. (details in [4])

2.5. Feasibility of SANS for SAFARI reactors

A feasibility study, including modeling, space and financial constraints, was carried out, using in-pile beam-tubes and neutron or curved guides in front of the collimator. The study revealed that the best option would be to build a pinhole camera-type SANS using a velocity selector. For budgetary reasons a first version of a SANS instrument was designed on an in-pile beam tube containing a silicon filter for fast neutrons.

NECSA has successfully applied for financial support by the IAEA in obtaining a velocity selector collimator system, detector electronics, and some basic components for its SANS design. A TC project is under implementation.

3. DISCUSSIONS DURING THE FINAL RCM

3.1. Components of SANS

3.1.1 *Source part*

The tailoring of neutron beams for SANS instruments installed at low-flux reactors has to be done with particular care to achieve the best possible signal-to-background ratio. The choice of the main beam line characteristics for a SANS should favour simple solutions, adapting to lower technology requirements which are easier to maintain locally.

3.1.2 *Reducing the background*

Careful shielding of the beam port and instrument has to be achieved. Many workable and thoroughly tested solutions have been developed at advanced centres, and bilateral collaboration in this respect can prove useful in speeding up the design and construction.

3.1.3 *Filtering*

It is very important to achieve an effective filtering of the beam. This could be done by means of adequate crystals and/or by the use of curved neutron guides:

(i) Neutron guides can very effectively eliminate both fast and epithermal neutrons. On the other hand, neutron guides have certain disadvantages, like occupying a large space, cutting off the lower wavelength neutrons from the beam and being expensive.

(ii) The option of using crystals as filters seems thus a better solution for small reactors without a cold source. A sapphire or Si single crystal may be used as fast neutron filters. Both filters reduce considerably the fast neutrons with little attenuation of the thermal neutrons. However, the cooling of an Si crystal to liquid nitrogen temperature improves the thermal neutron intensity by about 20%.

3.1.4. *Improving the signal*

For applying a pinhole instrument it is important to choose a suitable collimator divergence and to use the maximum available source size. In addition, solutions capable of increasing the intensity of the sample, using converging devices like multi-collimation arrangements, have been considered.

3.2. Monochromatization and incident beam divergence

Wavelength selection by means of crystal monochromators leads to an unnecessarily small $\Delta Q/Q$ value, resulting in poor intensity, a situation that should be avoided in small flux reactors.

The use of mechanical velocity selectors seems to be a better choice, since they allow to choose the wavelength with $\Delta\lambda/\lambda$ of the order of 10%.

3.3. Detectors

The development of low-cost detectors is an important task requiring the common efforts of all participants of the present CRP. However, cost is just one consideration. The robustness and ease of maintenance, or simplicity in the replacement of individual detector components,

are equally important. The aim of this project was a feasibility study and the testing of SANS detection systems based on commercially available linear-position sensitive detectors (PSDs).

To evaluate the feasibility of using linear position sensitive detectors (PSDs) for meaningful SANS analysis, a variety of detectors and geometries has to be studied. Documentation showed that almost no experimental results (performance, availability) have been obtained so far on available 1D-PSD counters and electronic concepts used for SANS purposes. Therefore, neutron tests have to be performed comprising measurements of spatial resolution, SANS scattering from various standard samples, reproducibility tests and estimates of dead time and total count rate capabilities. Different arrays of 1-D detectors in rectangular or star-like configurations have to be considered for replacing 2-D multi-wires detectors.

Selected 1D-PSDs have been tested on cold neutrons under SANS conditions at HMI with the following results:

- A combination of four Reuter-Stokes 1-D PSDs and electronics from Mesytec;
- A Greek detector Reuter- Stokes tube with Studsvic-type electronics;
- The prototype of a RUDETEC 1-D PSD detector developed at NECSA, SA using Mesytech electronics.

Detector electronics have to be selected which would allow the multiplexing of several 1-D PSDs.

In simple data acquisition systems this modular electronic system should allow to assemble a detection array of variable numbers of PSDs where individual PSDs can easily be replaced and the geometric arrangement can be modified.

3.4. USANS

One of the remarkable developments within the last few years has been the Ultra-Small angle-Neutron Scattering (USANS), which allows access to the evaluation of spatial density fluctuations on a large-length scale extending up to the micrometer range.

The instrument is comparatively smaller than the conventional pin-hole cameras and therefore easier to install and operate. The realization of such an instrument is presented by S.Mazumder in this document. The instrument is based on the Bonse-Hart technique. A neutron beam, doubly diffracted by two perfect parallel single crystals, yields a very high angular and momentum (Q) resolution. The sample is placed between the two crystals and the scattering profiles are recorded by rotating the second crystal with respect to the first one. The Q domain covered by this device extends from 10^{-3} to 10^{-1} nm^{-1}.

The sensitivity of the instrument is poor at high momentum transfer due to the background caused by the tails of the crystal reflection curves. This can be improved by using triple-bounce channel-cut crystals for both the monochromator and the analyzer. The use of Agamalian-cut crystals results in further improvement.

3.5. Time-of-flight

Time-of-flight is an alternative method to measure the scattered intensity as a function of momentum transfer. It avoids the utilization of a monochromator, single crystal or mechanical selector. The installation of such an instrument is simple and cheaper. Pulses of polychromatic neutrons are obtained by using a chopper, and the scattered spectrum from each pulse is recorded as a function of the time–of-flight.

The instrument consists of a small chopper and a detector with a time-of-flight (TOF) data acquisition system. Besides its simplicity, the advantage of the system is that it covers in a

single run all the Q range, and has a lower level of background due to the lock-in principle. The Q dependence of the scattered intensity is easily reconstructed from the recorded TOF spectra. Obviously both single and PSD detectors are compatible with the system.

As in all SANS experiments, the scattering is assumed to be totally elastic. For a given detector position, the momentum transfer is defined by the scattering angle and sample-to-detector distance, but at different times scattered neutrons are distributed in time channels corresponding to different wavelengths. As a consequence, essentially the entire scattering function is measured at a single position of the detector. The use of multi-detectors or a PSD allows for the study of anisotropic scattering. The typical Q range accessible is 10^{-2} to 1 nm^{-1}.

The choice of parameters, such as velocity of the chopper, width of the pulse and width of the time channels, permits a continuous variation of the Q domain and the Q resolution.

4. CONCLUSIONS

The two techniques discussed above may represent an ideal alternative way to start SANS measurements on a very small investment. Reduced to their simplest version, each of the techniques implies only the acquisition of a double single-crystal in the case of the USANS, or of a small chopper, a detector and a collimation system for the TOF machine.

USANS is in any case a technique that complements the information obtained by SANS. It extends the usual Q-range, allowing for the use of neutron scattering in situations normally accessible only by microscopy or light scattering.

Time-of-flight is also a technique totally compatible with the installation of a classical pinhole SANS installation. The use of one or the other technique is a matter of advantages or inconveniences.

REFERENCES

[1] RICHTER D., SPRINGER, T., A Twenty Years Forward Look at Neutron Scattering Facilities in the OECD Countries and Russia, Technical Report, European science Foundation and Organisation for Economic cooperation and Development (OECD), (1998)
[2] CARVALHO, FREDERICO GAMA, “Study and design of a new generation of SANS instrument: smaller, modular, with enhanced capability and low service requirement” (these proceedings).
[3] POUTCHKOV ALEXANDER V., “Optimization of velocity monochromators for low power research reactors” (these proceedings).
[4] MAZUMDER, S., SEN, D., PATRA, A.K., “Use of SANS for the microstructural characterization of advanced materials during processing and application; installation of high resolution SANS at Trombay” (these proceedings).

VIABILITY STUDY FOR THE INSTALLATION OF A SANS BEAM-LINE AT IPEN-CNEN/SP

J. Mestnik Filho[1], J. Teixeira[2]

[1]Nuclear Physics Department, Instituto de Pesquesas energeticas e nucleares, Comissao nacional de Energia Nuclear, Sao Paulo, SP, Brazil

[2]Laboratoire Leon Brillouin, Centre d'Etudes de Saclay, France

Abstract: Upon assessing the viability of installing a SANS device at the IEA-R1 reactor, it was concluded that a standard SANS spectrometer would attenuate the neutron flux too much, causing a poor signal-to-background ratio. The performance can, however, be considerably enhanced by the use of multi-channel converging collimation, and further improved when combined with stacked neutron guides for fast neutron filtering.

1. INTRODUCTION

The small angle neutron scattering (SANS) technique is used to study structural properties of materials on the so-called mesoscopic scale covering the length range of 10 to 1000 Å, and is widely applied in materials science, polymer chemistry, biology and magnetism. Specifically, structures of large molecules such as colloid particles and micelles, magnetic inhomogeneities, microvoids, defect properties and precipitates can be studied with SANS and its X-ray counterpart SAXS.

As in any scattering experiment, the measured quantity is the intensity of the scattered monochromatic neutrons (or X-rays) as a function of the scattering angle by a sample under study, with the aim to determine the scattering cross-section as a function of the wave vector transfer given by $Q=4\pi\sin\theta/\lambda$, 2θ being the scattering angle and λ the neutron wavelength. The scattered intensity distribution with a width $\sim 2\pi/R_0$, centred around $Q_0=2\pi/R_0$, reflects the presence of particles with a radius of R_0 [1]. Owing to the range of particle sizes of interest, a SANS instrument has to cover the lower limit in the wave vector transfer, typically $5\text{x}10^{-4}$ Å $^{-1} < Q < 0.5$ Å^{-1}, attainable only at small scattering angles with large neutron wavelengths (4-20Å). Since these low-energy neutrons are only a small fraction of the reactor neutron spectrum, the SANS technique is more limited to medium flux reactors, since it restricts the type of systems that can be studied [1,2].

The purpose of this project is to study the viability of implementing a SANS facility at one of the beam ports of the IEA-R1 reactor at IPEN, with special emphasis on determining the potentials and limitations. The motivations for this study are:

- The number of potential users among the Brazilian scientific community is known to be sufficient to justify the investment and has been growing during the last years.
- The SAXS line of the synchrotron light laboratory at Campinas, São Paulo, is now well established, and it could be attractive for regular SAXS users to perform new or complementary experiments on a SANS line.
- Possibility to run SANS experiments on medium flux reactors such as IEA-R1 [2].
- The IEA-R1 reactor represents the unique place in Brazil where a source of neutrons is available.

The experiences on neutron beam lines at IPEN, the technical description of the IEA-R1 reactor and an outline of the research work proposed to accomplish this project will be presented here.

2. DESCRIPTION OF THE IEA-R1-REACTOR

The reactor is a material testing reactor (MTR) with a 10 meter-deep open pool as shown in figure 1. It is designed to facilitate access to the core to insert and withdraw materials for irradiation and, at the same time, a neutron and gamma ray source to the beam lines and to an irradiation device controlled by a pneumatic system for sample transfer. For maintenance purposes the reactor core can be moved to a second section of the pool at ~3 meters from its normal operating position. It can operate at 5 MW power, with the heat removed by forced water circulation provided by pumps in its primary circuit. A second and independent circuit removes the heat trough a heat exchanger and sends it to a cooler system, which in turn transfers the heat to the atmosphere. Some technical data about the IEA-R1 reactor are given in table 1.

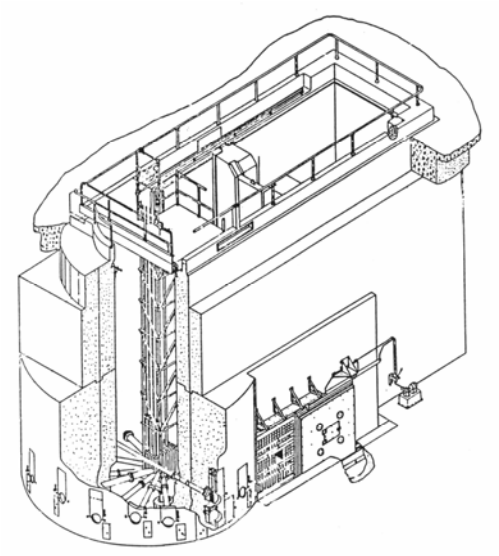

Fig. 1. Sketch of the IEA-R1 reactor

The reactor fuel elements are composed of thin (1.52 mm) fuel slabs assembled side by side, with a space between them (2.9 mm) filled with water that serves as moderator and cooler. The assembly forms a long (714.4 mm) piece with nearly square shaped (76.1 x 79.76 mm^2) cross-section. The technical data of fuel element are given in Table 2.

Table 1: IEA-R1 Reactor technical data

Type: Open pool
Maximum Power: 5 MW
Average thermal neutron flux: 4.6×10^{13} $n/cm^2 \cdot s$
Peak thermal neutron flux: 1.17×10^{14} $n/cm^2 s$ at centre of the core - Beryllium irradiation station
Average epithermal flux: 1.3×10^{14} $n/cm^2 \cdot s$
Thermal flux at the pneumatic irradiation system: 2×10^{12} $n/cm^2 \cdot s$
Moderator and cooler: light water
Reflector: graphite
Operating cycle: 24 hours a day, 2.5 days a week
Date of first operation: 16 September 1957
Safeguards: IAEA and ABACC

Table 2. Fuel element technical data

Dimensions of slabs: 625 x 70.8 x 1.52 mm^2
Spacing between slabs: 2.9 mm
Number of slabs per standard element: 18
Number of slabs per control element: 12
Cladding material: Aluminium
Cladding thickness: 0.38 mm
Fuel material: U_3O_8 and U_3Si_2Al
Fuel thickness: 0.76 mm
Uranium density: 2.3 and 3.0 g/cm^3
U^{235} enrichment: 20% by weight
Manufacturer: IPEN-CNEN/SP
Number of standard elements: 21
Number of control elements: 4
Minimum critical mass: 3.6 Kg
Maximum burn-up: 50%
Average burn-up: 30%

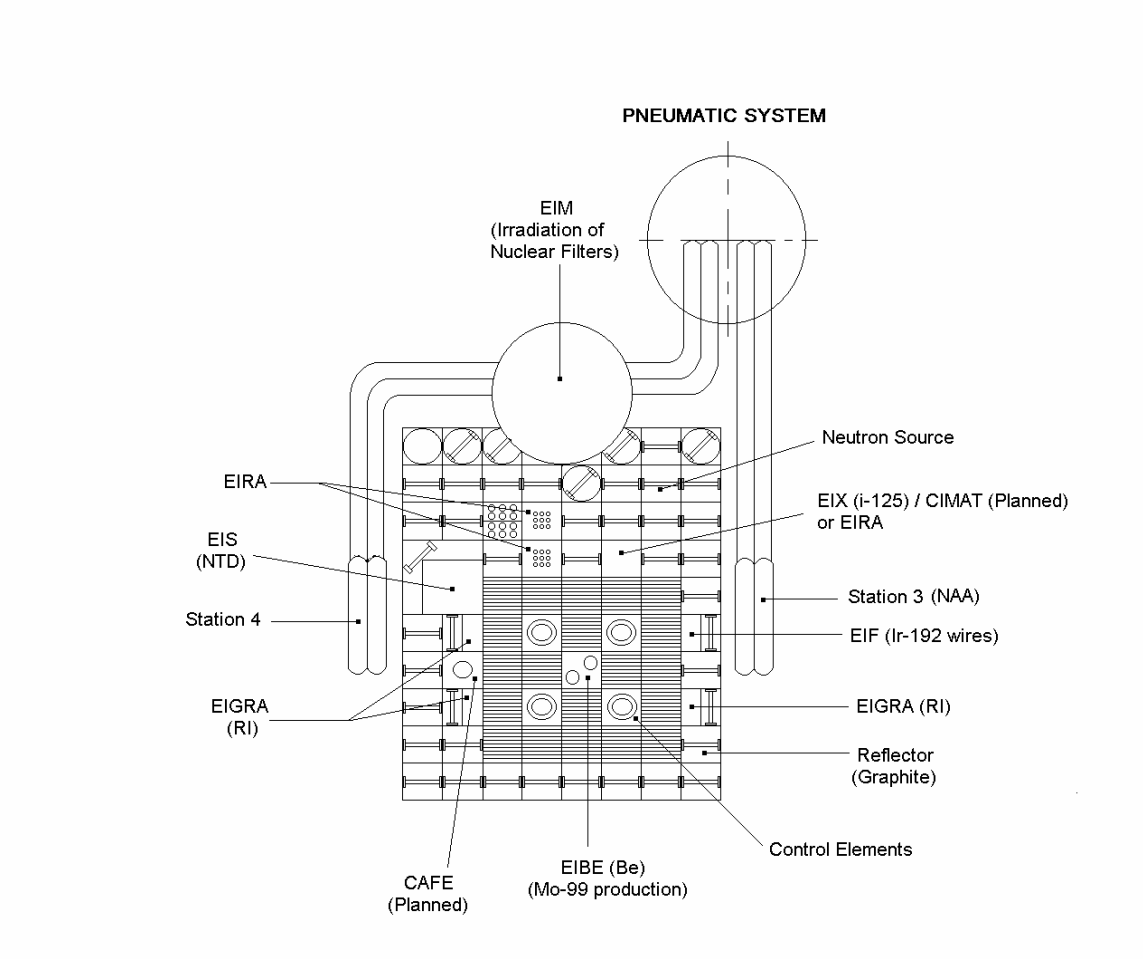

Fig. 2. IEA-R1 reactor core configuration

There are standard fuel elements with 18 slabs and control fuel elements with 12 slabs, whose resulting central space is used to insert the reactor control rods made with neutron absorbing materials. The standard reactor configuration consists of a 5 x 5 array of fuel elements, 4 of them being control elements, surrounded by graphite reflectors. In the actual configuration the central position is occupied by a system (EIBE) designed for ^{99}Mo production, made of beryllium, as can be seen in figure 2.

There are 10 beam ports available for experiments, as can be seen in figure 3. Eight of them, directed toward the centre of the core, are called radial beam holes, whereas the other two constitute the ends of a unique tube with a tangential direction relative to the core. In the tangential tube, the extracted radiation can be present only after scattering from some material inserted in the middle of the tube. Eight of the tubes have an internal diameter of 152.4 mm, whereas the other two have one of 203.2 mm. For safety reasons it is necessary to insert another tube that contains collimators, filters or other devices, into a reactor tube to perform beam experiments, and the small gap in between is filled with water. The radial tubes have an average length of 2.65 m and the measured thermal neutron flux emerging from the beam hole No. 10 is 2.3×10^7 n/cm^2·s, with the reactor operating at a power level of 2 MW. This line ends with a 5 x 5 cm^2 aperture with a Soller collimator with 30 min horizontal divergence.

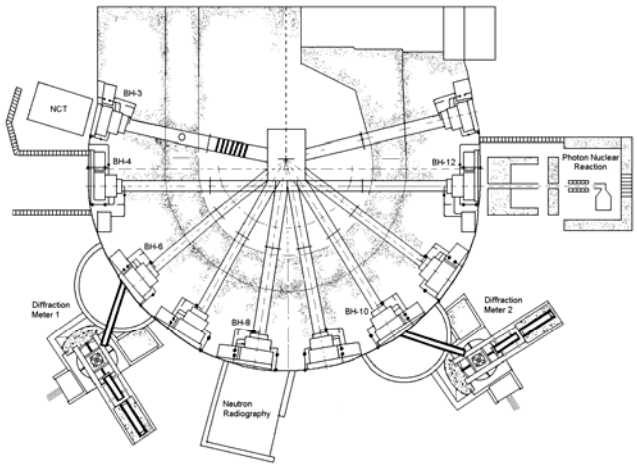

Fig. 3. Disposition of the beam lines in the IEA-R1 reactor

3. COMPARISON OF THE PERFORMANCE OF A TRADITIONAL SANS SPECTROMETER WITH ONE USING A CONVERGING MULTI-CHANNEL COLLIMATOR

3.1. Fundamentals of SANS

In a scattering experiment, a pattern of scattered particles from a sample is determined with the aim to get information about the form and spatial arrangement of the elementary components of the sample, i.e., about the structure of the sample. A collimated beam of particles (visible light, X-rays, neutrons) is made incident upon the sample and the intensity of scattered radiation as a function of the scattering angle is measured. The fundamental relationship governing the experiment is given by the *scattering amplitude*:

$$f = \int \mathrm{d}V.n(\mathbf{r}).\exp(-i\mathbf{Q}.\mathbf{r}) \qquad (1)$$

The square of f determines the scattered intensity. Here, the integral is extended over the volume of the sample, $n(\mathbf{r})$ is the charge (X-ray) or mass (neutron) density and **Q** is the scattering vector, given by:

$$\mathbf{Q} = \mathbf{k_0} - \mathbf{k_1} \qquad (2)$$

$\mathbf{k}_0$ and $\mathbf{k}_1$ being the incident and scattered wave vectors respectively. The magnitude of the scattering vector is:

$$Q = \frac{2\pi}{\lambda}\sin\theta \qquad (3)$$

where λ is the wavelength of the neutrons and θ the scattering angle. The quantities **Q** and **r** in equation 1 are reciprocally related (Fourier transform) and, as a consequence, in order to probe greater spatial inhomogeneity, smaller regions of Q have to be scanned or, according to equation 3, smaller scattering angles for fixed wavelengths.

The periodic arrangement of atoms in solids can be observed by 1 Å neutrons or X-rays scattered over an angular range of 10 to 120 degrees. The small scattering angle range (~ 0.1º to 3º) provides information on spatial inhomogeneities with dimensions of 10 to 1000 Å. Larger wavelengths are advantageous in this case and neutron wavelengths of up to 20 Å have been utilized.

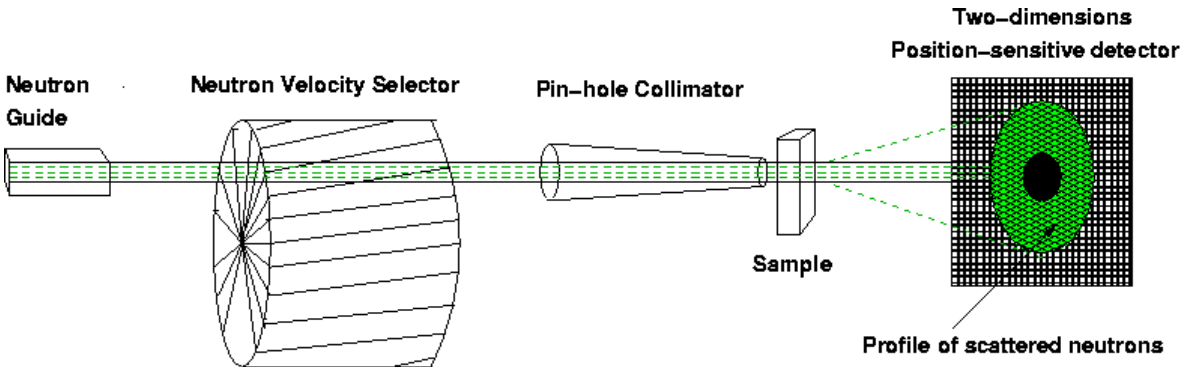

Fig. 4. Sketch of a traditional SANS instrument

In order to cover such small angles, a beam of high intensity, small cross-section (~1 mm^2) and a sample-to-detector distance of around 1 meter are needed. These figures are usually found in experiments with X-rays in synchrotron radiation facilities. In the case of SANS, due to the much smaller beam densities, the sample-to-detector distance can reach more than 50 meters, since a wider beam (~ 1 cm) is needed in this case. A sketch of a traditional SANS instrument is depicted in figure 4.

3.2. The optics of a SANS instrument

The performance of a SANS instrument depends basically on the magnitude of the pinhole collimator aperture and dimension, as well as on the distances between sample and detector, as shown in figure 5. The entrance and exit collimator apertures are R_{ns} and R_s respectively. L_1 is the collimator length and L_2 is the sample-to-detector distance [1]. The detector is considered to have a pixel of size Δl. Relations between these variables can be obtained to get a higher counting rate at the detector for a given resolution of the instrument. These are:

$$L1=L2 \quad \text{and} \quad R_{ns} = 2\,R_s = \Delta l \qquad (4)$$

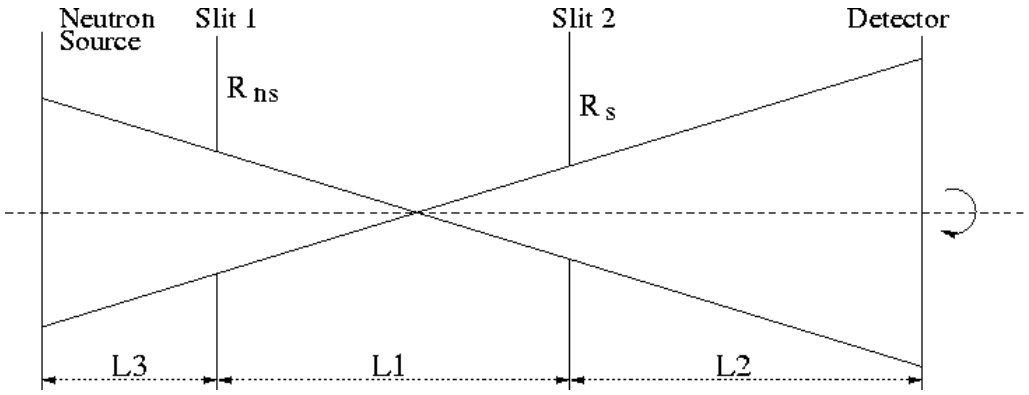

Fig. 5. Neutron optics of a SANS instrument

The magnitude of the scattering vector corresponding to the *n*'th detector pixel from the centre of the detector is

$$Q_n = \frac{2 \cdot \pi}{\lambda} \cdot \frac{n \cdot \Delta l}{L_2} \tag{5}$$

whereas the minimum *Q* is given by:

$$Q_{\min} = \frac{2 \cdot \pi}{\lambda} \cdot \left(2\frac{R_{ns}}{L_1} + \frac{\Delta l}{L_2} \right) \tag{6}$$

$Q_{\max}$ is determined by (5) with $n = n_0$, the outermost pixel of the detector.

The resolution of the spectrometer and the number of neutrons hitting the sample per unit time, are respectively given by:

$$\frac{\Delta Q}{Q} = \left[\left(\frac{\Delta \lambda}{\lambda} \right)^2 + \left(\frac{\Delta \Theta}{\Theta} \right)^2 \right]^{1/2} \tag{7}$$

(8)

$$N_s = \frac{\Phi_0 \pi}{4} \frac{{R_{ns}}^4 {L_2}^2}{\left(L_1 + L_2\right)^2 {L_1}^2} \bullet \left\{ 1 + \frac{1}{3} \frac{L_2^2 L_3^2}{\left(L_1 + L_2\right)^2 \left(L_1 + L_3\right)^2} \right\}$$

Where λ is the neutron wavelength, $\Delta\Theta$ is the angular spread of scattered neutrons defined as the full width at a half maximum (FWHM) of a Gaussian distribution:

$$\Delta\Theta = \sqrt{2 \ln 2} \left[2\left(\frac{R_{ns}}{L_1} \right)^2 + \frac{1}{3}\left(\frac{\Delta l}{L_2} \right)^2 \right]^{1/2} \tag{9}$$

and Φ_0 is the neutron flux at the neutron source. L_3 is the distance between the neutron source surface and the entrance slit of the collimator.

3.3. Performance of a traditional SANS spectrometer

Figure 6 shows the result of a performance simulation of a hypothetical SANS instrument running at the beam port #10 of the IEA-R1 reactor. The temperature of the Maxwell distribution of thermal neutrons was estimated to be 350 K. The available space at this position is 16 m long. The length of the instrument, $L_1 + L_2$, was taken to be 10 m, with the rest of the available space supposed to be reserved for the exit portion of a stacked neutron guide, a neutron velocity selector and the sample environment. The detector is a typical 64 x 64 pixels, two-dimension position sensitive, with a pixel size of 1 cm x 1 cm. The width of the neutron wavelengths impinging the sample was taken to be 5 % around the mean wavelength.

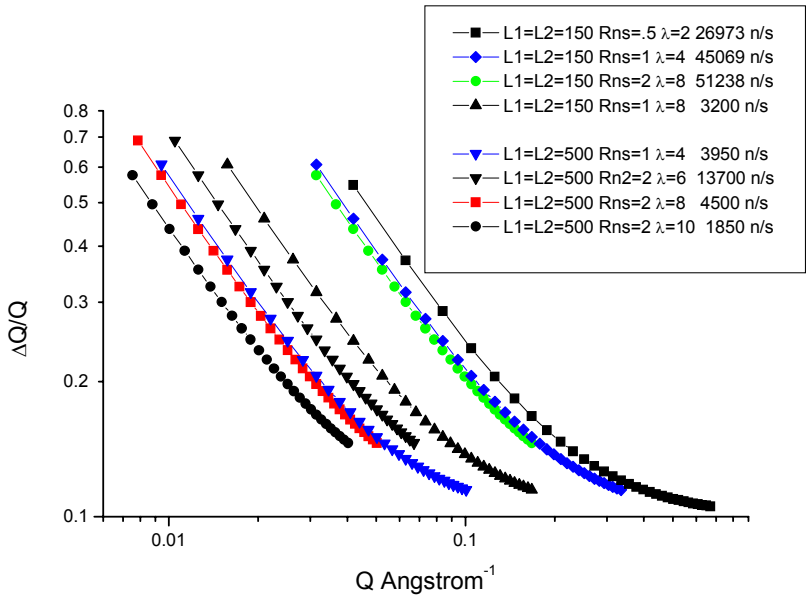

Fig. 6. Plots of the FWHM of the resolution as a function of the momentum transfer. In the insert the conditions for each curve are shown. Lengths are in cm, wavelengths in Å. The last column represents the number of neutrons hitting the sample per second. Neutron flux at the reactor core $\Phi_0 = 10^{12}$ n.cm^{-2}.s^{-1}, temperature of the Maxwell distribution T=350 K.

In figure 6, several curves representing the instrument resolution $\Delta Q/Q$ as a function of the momentum transfer Q are presented. The parameters for each curve are shown in the insert together with the number of neutrons hitting the sample per second at a given condition.

The acceptable minimum for the neutron rate at the sample position is taken to be 10^4 neutrons per second. Bearing in mind that only 10 % of these are useful for the experiment in order to avoid multiple scattering and considering the losses on the neutron filter and on the monochromator that together can easily be 70%, around 300 neutrons per second would be necessary for a reliable count. A typical experiment with good statistics would last about one hour and more if one considers the background counting, as it is expected to be high in this case since the spectrometer has to be installed in the reactor room.

As can be seen in figure 7 in the case that $\lambda = 4$ Å, $L_1 = L_2 = 5$ m and $R_{ns} = 1$ cm, corresponding to the matched condition with $R_{ns} = \Delta l$, the neutron rate in the sample will be less than the required minimum by a factor of ≈ 3, thus restricting the possibility to run an experiment under these conditions. For higher wavelengths the neutron rate will be even

smaller. In order to get some idea of other performance parameters, let us keep to these conditions. The minimum attainable value for the momentum transfer Q_{min} would be 0.01 Å^{-1} and the maximum would be Q_{max} = 0.1 Å^{-1}. The resolution at Q_{min} is very poor, attaining $\Delta Q/Q$ of 0.6 FWHM. This feature is, however, characteristic of any SANS experiment, the remedy being to decrease the low limit for Q. If we restrict ourselves to a maximum of 20 % in the resolution, the useful Q range would be 0.03 to 0.1 Å^{-1}. This means that in the range of Q values between 0.01 - 0.03 Å^{-1} only experiments that do not depend too much on the resolution should be performed, like the cases in which a monotonic behaviour of the scattered intensity as a function of Q is expected.

The unmatched condition in which R_{ns} = 2 cm and λ = 6 Å, (L_1=L_2=5 m) results in a sufficient neutron rate in the sample. The low Q limit would be slightly increased over 0.01, the resolution at Q_{min} increases to 0.7, and Q_{max} decreases to 0.07 Å^{-1}. The range of Q values corresponding to $\Delta Q/Q$ less than 0.2 is 0.04 - 0.07 Å^{-1}.

These findings indicate that the experiments on a traditional SANS instrument at the IEA-R1 reactor should be performed with an unmatched condition when L_1 = L_2 = 5 m. The minimum Q would be close to 0.01 Å^{-1} at the worst resolution of 0.7, whereas at a better resolution lower than 0.2, Q_{min} = 0.04 Å^{-1}.

Combining one measurement with this setting with others with lower values of L_2 and λ, it is possible to reach $Q_{max} \approx$ 0.5 Å^{-1} at resolutions better than 20 %.

In short, it can be concluded that a traditional SANS instrument at the IEA-R1 reactor would present a useful Q range of 0.04 - 0.5 Å^{-1} with a resolution better than 20 %, and a Q range of 0.01 - 0.04 with poor resolution.

As can be seen, these figures represent a very modest SANS spectrometer performance. Even in this case several studies on colloid particles and micelles can be performed, but there are other cases, like in polymer science, in which the application of such a facility would be very limited and an improvement in performance would be highly desirable.

3.4. A SANS spectrometer based on a converging multi-channel collimator

A possible way to improve the SANS spectrometer performance, not yet developed at present, is the utilization of a stack of multiple pinhole collimators, as depicted in figure 7.

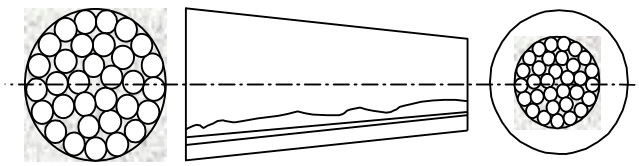

Fig. 7. Stack of multiple pinhole collimators

The motivation for such an idea is the fact that usually the neutron source area seen at the entrance aperture of a single pinhole collimator is small compared to the available neutron source area. In our example R_{ns} = 2 cm, whereas the beam hole radius is 7.5 cm. If all this area could be used for the experiment, a gain factor of 14 could be achieved in the neutron flux at the sample position. However, since the entrance slit of the collimator is located at a distance L_3 from the neutron source (see figure 6), the gain factor will be less than this value. Even with this limitation it seems to be advantageous to construct a spectrometer with this

device, since the condition $L_1 = L_2$ would be no longer necessary and thus a greater sample-to-detector distance could be utilized in the same available space.

The following relations hold for this case:

$$N_s = \frac{\Phi_0 \pi}{4}\left(\frac{L_2}{L_1+L_2}\right)^2\left(\frac{R_{ns}}{L_1}\right)^2 {R_N}^2\left(\frac{L_1+L_2}{L_1+L_2+L_3}\right)^2 \tag{10}$$

where R_N is the radius of the neutron source at the entrance (bottom) of the beam-hole. The neutron rate in the sample, $N_{s,}$ can also be given by:

$$N_s = \frac{\Phi_0 \pi}{4}\left(\frac{L_2}{L_1+L_2}\right)^2 \frac{3\Delta\Theta^2}{14\ln 2} {R_N}^2\left(\frac{L_1+L_2}{L_1+L_2+L_3}\right)^2 \tag{11}$$

where a dependence on the square of the angular spread is shown, as compared to the fourth power in the case of a unique pin-hole collimator. The following conditions must hold to obtain the maximum resolution for a given neutron rate at the sample position:

$$R_s = R_{ns}\frac{L_2}{L_1+L_2} \tag{12}$$

and

$$\frac{R_{ns}}{L_1} = \frac{\Delta l}{L_2} \tag{13}$$

Table 3 presents the expected performance parameters for a hypothetical SANS spectrometer that utilizes a converged multi-channel collimator.

As can be seen in table 3, the performance parameters of a SANS spectrometer are improved as compared to the case in which just one pinhole collimator is used. It is possible to enlarge the sample to detector distance L_2 and to increase the neutron rate at the sample position. In this way, the minimum value of Q can be decreased to 0.003 $Å^{-1}$ and Q_{min} for $\Delta Q/Q$ less to 0.2 can also be decreased to 0.01 $Å^{-1}$, utilizing 6 Å neutrons with a perfectly matched spectrometer, contrary to the previous single-pinhole collimator case. The maximum value of Q can still be reached as before if 2 Å neutrons are available. The conditions seen in table 1 were chosen bearing in mind the space limitations in the IEA-R1 reactor room. Other limitations occur due to the high temperature of the thermal neutron flux distribution.

There are, however, some drawbacks that have to be solved in order to build up a spectrometer with a CMC. First, as is seen in table 3, the tubes that compose the multi-channel collimator are somewhat thin and long, the aperture radius being 0.2 cm and the length 2 m. The walls of the tubes should be as thin as possible, since the relation between the open area of the tubes and the wall thickness will ultimately define the transmission efficiency

of the collimator. A shorter collimator must necessarily have a thinner aperture. These tubes, too, are converging, i.e., they start with a radius R_{ns} and end with a radius R_s. The second drawback is that the radii of the tubes have to change in accordance with the setting of the sample to detector distance L_2, otherwise the spectrometer would not be focused. This requirement can be accomplished by building up a collimator with continuously variable diameters or by utilizing a set of interchangeable collimators. The diameter has to vary in a large range of about a factor of 5. The third drawback is related to the fact that the diameter of the neutron beam at the collimator entrance will be larger, in our case ~ 6 cm, requiring that the beam transmitted by the velocity selector be as wide. This can impose restrictions on the construction of the neutron velocity selector, as larger discs for this device could be needed.

Table 3. Performance parameters for a hypothetical SANS instrument at the IPEN-CNEN/SP reactor that utilizes a converging multi-channel collimator. Reactor flux at the entrance of the beam hole $\Phi_0 = 10^{12}$ n.cm^{-2}.s^{-1}, temperature of the neutron flux distribution $T_n = 350$.

λ (Å)	N_s (n.s^{-1})	Q_{min} (Å^{-1})	Q_{min} (Å^{-1})	Q_{max} (Å^{-1})	Conditions
			$\Delta Q/Q < 20\%$		
4	7.5x10^4	0.0047	0.015	0.05	L_1= 2 m
6	1.6x10^4	0.0031	0.010	0.033	L_2 = 10 m
8	5.3x10^3	0.0023	0.0086	0.025	R_{ns} = 0.2 cm
4	2.6x10^5	0.024	0.078	0.25	L_1 = 2 m
6	5.8x10^4	0.016	0.052	0.16	L_2 = 2m
8	1.9x10^4	0.012	0.039	0.13	R_{ns} = 1 cm

3.5. SANS with CMC and time-of-flight technique

Usually a SANS spectrometer utilizes a neutron velocity selector as a monochromator device. An alternative method is to use the time-of-flight technique to determine the neutron wavelength. In this method, the incident beam is opened in regular intervals by means of a chopper, usually made of a rotating absorbing disk with one or more windows, and the neutron wavelength is determined by the time needed for a neutron to travel a known distance. In our case, the interest in this method is due to two reasons. Being a disk, a chopper device is in principle shorter than a velocity selector, saving some space in order to increase L_2. The second reason is that, also in principle, it is easier to build a large disk chopper instead of a large disk neutron velocity selector.

In table 4 several parameters are presented for the operation of a hypothetical SANS spectrometer as discussed above in the time-of-flight mode in two settings of the sample to detector distances L_2. The chosen requirements were that the system would use the neutrons in the 2 - 8 Å interval and that the pulse width should be such that $\Delta t_0/t_0 = \Delta\lambda/\lambda = 0.1$ for the 2 Å neutrons, where t_0 is the time of flight. The 8 Å neutrons define the rotation speed of the chopper disk, whereas Δt_0, the time of flight of 8 Å neutrons t_{max} and the beam radius, define

the chopper disk radius. The window of the chopper is taken to be of the same size as the beam. The multi-channel analyzer should have a width equal to Δt_0 and the number of channels should be $t_{max} / \Delta t_0$.

Table 4. Time-of-flight data parameters for two sample-to-detector distances; t_{min} and t_{max} are the times needed for 2 and 8 Å neutrons to travel the L_2 distance, R_{beam} is the radius of the beam at the entrance of the chopper (equal to the sample radius), Δt_0 is the width of the neutron pulse, R_{disk} is the radius of the chopper disk, and RPM is the number of rotations per minute of the chopper.

L_2(m)	t_{min}(ms)	t_{max}(ms)	R_{beam}(cm)	Δt_0(μs)	R_{disk} (cm)	RPM
2	1.0	4.0	1.6	100	20.4	15000
10	5.0	20.0	4.4	500	56.2	3000

The duty cycle of the chopper in our example is $\Delta t_0 / t_{max} = 0.025$. This is more than one order of magnitude higher than the fraction of the spectrum transmitted by the velocity selector with $\Delta\lambda/\lambda = 0.1$ at 4 Å. Thus, compared with the traditional velocity selector, the time-of-flight method also results in a gain in the counting rate. This can be used to increase the resolution by a factor of 3 and, as a consequence, to decrease Q_{min} by the same amount. However, a detector with smaller pixel size is needed for this purpose since there is not enough space to increase L_2.

4. BEAM FILTER SYSTEM

There are two ways to accomplish the filtering of the neutron beam for fast neutrons and gamma radiation. The simplest method is just to transmit the neutron beam through suitable materials that have a small total cross-section for neutrons of interest and a high cross-section for the unwanted radiation. One of the most efficient materials for filtering against fast neutrons is polycrystalline beryllium, usually cooled to liquid nitrogen temperature to decrease the inelastic scattering cross-section for the transmitted neutrons. Only neutrons with a wavelength higher than 4 Å are transmitted. Neutrons with smaller wavelengths are scattered out of the beam and are absorbed in the reactor wall (shield). Good filtering against fast neutrons is achieved when the thickness of the filter is of the order of 50 cm.

One of the disadvantages of the polycrystalline beryllium filter is that it removes long-wavelength neutrons by absorption, since the absorption cross-section depends linearly on the wavelength. Around 20 % of the 6 Å neutrons are removed by absorption after passing through 50 cm of beryllium. Another disadvantage is that it does not transmit neutrons with a wavelength of less than 4 Å, thus limiting the Q_{max} that can be accessed with a SANS spectrometer. A third disadvantage is that polycrystalline beryllium does not remove efficiently the gamma radiation because it is a material with low electronic density. Heavier materials such as bismuth or lead must be utilized in conjunction with beryllium to accomplish this task. However, these materials must be single crystals since they present a higher neutron wavelength cut-off. Since the neutron absorption cross-sections of these materials are quite high compared with that of beryllium, they must necessarily be short and, as a consequence, the removal of gamma radiation would never be satisfactory.

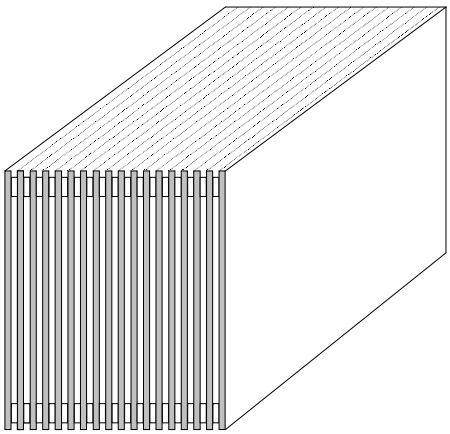

Fig. 8. Section of a stacked neutron guide.

The second filtering method, initially proposed by the group at IRI in Delft, The Netherlands, is the utilization of the so-called stacked neutron guides [3]. It consists of a stack of thin neutron guides made of 1 mm-thick silica glass plates with spacers also 1 mm thick of the same material. A sketch of a small section of such a device is presented in figure 8. The internal walls of the guides are coated with Ni^{58}, a suitable material for the total reflection of the neutrons that impinge the surface at grazing angles less than the critical value. The guide is 3 m long and has a curvature radius of 200 m. Neutrons reflected from the internal walls are transmitted only to the end of the guide. Fast neutrons and gamma radiation are absorbed in the walls. The transmission efficiency is ~ 60 %, whereas the contamination of the beam by gamma radiation and fast neutrons is ~40 and ~1000 times smaller as compared to a typical transmission filter.

Another advantage of a stacked neutron guide is that it transmits a wider neutron spectrum as compared to the crystalline beryllium filter. The transmitted spectrum begins at 1.5 Å and there is in principle no limit for a higher neutron wavelength, since the transmission efficiency increases as a function of the neutron wavelength due to the fact that the critical angle for reflection is given by $\theta_c=\gamma_c\lambda$, with γ_c=2.05 mrad/Å for the coating material Ni^{58}.

In our example of a SANS spectrometer at the IEA-R1 reactor, utilizing the multi-channel collimator, a stacked neutron guide of a cross-sectional area of 10 x 10 cm^2 would be adequate, but a serious limitation exists. It is related to the fact that the neutron beam emerging from such a device is too much collimated, i.e., the beam semi-divergence is too small, being 8.2 mrad for 4 Å neutrons. This does not cause problems when the spectrometer runs at the large sample-to-detector distance L_2 = 10 m. In this case a beam semi-divergence of 5 mrad is enough for the neutrons that emerge from the sides of the guide to reach the centre of the detector. In the case when L_2 = 2m, however, only a very small portion of the sectional area of the guide will be effective, i.e., the one inside a circle with a radius of 1.6 cm, since a much larger beam semi-divergence would be needed for the neutrons that emerge from the sides of the guide, i.e., 30 mrad. This limitation practically destroys every gain that was achieved with the utilization of the CMC. The unique way to overcome this problem is to try to use a stacked neutron guide of a different design. One possibility is to use converging neutron guides, since in this case greater divergence can be achieved. Anther possibility is to choose coating materials with higher critical angles for total reflection.

5. CONCLUSIONS

In conclusion, it was shown that a traditional SANS spectrometer at the IEA-R1 reactor would have a very modest performance. A greatly improved performance can be achieved if a SANS spectrometer is made with a converging multi-channel collimator besides running with

the time-of-flight methodology. The following technical problems have to be solved: a) the construction of the CMC, b) the construction of the chopper disk, and c) the small divergence of the stacked neutron guide.

REFERENCES

[1] INTERNATIONAL ATOMIC ENERGY AGENCY, Trends and Techniques in Neutron Beam Research for Medium and Low Flux Research Reactors**,** IAEA-TECDOC-974, IAEA, Vienna (1997).

[2] MARGAÇA, F.M.A., FALCÃO, A.N., SALGADO, F.J., CARVALHO. F.G., Multichannel collimation for SANS instruments, Physica B **276-278** 189 (2000).

[3] WELL, A.A.Van., HAAN, V.O.de, REKVELDT, M.Th., Stacked neutron guides at IRI Delft**,** Neutron News, **2**, No.3, 28 (1991)

INVESTIGATIONS FOR THE DEVELOPMENT OF SMALL ANGLE NEUTRON SCATTERING APPARATUS AT A LOW-POWER REACTOR

K. Mergia, S. Messoloras

National Centre for Scientific Research, "Demokritos", Greece

Abstract: A 1D ^{3}He position sensitive neutron detector was tested for various parameters such as efficiency, signal-to-background ratios and gamma/neutron sensitivity. Transmission and scattering cross-sections were measured for samples of silver behenate and glassy carbonate. To estimate the Q measurement resolution the Guinier approximation was used. When determining lengths in the order of particle sizes, resolution itself may not be as important a factor as the question of applicability of the Guinier approximation. The maximum measurable size was calculated for different collimation means. Indications are that pinhole collimation might not necessarily be the best option when measuring larger sizes (~nm) in reactors where space is a restriction.

1. POSITION SENSITIVE DETECTOR (PSD) FOR A SANS INSTRUMENT IN A LOW POWER REACTOR

1.1. Detector characteristics

The detector type used for the underlying work was a Reuter-Stokes ^{3}He Position Sensitive Detector RS-P4-0824-208, filled to a pressure of 8 atm ^{3}He and 4 atm Ar with 0.5% CO_2. The detector is cylindrical, of a diameter of 25.4 mm, and has walls of 0.508 mm stainless steel, while its active length is 609.6 mm. Position determination is accomplished by the charge division method. In practice, it is not the charges that are measured but the digitized voltage representations of these charges produced by the Analog-to-Digital Converters (ADC).

When a neutron strikes the detector whose anode is biased with a high DC voltage of up to 2000 V, it will be absorbed in ^{3}He according to the reaction

$$^3He + n \rightarrow {}^3H + {}^1H + 768keV \qquad (1)$$

Electrons from ionization of the fill gas created by the neutron absorption reaction products are accelerated towards the anode by the bias voltage-producing additional ionization by electron impact. The final result of the neutron capture is the deposition of a negative charge on the anode and of an equal positive charge on the detector cathode. The charge passes down the resistive anode, out of both ends of the detector, and into the pre-amplifiers shown in figure 1. The pre-amplifiers convert the charge into a voltage signal, which passes through a pulse amplifier. The amplifier outputs are processed by two 8-bit analog-to-digital converters (ADCs). The ADCs used are the Motorola MC10319. The ADC outputs are directed to the main processor (LCA) and afterwards to the Personal Computer (PC).

The basic component for this arrangement is the LCA (Logic Cell Array), which is the XC4006E-PG156-3 of Xilinx and belongs to the FPGA (Field Programmable Gate Array) family. The software includes a schematic part, a simulation part and the creation of a bit-stream-type file (*.RBT) to programme LCA.

In our arrangement we select ten points for each pulse, and these points simulate the pulses. The pulses are separated in 255 levels (from 0-255). This level selection occurs as a consequence of the use of the ADC, which is an 8-bit converter. Over 255 levels the ADC gives an overflow (over-range), which means that pulses higher than the 255 level cannot be measured. The choice from which level to start the ten-point selection is usually level 48. The clock frequency for both the ADC and the LCA is 20 MHz.

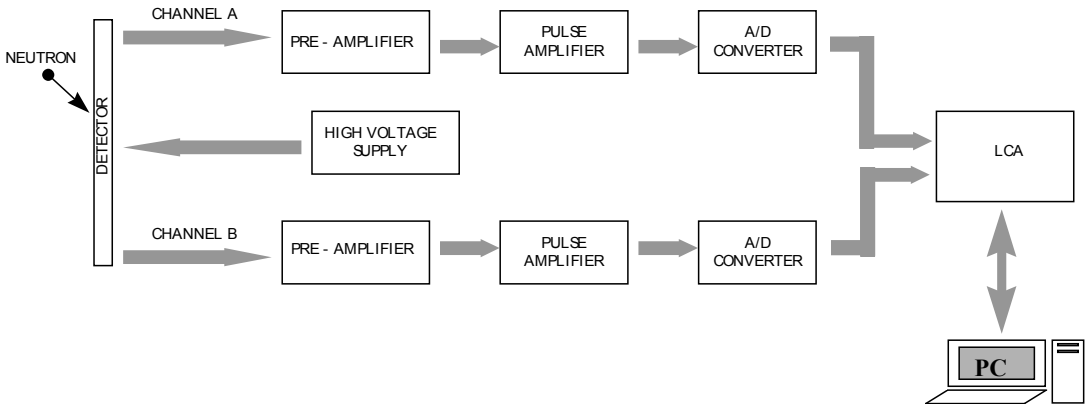

Fig. 1. General Diagram for the Electronic Arrangement

In order to determine the position of the neutron absorption on the detector, the following calculation has to be performed:

$$R_A = \frac{V_A}{V_A + V_B} * 1024, \quad \text{If } V_A > V_B \tag{2}$$

$$R_B = \frac{V_B}{V_A + V_B} * 1024, \quad \text{If } V_B \geq V_A \tag{3}$$

where 1024(=2^{10}) is the number of channels which correspond to the active length of the detector. The above calculation is performed using the LCA, and the result is directed to an external RAM (Hitachi HM628128). R_A and R_B are the resistances of the wire from the A and B ends of the anode wire to the point of neutron detection, and V_A and V_B represent the voltages at the A and B ends of the anode wire respectively.

2. EFFICIENCY DETERMINATION OF A PSD

For the detector efficiency determination along the detector length an Am-Be neutron source was used, which was placed in the centre of a wax sphere of 10 cm diameter. The pattern received is shown in figure 2. This pattern can be easily explained. When we move from the center to the edges of the detector, the signal at the one edge of the detector tube increases whereas at the other end decreases. So there will be events giving pulses higher than the digitization threshold or below the discrimination threshold.

2.1. Calibration of PSD parameters

In our electronics design there are two levels which determine whether a pulse at the ends of the detector tube is going to be measured. The first (to be referred to as A level) determines the level above which the digitized neutron pulse coming from either the right or the left edge of the detector tube is accepted.

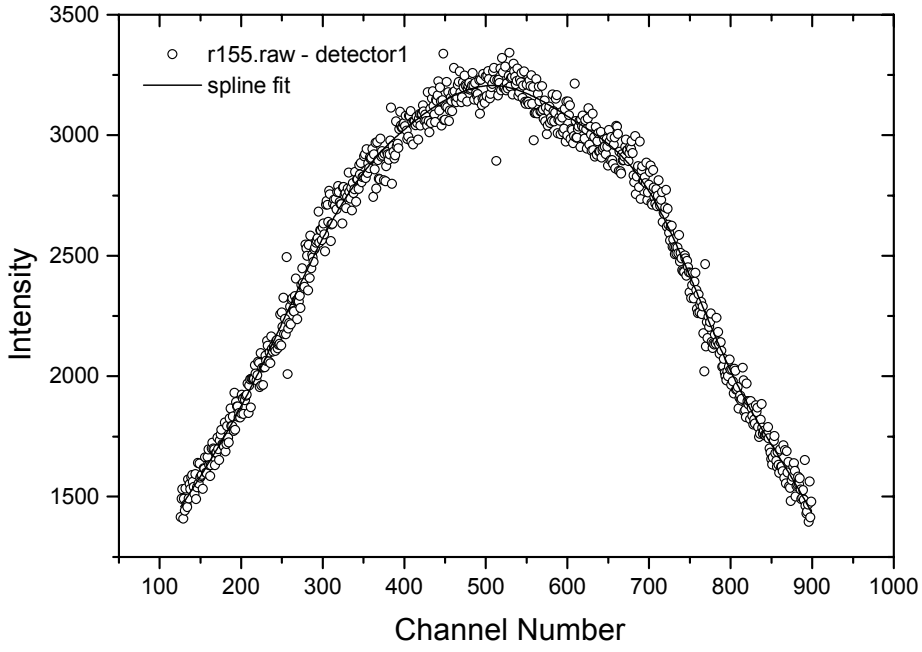

Fig. 2. Efficiency determination of a linear position sensitive detector

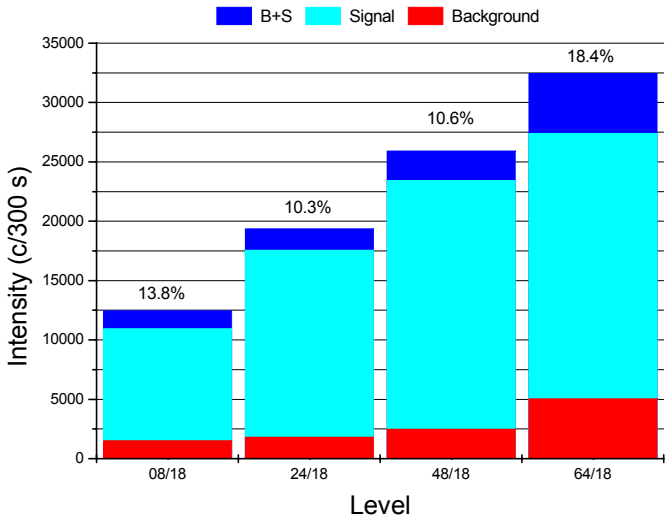

Fig. 3. Background, signal and signal with background included for different A levels. The numbers correspond to the background-to-signal ratio.

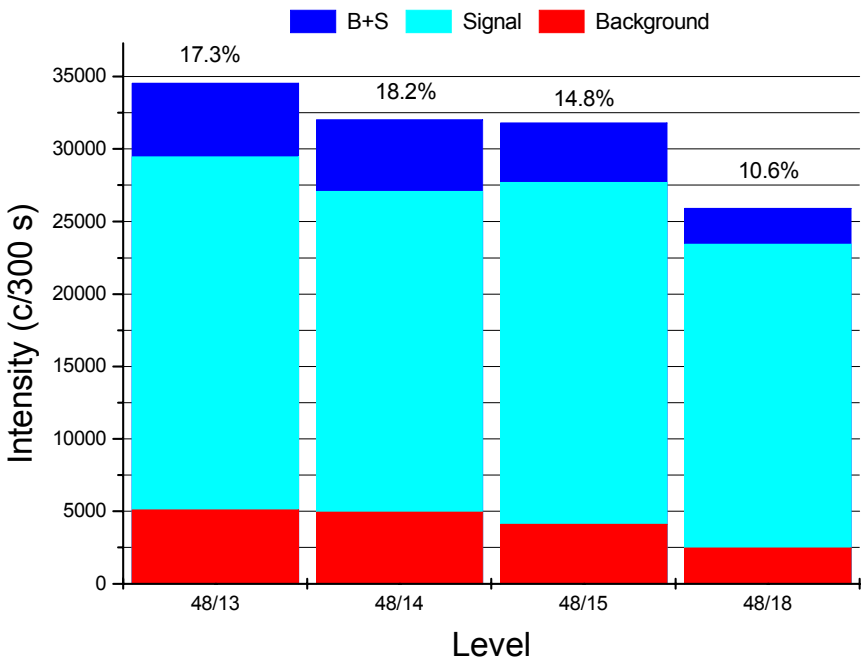

Fig. 4. Background, signal and signal with background included for different A+B levels. The numbers correspond to the background-to-signal ratio.

The second level (A+B level) refers to the summation, A+B, of the two digitized pulses from the two edges of the detector tube. We performed measurements with different detector configurations, i.e., with different combinations of the two levels. Each configuration is described by two numbers; the first one refers to the first level and the second one to the second level, as described above, i.e., xx/yy. Two of the criteria for the optimization of the levels used is the background-to-signal ratio, which has to be as low as possible, and the counting rate, which has to be as high as possible. The histogram in figure 3 shows the background, the signal and the signal with the background included, for different A levels and for the same A+B level. The different percentages shown in figure 3 correspond to the background-to-signal ratio. We observed that the smaller ratio was for levels 24 and 48, which were about the same, but the counting rate for level 48 was higher. Thus level 48 was chosen as A level. Then, by keeping the A level constant and equal to 48, we varied the A+B level. The results are presented in figure 4 where one observes that for level 13 the counting rate becomes maximum, but for level 18 the background-to-signal ratio becomes minimum. So level 18 was chosen as the optimum one. Level 18 corresponds to a cut-off value of 1280 for the sum of the two pulses.

The γ against the neutron sensitivity of the detector was also measured for different A+B levels, using a 370 kBq Co60 γ source and a 30 mCi AmBe neutron source. In figure 5 the total counts and the γ over neutron ratio for the different A+B levels are presented. At level 18 (cut-off value 1232) the γ sensitivity becomes very low (95 % decrease), while the neutron counting rate remains quite high (21 % decrease).

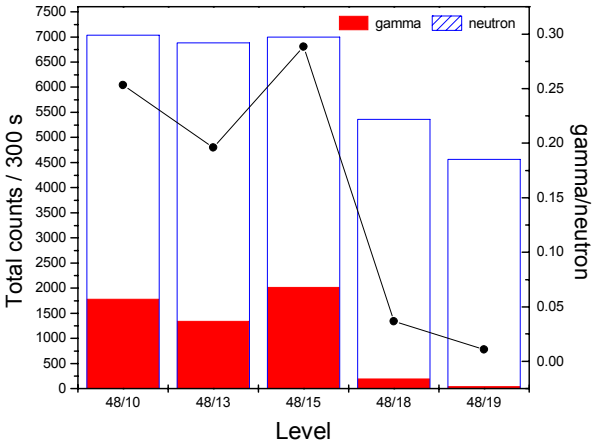

Fig. 5. Total counts for neutron and γ source versus the different discrimination levels. The points correspond to the γ-to-neutron ratio.

2.2. Results from standard samples

The detector test measurements were carried out at a V4 instrument at the Hahn-Meitner Institut. The geometry used is depicted in figure 6. The detector was placed vertically at a distance of 634 mm from the sample position, with the neutron beam at a height of 285 mm from its down edge. A beam stop of boron carbide was placed on the detector where the beam impinged on it.

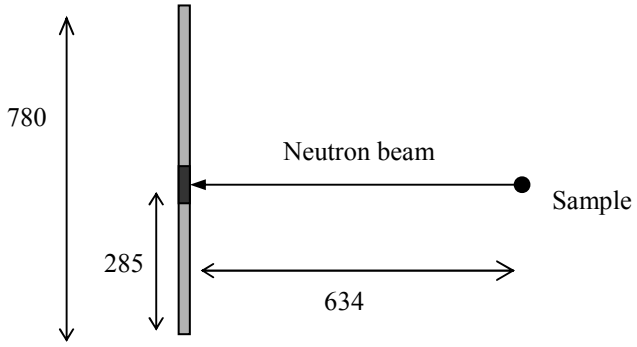

Fig. 6. The geometry used for the detector measurements. All numbers in mm.

Two standard samples of silver behenate (AgBE) and glassy carbon were measured at the two different wavelengths of 6.07 and 12.10 Å. The collimation used was 4 m and the aperture was 5 mm in diameter. The data were corrected for background, transmission and efficiency, and finally absolute values were derived by water measurements. The water measurements were also used for the detector efficiency corrections.

For the correction of the data the following formula was used:

$$\frac{d\sigma}{d\Omega} = \frac{(I_s - I_{Cd})/T_s - (I_{ec} - I_{Cd})/T_{ec}}{(I_{H_2O} - I_{Cd})/T_{H_2O} - (I_{ec} - I_{Cd})/T_{ec}} \cdot \frac{sc(H_2O)}{sc(sample)}$$
$$sc(H_2O) = \frac{A_{H_2O}}{T_{H_2O}} \frac{1 - T_{H_2O}/T_{ec}}{4\pi}, \quad sc(sample) = A_s d \tag{4}$$

where

I_s : is the scattering of the sample

I_{Cd} : is the background scattering

I_{ec} : is the scattering of the empty cell

I_{H_2O} : is the water scattering

T_s : is the sample transmission

T_{ec} : is the empty cell transmission

T_{H_2O}: is the water transmission

$A_{H_2O/s}$: is the area of the water or sample being illuminated

d : is the sample thickness

The transmission of a sample is defined as the ratio of the scattering intensity of the sample over the scattering intensity of the empty hole.

2.3. Silver Behenate

The raw data for AgBE for the two wavelengths are shown in figure 7. These data are presented versus the electronic channel number. Each electronic channel corresponds to approximately 0.67 mm. The raw data from water, empty cell and background are presented in figure 8 normalized to time for λ=6.07 Å.

The corrected data for AgBE at the two wavelengths λ=6.07 Å and λ=12.10 Å are presented in figure 9. These data have been corrected for background, empty cell, background, transmission and absolute intensities according to the formula of eq. (4).

The data have also been corrected for detector efficiency, using the data from water. For the transformation of the electronic channels to positions and subsequently to scattering angles, the data from a cadmium mask have been used. This mask is constructed in the form of a cadmium sheet with 25 sets of holes of 2 mm diameter at certain distances along the length of the detector. As a sample a strong scatterer (perspex) was used, and from the spectrum, which is actually a set of Gaussian peaks, the parameters for the channel transformation to position were determined.

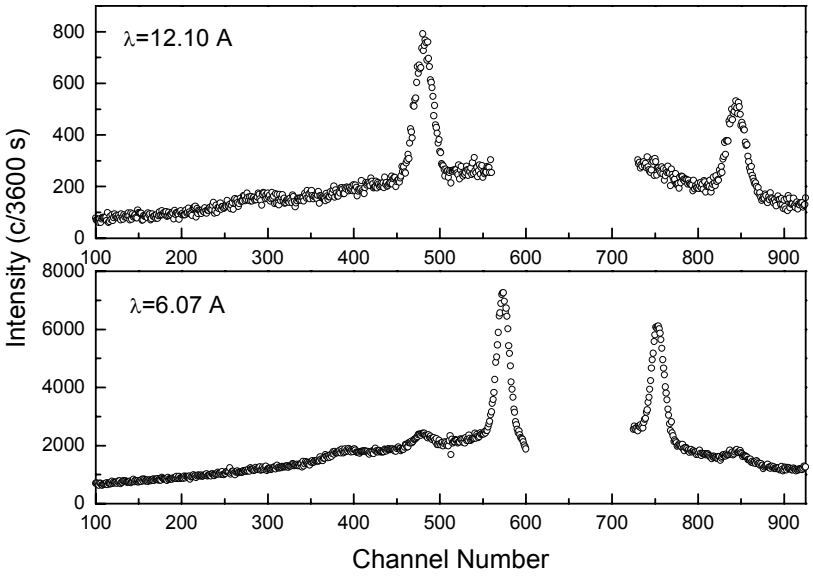

Fig. 7. The raw data for AgBE at the two wavelengths 6.07 Å and 12.10 Å

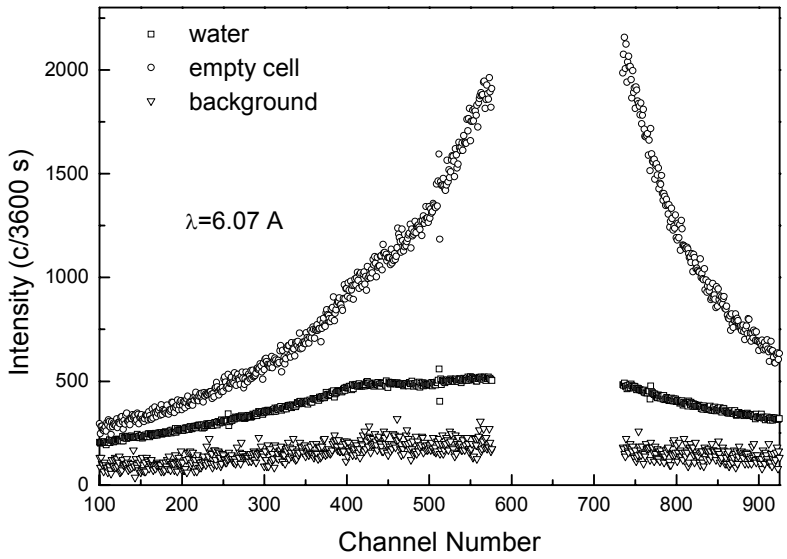

Fig. 8. The time normalized raw data from water, empty cell and background for λ=6.07Å.

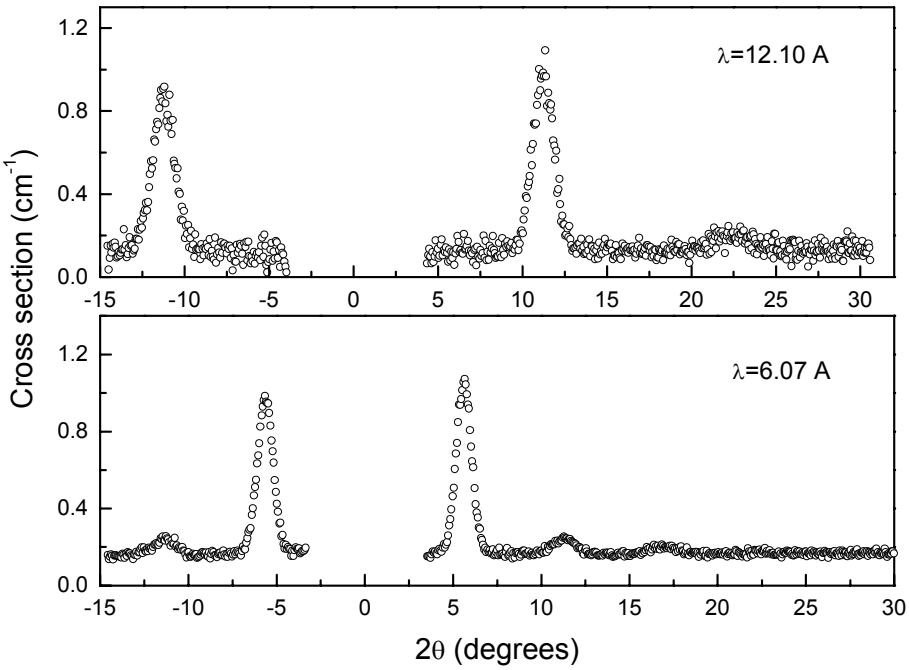

Fig. 9. The corrected data for AgBE at two wavelengths 6.07 and 12.10 Å

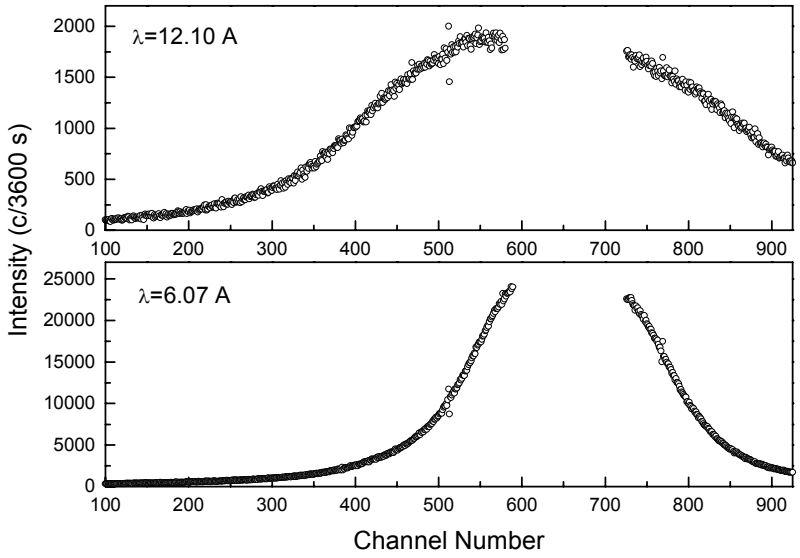

Fig. 10. The raw data from glassy carbon at the two wavelengths 6.07 and 12.10 Å

The data from the mask were also used for correcting unequal amplifications at the two ends of the detector, i.e., an amplification mismatch of 1%, which is difficult to correct electronically. The mask data for different sample-detector distances were used for the correction of the geometric effect that was due to the fact that the beam spot was not formed

exactly behind the mask hole, and consequently the angle of the scattered beam relative to the normal to the detector wire passing from the sample centre had to be taken into account. At this sample-detector distance, i.e., 634 mm, the FWHM was 61.2′ for λ=6.07 Å and 90.8′ for λ=12.10 Å.

2.4. Glassy Carbon

Glassy carbon was also measured at the two wavelengths of 6.07 and 12.10 Å. The raw data are presented in figure10, and the corrected curve in figure 11. Again corrections for empty cell, background, transmission, detector efficiency and absolute measurements have been performed (eq. (4)).

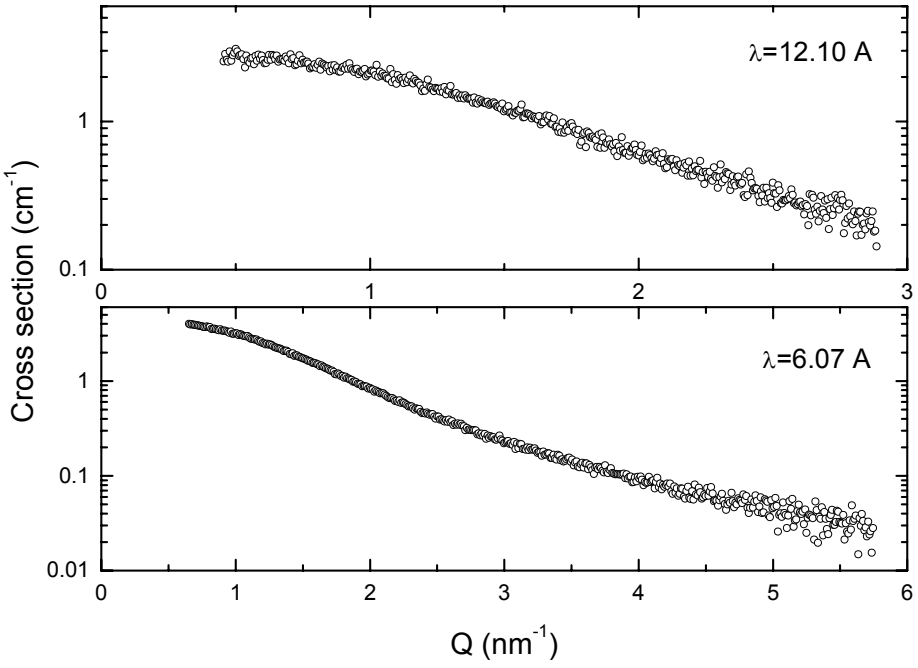

Fig. 11. The corrected data from glassy carbon at the two wavelengths 6.07 and 12.10Å

3. SOME ASPECTS OF A SANS INSTRUMENT IN A LOW-POWER REACTOR

3.1. Introduction

With SANS we want to measure structure scales from 1nm to μm. In a first approach to the problem of developing a SANS instrument in a low-power reactor without a cold source, we will be restricted to structures of isolated particles, and any interference scattering between the particles and the effects of a size distribution will be ignored. Once the feasibility of a SANS instrument within the conditions of low power and the lack of a cold source and the limited requirement of measuring sizes has been established, more sophisticated structures could be examined. For large sizes a USANS facility would be appropriate, and our calculations show that such an instrument would be successful in our reactor. Using Si bent crystals (Double-Crystal SANS Diffractometer DN-2, NPI, Prague) seems to be a good choice. With such an instrument the maximum Q to be expected might be around 5×10^{-2} nm^{-1},

which implies that the minimum size which could be detected would be around $R_g = 30\text{nm}$. Thus another instrument would be needed to cover for smaller sizes.

3.2. Initial considerations

Since we are only interested in determining sizes, we need only consider the Guinier region of the SANS which can be expressed as

$$S(QR_g) \sim (\Delta b)^2 \, nR_g^6 \exp\left(-\frac{Q^2 R_g^2}{3}\right) \tag{5}$$

where Δb is the contrast, n the number of particles and R_g the radius of gyration. The Guinier approximation is valid for up to $Q_{\max} R_g \sim 1.5$ where the intensity is around 50 % of the maximum value at $Q = 0$. In order to determine the value of R_g an extended Q range is required and we may set $Q_{\min} R_g \sim 0.5$ (intensity around 90% of the maximum).

3.3. Resolution

Next we need to consider the resolution for such a measurement. For the resolution we have

$$S(Q_0 R_g) = \frac{1}{2\Delta Q} \int_{Q_0 - \Delta Q}^{Q_0 + \Delta Q} \exp\left(-\frac{Q^2 R_g^2}{3}\right) dQ = \exp\left(-\frac{Q_0^2 R_g^2}{3}\right) F\left(Q_0 R_g, \Delta Q R_g\right) \tag{6}$$

where $F\left(Q_0 R_g, 0\right) = 1$. In figure 12 the function $F\left(Q_0 R_g, \Delta Q R_g\right)$ is plotted against $Q_0 R_g$ and for different values of $\Delta Q R_g$. Figure 12 shows the deviation from the Guinier approximation, which is independent of the value of R_g, for the different values of $\Delta Q R_g$. Since we are interested in the error in determining the value of R_g, this error is given in figure 13. In the simulations the Q range used is from QR_g 0.5 to 1.5 and the values of R_g used are from 2 to 70 nm. The error is independent of the value of R_g, provided the above defined Q range is used.

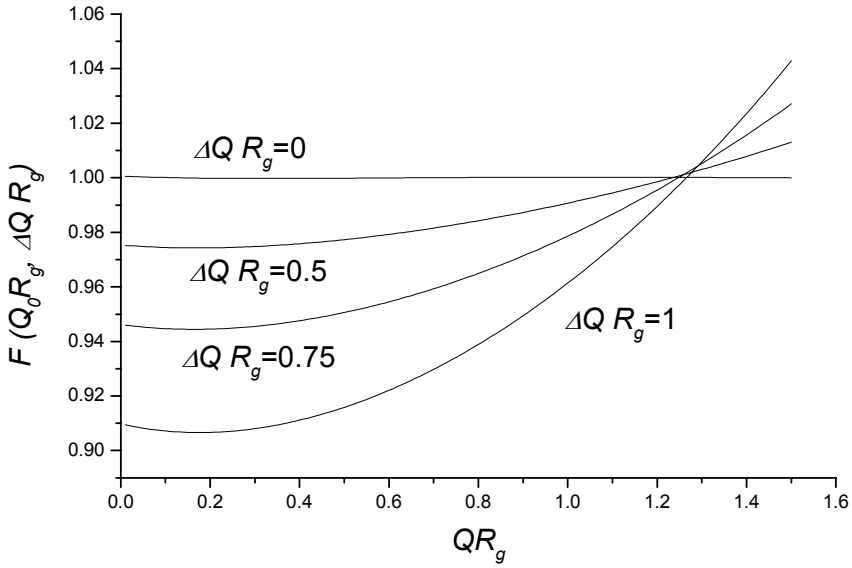

Fig. 12. $F\left(Q_0 R_g, \Delta Q R_g\right)$ *versus* $Q_0 R_g$ *and for different values of* $\Delta Q R_g$

From figure 13 it is apparent that a reasonable value of $\Delta Q R_g$ is around 0.6 ($\Delta R_g / R_g \sim 4\%$), which gives a value of $\Delta Q / Q$ around 0.4. This relaxation of the resolution is very important for a low-power reactor.

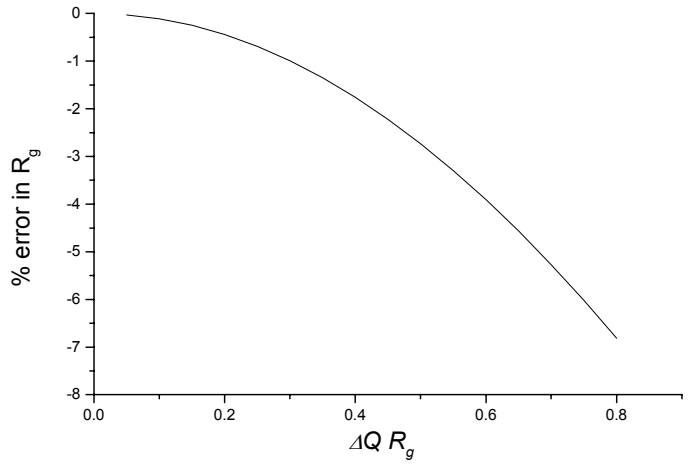

Fig. 13. The error in R_g *for different values of* $\Delta Q R_g$

In conclusion, the resolution is not the all-important factor in determining the size of particles; of more importance should be considered the applicability of the Guinier approximation and the measurement of a Q region, which corresponds to the Guinier region. For the latter it is necessary that the Q range be extended up to $2.5 / R_g$.

3.4. Maximum size

The maximum size which can be determined is given by

$$R_{g,\max} = \frac{0.5}{Q_{\min}} \tag{7}$$

In an optimized pinhole system we have

$$Q_{\min} = \frac{24\pi}{\lambda}\frac{S}{D} \tag{8}$$

where $2S$ is the sample diameter and D the sample detector distance. Using equation (7), we obtain

$$\frac{R_{g,\max}}{\lambda} = \frac{1}{48\pi}\frac{D}{S} \tag{9}$$

The divergence of the incident beam $\delta\theta_0$ is given by

$$\delta\theta_0 = \frac{3S}{D} \tag{10}$$

Taking $2S = 1\text{cm}$, we have $\delta\theta_0 \sim 10'$ for $D = 500\text{cm}$. Such an incident beam divergence may be produced by another collimating system, e.g., soller collimators.

Assuming a divergence of the incident beam of $\delta\theta_0$ the $Q_{\min}$ is given approximately as

$$Q_{\min} = \frac{4\pi\sin\theta}{\lambda} \approx \frac{4\pi}{\lambda}\left(\frac{S}{D} + \delta\theta_0\right) \tag{11}$$

and the maximum detectable size as

$$\frac{R_{g,\max}}{\lambda} \approx \frac{1}{8\pi}\left(\frac{S}{D} + \frac{3}{2}\delta\theta_0\right)^{-1} = A\left(\frac{D}{S}, \delta\theta_0\right) \tag{12}$$

where the detector element is $D\delta\theta_0/2$. The function $A\left(\frac{D}{S}, \delta\theta_0\right)$ is plotted in figure 14 against D/S together with equation (10).

We observe that the pinhole geometry in comparison, say, with a collimation of 10' gives larger sizes for longer distances. If we decrease the incident beam collimation to 5' we will be able to determine much larger sizes, and only a very long instrument could compete with such an arrangement. For $A \sim 10$ for pinhole geometry we must have $D/S \sim 1500$, whereas for $\delta\theta_0 = 5'$ we need $D/S \sim 500$. This would imply either larger sample areas and/or reduction of the instrument length.

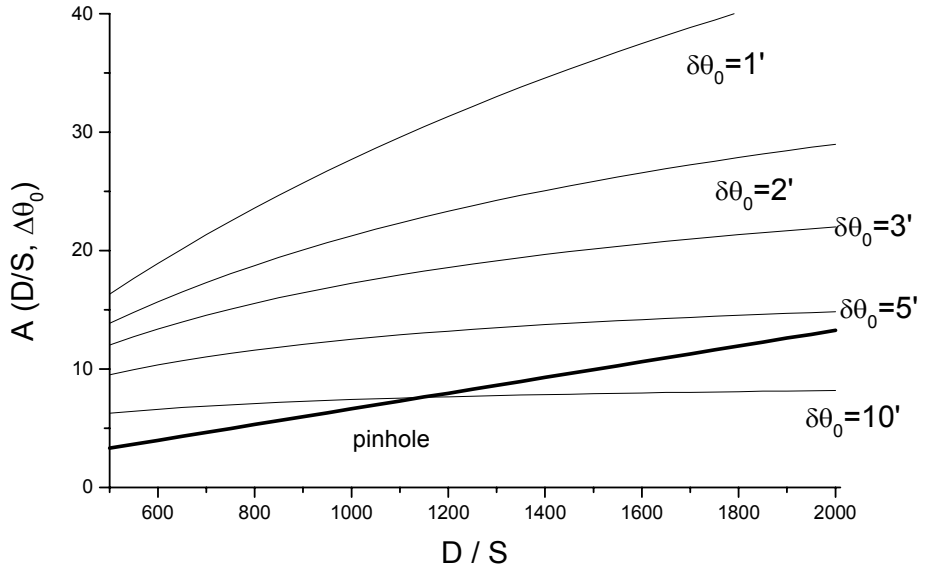

Fig. 14. The function $A\left(\frac{D}{S}, \delta\theta_0\right)$ *versus* D/S

We may conclude from the above that it is worth examining whether a pinhole arrangement would be the best choice for a low-power reactor and where restrictions of the available space exist. In addition, the cost of a shorter instrument would be reduced. Detailed calculations of the neutron intensity in such an arrangement are underway.

3.5. Long wavelengths

In order to detect large sizes (see equations (9) and (12)) it is necessary to employ long wavelengths. In a reactor without a cold source it is questionable up to what wavelength could be employed to have enough intensity for an experiment. In order to have a first approach at the problem we assumed a sample in which the size of the particles increased but their volume fraction and their contrast remained the same. This is the case in the precipitation phenomena. Under these conditions the scattering will be as

$$I \sim cR_g^3 \exp\left(-\frac{Q^2 R_g^2}{3}\right) n(\lambda)\Delta\lambda \exp(-a\lambda) \tag{13}$$

If we detect a size R_g using a wavelength λ according to equations (9) and (12), in order to detect a larger size R_g' we need to increase the wavelength as

$$\frac{R_g'}{R_g} = \frac{\lambda'}{\lambda} \tag{14}$$

For the same scattering angle or detector element we have

$$Q'R_g' = QR_g \tag{15}$$

The ratio of the scattering from sizes R_g and R_g' will be given as

$$\frac{I(\lambda')}{I(\lambda)} = \left(\frac{\lambda'}{\lambda}\right)^3 \frac{n(\lambda')\lambda'\exp(-a\lambda')}{n(\lambda)\lambda\exp(-a\lambda)} \tag{16}$$

where it is assumed that $\Delta\lambda/\lambda$ is constant. Using as λ the maximum wavelength of the Maxwellian and writing λ' as λ we have

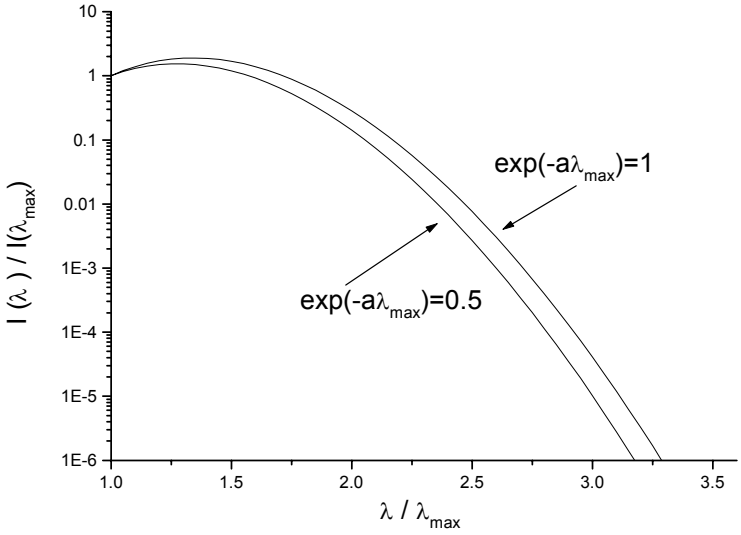

$$\frac{I(\lambda)}{I(\lambda_{\max})} = \left(\frac{\lambda}{\lambda_{\max}}\right)^9 \exp\left(-\frac{5\lambda^2}{2\lambda_{\max}^2}\right)\exp\left(-a\lambda_{\max}\left(\frac{\lambda}{\lambda_{\max}}-1\right)\right) \tag{17}$$

Fig. 15. $I(\lambda)/I(\lambda_{\max})$ *versus* $\lambda/\lambda_{\max}$ *(eq. (17))*

The last equation is plotted in figure 15. From this it is apparent that in the best situation in a low-power reactor the maximum value of $\lambda/\lambda_{\max}$ could be around 3.5, which would give a value of $\lambda \sim 0.6\text{nm}$, and, taking into account the discussion in section 3.4, the maximum detectable size could be up to 6 nm.

Taking into consideration the current interest in nanotechnology, such an instrument would be very useful in this area. However, a collimating system with $\delta\theta_0 \sim 1'$ could increase the maximum detectable size to 24 nm. Still, in such a system the questions about the available flux remain.

4. Conclusions

To estimate the Q measurement resolution the Guinier approximation was used. When determining lengths in the order of particle sizes, resolution itself may not be as important a factor as the question of the applicability of the Guinier approximation.

The maximum measurable size was calculated as a function of the collimation divergence angle and the detector distance per typical sample dimension for different means of collimation, indicating that pinhole collimation need not necessarily be the best option when measuring larger sizes (~nm) in reactors where space is a restriction. The smaller the collimated beam divergence, the larger the measurable sizes, yet one must take into account that the price for a small divergence is reduced intensity, potentially causing problems when maintaining an acceptable signal-to-background ratio.

STUDY OF UPGRADING OF THE SMALL ANGLE NEUTRON SCATTERING DEVICE AT THE RESEARCH REACTOR OF THE ITN-NUCLEAR AND TECHNOLOGICAL INSTITUTE

L. Cser

Research Institute for Solid State Physics and Optics, Budapest, Hungary

Abstract. The main goals of the partnership between Hungary and Portugal are (1) To evaluate the usefulness of installing a neutron-beam guide at the ITN SANS facility and to carry out a model calculation of a neutron guide suitable for the SANS machine of the Instituto Tecnologico e Nuclear (ITN) in Sacavém, Portugal; (2) To develop a low-cost small, two-dimensional position sensitive detector which can potentially be used as part of a larger array for an area detector.

1. INTRODUCTION

Despite the rather moderate power of the research reactor (1MW swimming pool open core) operating in Sacavém its utilization in the area of small angle scattering (SANS) investigations promises interesting results.

The Portuguese research reactor operated by ITN is a 1 MW swimming pool open core reactor. The maximum thermal flux in the core is 2 x 10^{13} n/cm^{2}s^1. A study prepared in collaboration with the French Centre Nucléaire de Grenoble of the CEA shows that the existing shielding is adequate up to 5 MW. These features are very promising from the aspect of upgrading the reactor.

One tangential beam tube of 4 inches diameter was selected for installation of a SANS facility. The design of the instrument was optimized in consideration of the specific constraints of space, the geometry of the reactor hall and the detector used (ORDELA Model 2250N Position Sensitive Detector (PSD) with an active area of 25x25 cm^2). At present a vacuum tube with a diameter of 100 mm serves for the transportation of the neutrons from the source to the sample. A velocity selector installed at the reactor wall is used for the monochromatization of the incident beam. The flight path between the velocity selector and the sample position is 7 meters. The detector is placed in a 3-meter long vacuum vessel. Such geometry gives rise to at least two restrictions. First, the incident beam contains basically thermal neutrons, i.e., the short-wavelength (~1 Å) ones are dominant. Second, the rather short flight path imposes limitations on both the resolution and the type of samples to be investigated.

The CRP was launched in November 2000. Two months later, a seminar entitled "Application of Neutrons in the Research of Condensed Matter**"**, dealing with the possible application of the SANS study in this area of scientific activity, was held at the Instituto Tecnologico e Nuclear (ITN) in Sacavém, Portugal. . On this occasion the aims and the procedure of this bilateral cooperation initiated by the IAEA CRP were discussed in detail.with the ITN scientists

2. CONSIDERATIONS OF UPGRADING BY THE INSTALLATION OF A NEUTRON GUIDE

a) Increasing the flight path

Contemplating the general layout of the building incorporating the SANS facility, a rather long-neck room can be found behind the SANS facility. Provided that the argumentation presented in this paper will be accepted by the adequate authorities, this area can be used for

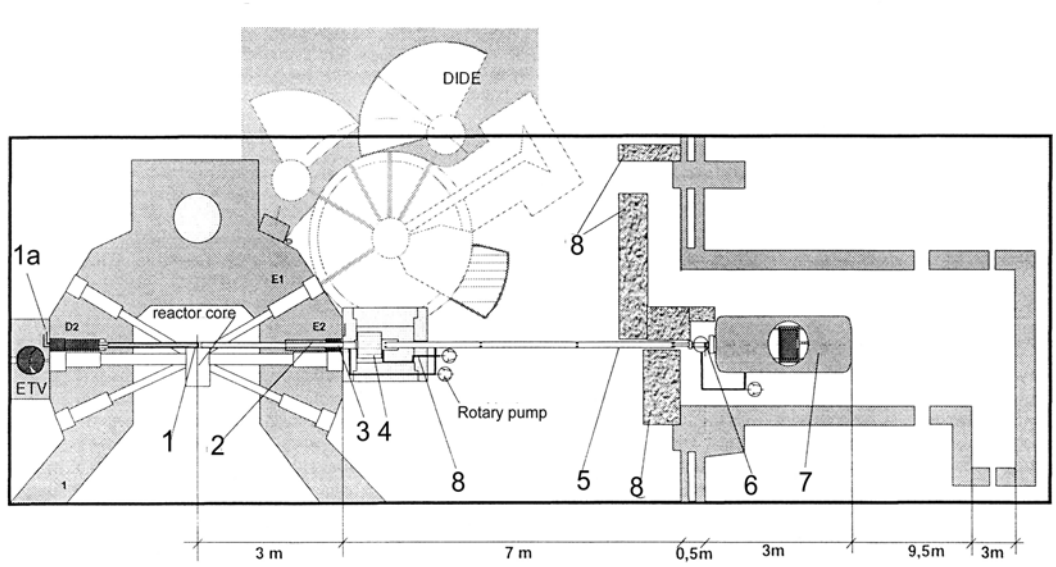

Fig. 1. General layout of the SANS instrument facility. 1- neutron scatterer; 1a- ends of the water circuit; 2- in-pile collimator assembly; 3- beam shutter; 4- mechanical velocity selector; 5- out-of-pile collimator; 6- sample chamber; 7- position sensitive detector; 8- shielding walls. DIDE is the nearby 2-axis diffractometer facility and ETV a time-of-flight diffractometer.

rebuilding the SANS facility in such a way that the distance between the velocity selector and the sample will be increased by 10 meters (Figure 1). Thus, the total flight path from the source to the sample would be equal to 23 meters (with a half-meter gap for the selector).

2.2 View of the ITN SANS installation plan

b) Installation of a neutron guide

Based on the experience obtained by a SANS group at the Budapest Neutron Centre, a neutron guide system coated with an Ni-Ti supermirror multilayer providing about 90 % reflectivity up to $2\theta_{critical}$ (Ni) should give rise to a significant increase in the incident neutron flux.

In order to start the discussion of the advantages of each of the above options we made sure on the reliability of our expectations. The schematic drawing (figure 1) shows that by lengthening the expected shape of the SANS facility should fit into the inner dimensions of the neutron hall. We agreed that the Hungarian side would carry out a series of Monte Carlo (MC) calculations to demonstrate the expected gain factors for various guide configurations.

The main geometrical constraint is the inner diameter of the 3-meter long in-pile tube. This diameter allows plugging in a guide of a 3 x 3 cm^2 inner cross-section, supposing that the thickness of the guide wall is not larger than 1 cm. At first sight this cross-section seems to be rather small. However, since the typical sample size is about one or two square centimetres, the above cross- section value would be reasonable.

During the MC calculations the following conditions had to be considered:

1. The total number of neutrons entering the guide was 10^6.

2. The velocity distribution of the neutrons was assumed to be Maxwellian with a characteristic temperature of 300 K.
3. The in-pile part had a fixed length at any time and its coating was accepted as equal to $2\theta_{critical}$ (Ni).
4. A gap of one meter was reserved for the velocity selector. The remaining part of the guide, i.e., between the velocity selector and the sample, could be varied.
5. The direct beam should not be let out at the end of the guide. In order to satisfy this condition the guide had to be either curved or deflected. In addition, to fulfill these requirements the horizontal dimension of the guide had to be decreased. Thus, the final accepted cross-section value was set at 2 x 3 cm^2.

The following situations were considered:

The full path of a neutron guide is curved. As requirement No. 5 the radius of the curvature was taken as R = 1350 meters. The gain factor is equal to about 10, i.e., the neutron flux at the end of the guide will be higher by an order magnitude compared to the case when the guide is not installed. The effective temperature of the spectrum of the neutrons is decreased below 100 K. This means that the neutron guide cuts out the short-wavelength neutrons but collects and transports the neutrons with larger wavelengths. The flux distribution of the neutrons at the end of the guide is quite flat in the vertical direction. The horizontal flux profile varies by a factor of two, while the effective temperature varies from 58 K to up to 129 K from the inner to the outer end.

a.) A much more homogeneous beam can be obtained if the last 2.5-meter section of the guide is straight. The gain factor is 15 and the effective temperature is 107 ± 8 K. (figure 2). For this situation the beam profiles in both, vertical and horizontal, directions were calculated at the end of the guide and at a distance of one meter from the end. The homogeneity in both directions was satisfactory.

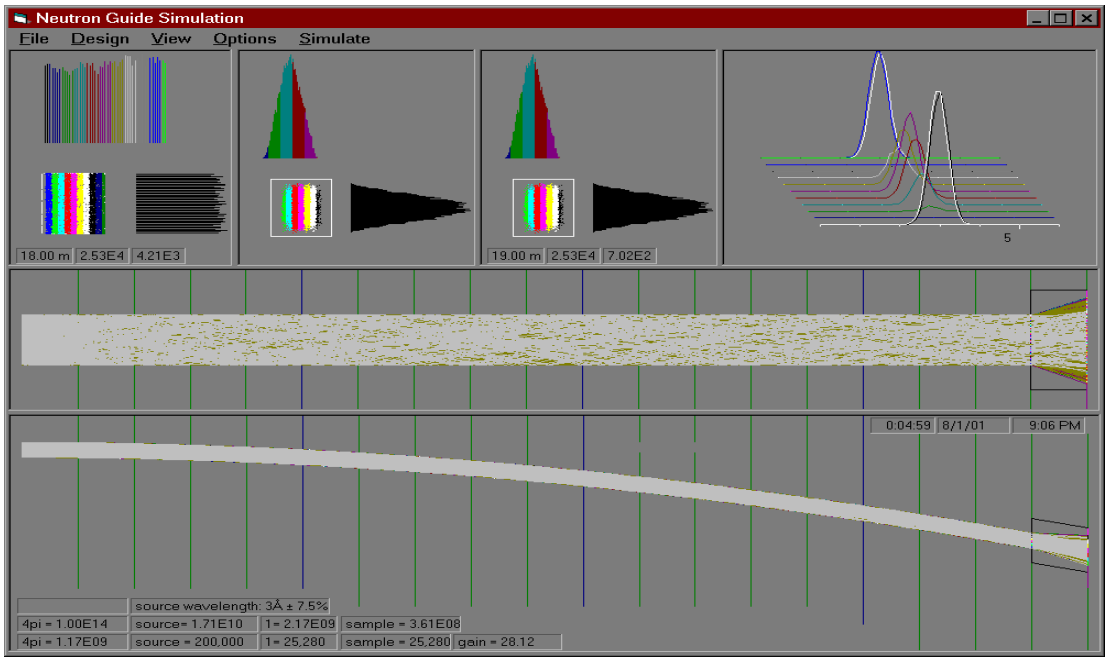

Fig. 2. The flux distribution at a distance of one meter from the end of the neutron guide

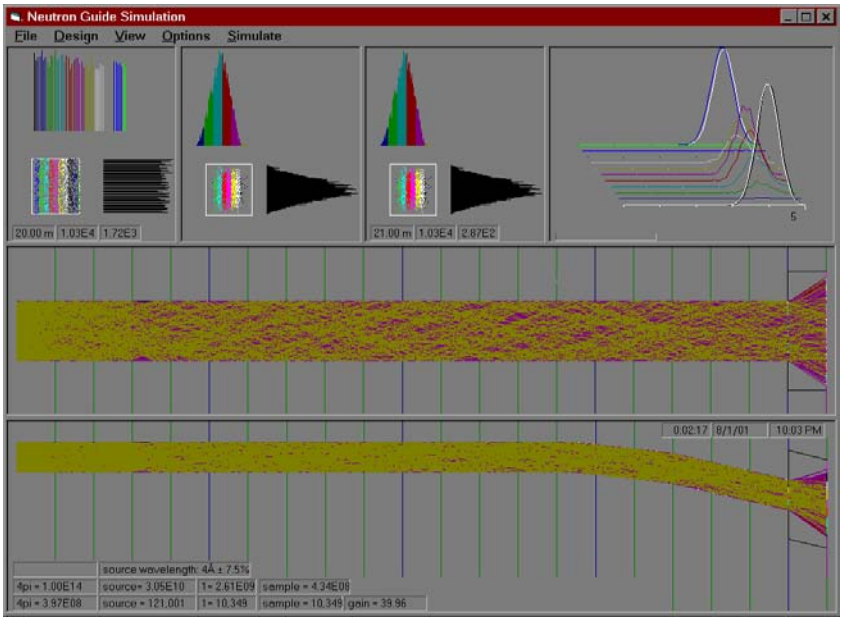

Fig. 3. The flux distribution at the sample position

b) A straight guide is divided into two halves and a 2.5-meter long straight section (deflector) coated with a $4\theta_{critical}$ (Ni) supermirror multilayer is placed in between. The gain is 13.9, i.e., not significantly lower than the gain in the previous version. The effective temperature and the homogeneity of the beam are almost equivalent to the version described in paragraph (a).

For the last two situations a more detailed study was done to clear up the divergence of the neutron beam at the end of the guide and at one meter distance free flight. This task is too complicated for an MC to deal with by the Maxwellian spectral distribution. For simplicity, two typical wavelengths: λ = 3 Å and λ = 4 Å, were chosen, and the divergence was calculated for these wavelengths.

The results obtained show that in both cases the flux is rather homogeneous at the end of the guides, while at a one-meter distance the flux distribution is triangular (see the upper insets in the figures). The divergence for λ = 3 Å is about ± 0.5 degree. This value for λ = 4 Å is only 10% higher. It is remarkable that the centre of gravity of the vertical profile is hardly shifted from the centre of the guide.

Taking the above divergences for the main source of the resolution (Δq) in the reciprocal space for wavelength 4 Å, the expected value of Δq is 0.0125 $Å^{-1}$. This value is quite acceptable and allows observation of the radius of gyration of about 100 Å with a rather small correction over the Guinier-range of the scattered intensity distribution.

3. CONSTRUCTION OF THE GUIDE SYSTEM

Thanks to the small cross-section of the guide it could be built up as a so-called free-standing performance, i.e., it did not need to be surrounded by a vacuum housing. The evacuation of the inner volume of the guide can be done by a relatively small vacuum pump operating without oil. The in-pile part of the guide will be inserted in a tube-shaped support. The alignment of this part will be done outside of the reactor and plugged into the corresponding channel afterwards. The remaining part of the guide will be mounted on a system of supports with a baseboard solidly fixed to the floor, supporting a strong rail made of steel. The guide

elements will be mounted on these rail frames. Each frame, made of aluminium, contains six screws to fix the guide elements in the prescribed positions. The positions are controlled by an auto-collimator providing an angular accuracy of less than 10 angular seconds.

3.1. Test of the proposed construction

The above calculations were tested by way of a study of quality of neutron guides at the Budapest Research Reactor [1]. The third neutron guide of this installation has similar parameters to those for which the model calculations were performed. The length of the guide is 16 meters, the curvature equal to 1350 meters, and the inner wall of the guide is coated by a $2\theta_{critical}$ (Ni) supermirror multilayer. The only difference is that the cross-section of the tested guide is 25 mm x 100 mm. Nevertheless, the results obtained are similar to those of a shorter and narrower guide. It was shown that the gain factor was 14 and thus in accordance with the MC modelling.

4. CONCLUSIONS

From the above considerations it follows that

- The installation of a neutron guide for the SANS facility at the 1MW research reactor operating in Sacavém gives rise to a gain of the total neutron flux of more than one order. In the wavelength range over 3 Å the gain is even more significant.
- The neutron spectrum gets considerably “softer”, i.e., the long-wavelength part of the neutron spectrum is more intensive (figure 4.)

Due to the increased distance between the source and the detector the background gets suppressed more than one order, i.e., the signal-to-noise ratio increases by more than two orders.

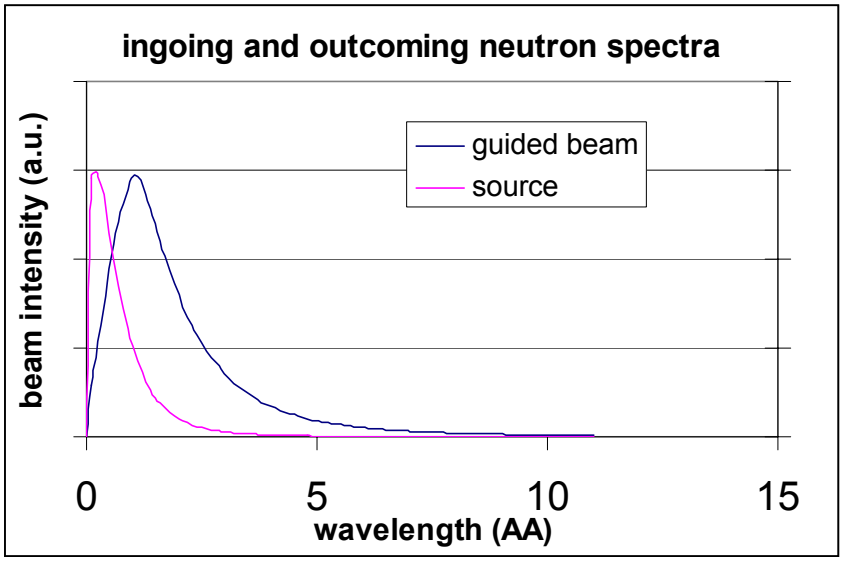

Fig. 4. The spectral distribution change due to the use of the neutron guide

Finally, from a technical point of view, the installation is feasible and the estimated price will to a large extent be remunerative.

Thus, the present considerations are a firm base for serious discussions to prepare a real design of a neutron guide system at the research reactor in Sacavém.

5. DEVELOPMENT OF 2-D POSITION SENSITIVE DETECTOR (PSD)

It was established that the existing ORDELLA type detector was too expensive. The development of a similarly sized but much cheaper detector would be desirable. A small-size detector would also be a first step towards the building-up of a large-size detector for SANS applications.

6. RESULTS

6.1. Development of a small (200 mm x 200 mm) PDS

A PSD neutron detector of the following specifications was designed and manufactured:

Construction: Sealed gas chamber with delay line encoding.

Overall dimensions	D~ 600 mm
Active area	200 x 200 mm^2
Detector window	Al (d=6mm)
Position encoding technique	delay line
Number of pixels	1024 x 1024
Spatial (position) resolution (FWHM)	1.7 mm x 1.7 mm
Filling gas	3 bar ^3He + 2 bar CF_4
Detection depth	20 mm ?
Anode and cathode wires	Gold-Tungsten
Wire spacing	1 mm
Detection efficiency (wavelength dependent)	50 - 85 %
Counting rate (global)	5 x 10^5 cps
Counting rate (local)	5 x 10^4 cps/mm^2
Integral non-linearity	4 x 10^{-2}
Differential non-linearity	± 10%
Dynamic range	single neutron detection
Timing resolution	2 microseconds

6.2. Electronic control and data acquisition system

Time to digital converter	Model: OTDCv1.11
Channel width	266.7 ps
Linearity	Automatic resolution adjustment
Differential non-linearity (for 256 x 256 pixel size)	5 %
Dead time (by using all channels)	1400 ns
Built in time delay (n=0….63, programmable)	8 ns + n x 5 ns
Minimum delay between the common and any of the other inputs	4 ns
Dimensions (for standard PC PCI slot)	90 x 160 x 20 mm^3
8-channel rate-meter (optional)	OTDC-RM8
X, Y, projection (optional)	OTDC-XY
6 channel constant fraction discriminator (CFD)	NEL 5.03.02
2-fold HV power supply	OHV-01
NIM crate with power supply	
Personal computer configuration	
Processor with required active memory	PENTIUM III.
Passive memory	HDD, Floppy (3.5"), CD
Screen	17” Colour monitor
Control	Mouse, Key-board
Connection	Internet card
Software	Windows’98
Connection cables, high voltage cable (mounted, tested)	Coaxial

The electronic control has a time-of-flight (TOF) option.

The view of the detector together with the control electronics is shown in fig. 5.

Fig. 5. The view of the 200 mm x 200 mm PSD (upper left corner) in ensemble with the high-voltage power supply, TDF (built in a NIM crate). The TDC is embedded in the PC shown on the right side.

7. TEST OF THE DETECTOR

In order to test the detector it was used in combination with another methodical development; a device devoted to hexapole magnetic focusing of a neutron beam was tested simultaneously.

7.1. Introduction

Six-pole magnetic fields yield a flux density gradient proportional to the radius and act as lenses upon neutrons flying along the field. Neutrons with spins oriented parallel to the field are defocused, while those having opposite orientation are focused. Such fields can be realized by using permanent magnet pieces with magnetization periodically rotated in space. When the magnetic material fills the available space and the magnetization turns smoothly from point to point (Halbach structure), the strongest field is obtained. A design approximating the Halbach structure using brick-shaped NdFeB permanent magnets has been realized, achieving two thirds of the ideal field strength, actually 47000 T/m^2 for a 7 mm diameter air gap.

7.1.1. Focal Length

The flux density of a six-pole magnetic field and the force acting upon neutrons with spins having an orientation anti-parallel to the field are:

$$|\boldsymbol{B}| = Cr^2 \ , \ \boldsymbol{F} = -s\nabla|\boldsymbol{B}| = -2sC\boldsymbol{r} \ , \qquad (1)$$

where C is the magnet constant and s the neutron spin. The focal length of a hexapole neutron lens, defined as the distance from the magnet entrance to the plane where a parallel beam is focused is

$$f = l + \frac{v_n}{\omega \tan \frac{\omega l}{v_n}} \ , \ \omega = \sqrt{\frac{2sC}{m}} \ , \qquad (2)$$

with m and v_n being the mass and velocity of the neutrons, l the magnet length. The focal length defined as the distance from the magnet median plane to the plane where a divergent beam is focused can be written as

$$F = \frac{l}{2} + \frac{v_n}{\omega \tan \frac{\omega l}{2v_n}} \ . \qquad (3)$$

7.1.2. Neutron Lens Design

The configuration of the constructed permanent magnet hexapole lens and the picture of a 75 mm long segment are shown in figure 6.

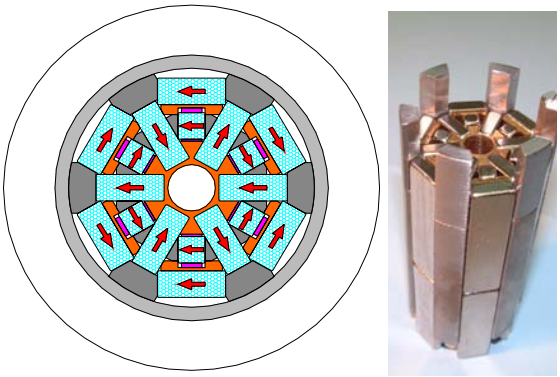

Fig. 6. Neutron lens geometry

Brick-shaped NdFeB permanent magnets were used with a remnant magnetization of 0.93 T, assembled into l = 0.45 m long hexapole lenses. The magnetic flux density (in mT) at a radius of 3.3 mm with respect to the azimuth angle (in 10°) was measured with a tiny Hall probe and averaged over the 6 lens segments.

The results yield a hexapole field constant of 47000 T/m^2, leading to $\omega = 737$ s^{-1} in eq. (2) and

$$f = 0.45 + \frac{5.68}{\lambda[\text{Å}] \tan 0.079\lambda[\text{Å}]} \quad [\text{m}] \ , \qquad (4)$$

respectively

$$F = 0.225 + \frac{5.68}{\lambda[\text{Å}]\tan 0.0396\lambda[\text{Å}]}\ [\text{m}]. \qquad (5)$$

7.1.3. Neutron Beam Experiments

Two experiments were performed using a white beam filtered by Be at room temperature. In the measurement set-up shown in figure 7 first only the upstream lens was placed into the beam, then both lenses. A 2-D position sensitive proportional detector was used in a time-of-flight mode. The focal plane for one lens placed at 2.875 m from the object aperture lies at 2.807 m behind the lens at 5.13 Å, yielding $\omega = 737\ s^{-1}$, while for both lenses the focal plane lies in the same position (where the detector is) at 6.55 Å. The results are consistent with the magnetic measurements, proving that the lenses have indeed $C = 47000\ T/m^2$.

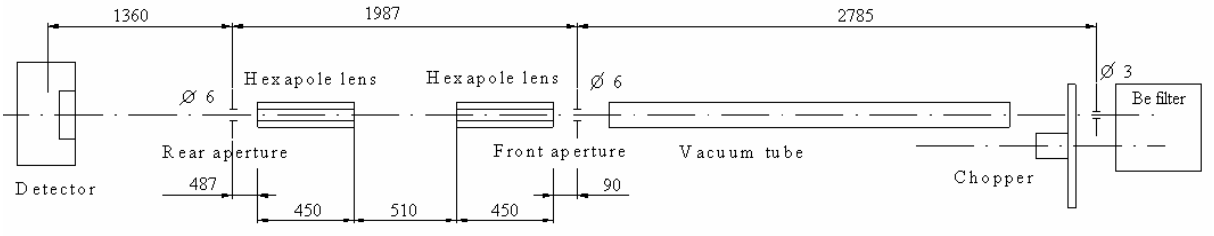

Fig. 7. Experimental setup for hexapole lenses.

The wavelength slices for the detected spot with two lenses are shown in figure 8. The corresponding images can be seen in figures 9 to 13.

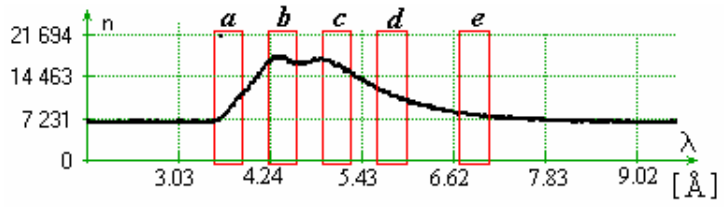

Fig. 8. Wavelength slices for plotted images (2 lenses)

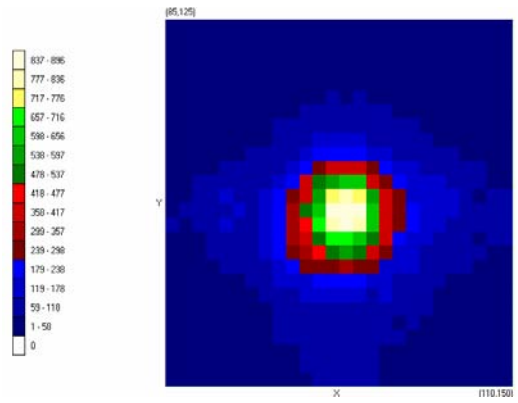

*Fig. 9. Wavelength slice **a** with two lenses.*

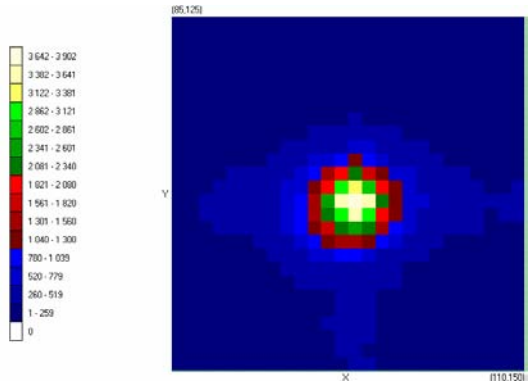

*Fig. 10. Wavelength slice **b** with two lenses.*

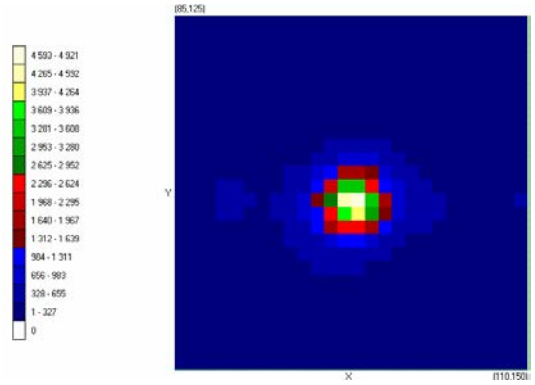

*Fig. 11. Wavelength slice **c** with two lenses.*

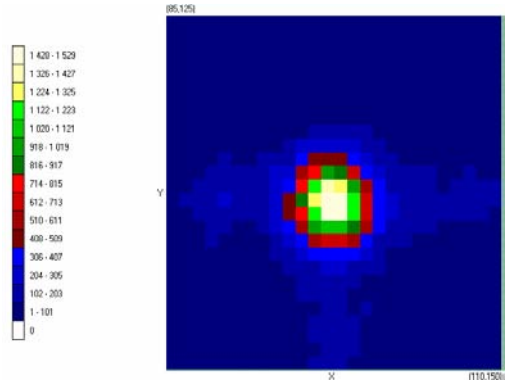

*Fig. 12. Wavelength slice **d** with two lenses.*

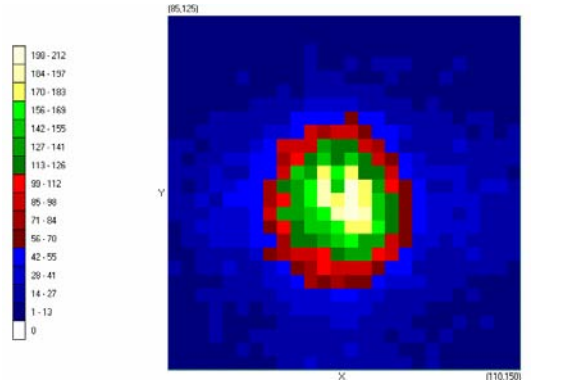

*Fig. 13. Wavelength slice **e** with two lenses.*

The wavelength slices for the detected spot with one lens are shown in figure 14. The corresponding images can be seen in figures 15 to 19.

The summed counts over the plotted area (figure 20) illustrate the signal-to-background ratio in the region of interest (much improved compared to the whole detector area ratios in figures 8 and 14).

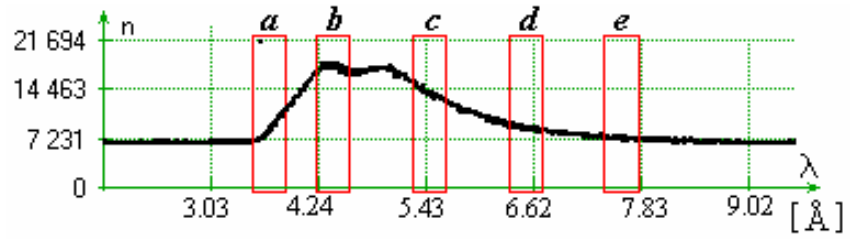

Fig. 14. Wavelength slices for plotted images (1 lens)

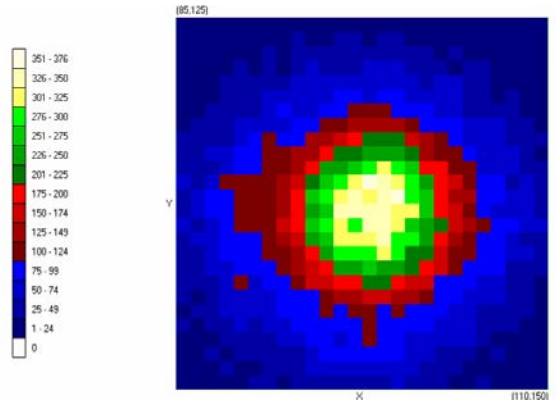

*Fig. 15. Wavelength slice **a** with one lens*

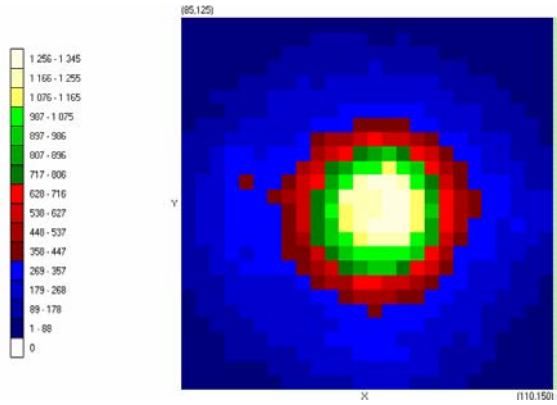

*Fig. 16. Wavelength slice **b** with one lens.*

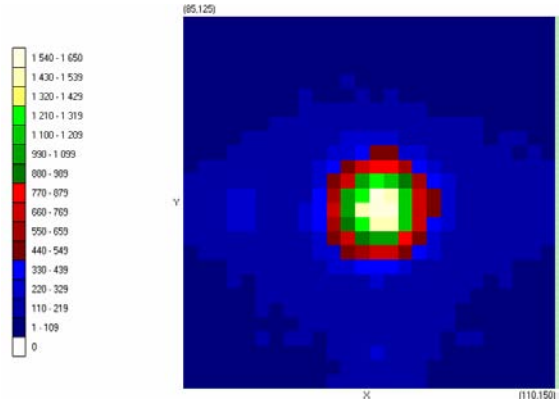

*Fig. 17. Wavelength slice **c** with one lens*

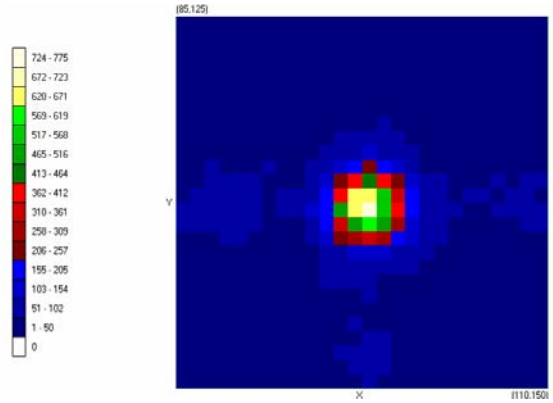

*Fig. 18. Wavelength slice **d** with one lens.*

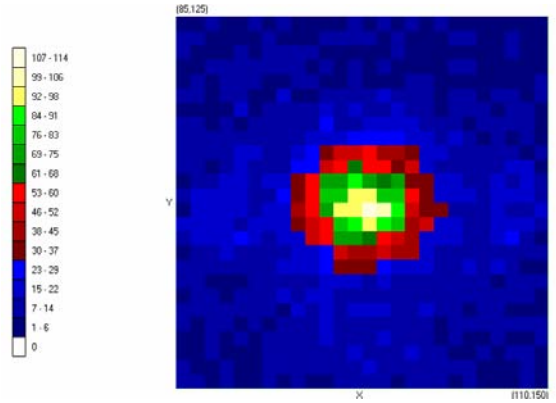

*Fig. 19. Wavelength slice **e** with one lens.*

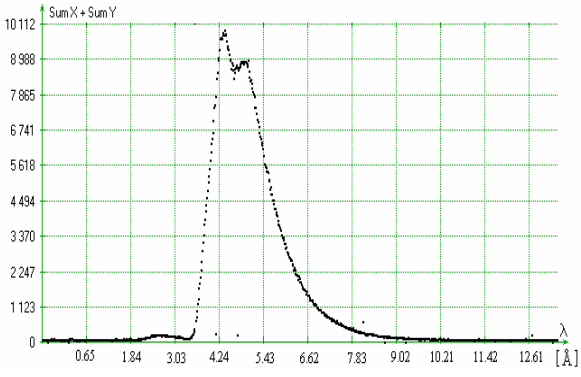

Fig. 20. Summed counts over the plotted area

The measurements were performed using the OTDC-TOF Four Channel Time-to-Digital Converter for 2-D Time-of-Flight Measurements, constructed by Open-Opto electronics Ltd.

http://www.openopto.kfkipark.hu

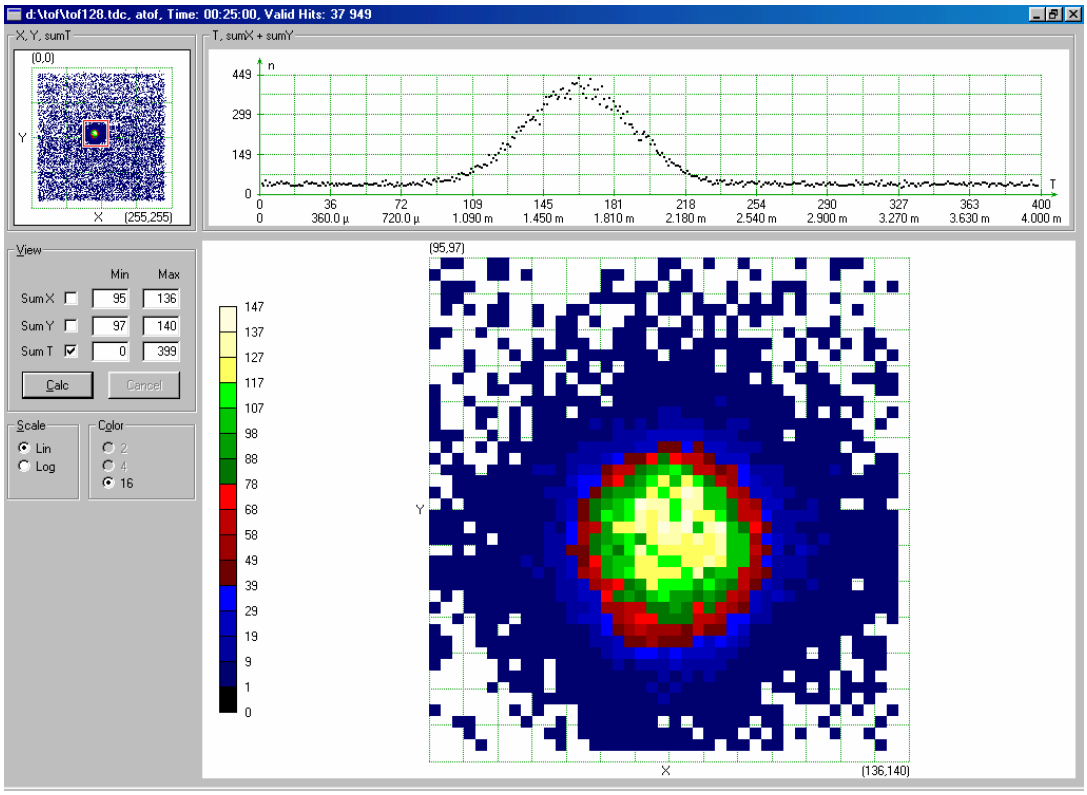

Fig. 21a. The focusing effect of the hexapole magnet, spot size without any focusing.

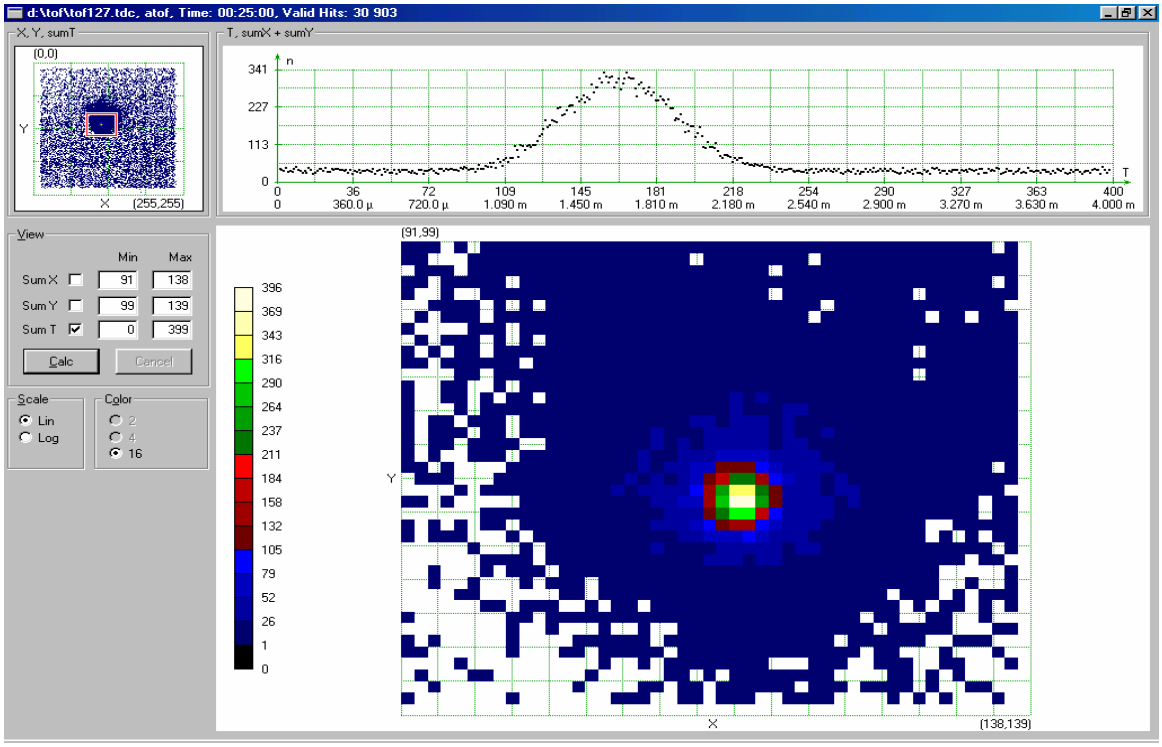

Fig. 21b. The focusing effect of the hexapole magnet, spot size with the focused beam.

8. CONCLUSIONS

8.1. Installation of a neutron guide

From the above considerations it follows that the installation of a neutron guide at the SANS facility at the 1MW research reactor operating in Sacavém would give rise to a gain in the total neutron flux of more than one order. In the wavelength range over 3 Å the gain would be even more significant. The signal-to-noise ratio can be significantly improved.

Finally, from a technical point of view, the installation is feasible and the estimated price would to a large extent be remunerative.

Thus, the present considerations are a firm base for serious discussions on preparing a real design of a neutron guide system at the research reactor in Sacavém.

8.2. 2-D PSD

It is shown that a small 2-D PSD with a delay line read-out can be manufactured for a reasonable price. The physical parameters of such a detector, i.e.; its efficiency and spatial resolution, are comparable (or even superior) to those of the commercially provided ORDELLA detector.

The efficiency of the 2-D PSD is especially pronounced in figure 21.

On the basis of the above achievements a large-size (600 mm x 600 mm) area detector is now under construction. This detector will satisfy the requirements of any SANS machine.

9. FINAL CONCLUSIONS

i. In the course of working on the topics of the present CRP it was shown that the efficiency of the SANS device at the ITN (Sacavém) could be improved by a relatively small financial investment.

ii. The experiment testing the small-size 2-D PSD serves as a good example that one of the important utilizations of low-power reactors is that of testing new ideas and devices before attempting to make use of them in large-scale facilities. In other words, the utilization of a SANS device should not be confined to the study of the properties of condensed matter. Methodological studies are just as important – or even more so – as studies on properties of a rather restricted variety of samples.

USE OF SANS FOR THE MICROSTRUCTURAL CHARACTERIZATION OF ADVANCED MATERIALS DURING PROCESSING AND APPLICATION; INSTALLATION OF HIGH RESOLUTION SANS AT TROMBAY

S. Mazumder, D. Sen, A.K. Patra

Solid State Physics Division, Bhabha Atomic Research Centre, Mumbai, India

Abstract. Double crystal based small angle scattering instruments are nowadays used extensively worldwide to access the large inhomogeneities commonly encountered in materials like cements, ceramics, magnetic materials with a mesoscopic magnetic domain etc. One of these instruments, with a single-bounce flat crystal both as monochromator and analyzer, has recently been installed at Trombay. The present instrument can access a q range ~ 0.003 - 0.173 nm^{-1}. This instrument has successfully characterized various technologically relevant materials like ceramics, alloys, rocks, etc. However, to increase the resolution and also to enhance the signal-to-background ratio, a triple-bounce channel-cut crystal-based ultra-small angle neutron scattering (USANS) instrument is under development. The project has been proposed in the form of an IAEA CRP in collaboration with Atom Institute, Vienna. The proposed facility will consist of a nondispersive (3,-3) setting of a pair of channel-cut perfect Si(111) crystals with a sample platform between them. Neutrons scattered from the sample are analyzed by angular displacement of the analyzer crystal in ultra-fine steps (of angular step size < 0.0001^o). the stability of the angular settings is maintained by mounting the DCD on a vibration-free platform. In this report we mention the progress made in the design and/or fabrication of (i) an ultra-precision rotation stage, (ii) a vibration isolation table and (iii) the relevant instrument electronics.

1. INTRODUCTION

Small angle neutron scattering (SANS) is an important non-destructive technique and its importance is increasingly realized with its potential applicability in different materials science problems. Conventional slit collimation instruments equipped with two-dimensional position-sensitive detectors are widely used for investigating problems in materials science and biology. The typical maximum accessible length scale for a slit collimation instrument is $\sim 10^2$ nm. However, large inhomogeneities as commonly encountered in cements, ceramics, macromolecules and magnetic domains are beyond the resolution limit of the conventional slit collimation instrument, where collimation is performed in real space by slits.

For investigations involving higher length scale, slit collimation instruments, with a few exceptions, such as D11 (ILL, Grenoble), become inefficient and impracticable owing to the necessity of employing long flight paths and small beam cross sections.

To access larger length scales, non-dispersive (1, -1) double-crystal (DC) based instruments are applied. These instruments use two parallel single crystals of high perfection. The extremely sharp Bragg condition of these crystals defines the q-resolution. The sample is placed between the two crystals and the scattering profiles of the specimens are recorded by rotating one crystal against another. This type of instrument is known as Bonse-Hart camera [1] in X-ray diffraction. In a double-crystal-based instrument, unlike a slit collimation instrument, the collimation is performed in the reciprocal space only by crystals, and the resolution in wave vector transfer q is independent of the beam cross-section. Because of the non-dispersive setting of both crystals the width of the rocking curve is independent of the divergence of the incoming beam. The high q-resolution exists in one dimension only and the recorded data are to be subjected to resolution corrections. The instruments can be compact and do not require long flight paths and two-dimensional position-sensitive detectors, as data are recorded through step-by-step rotation of the analyzer crystal. Doublecrystal-based SANS instruments are relatively much cheaper vis-a-vis slit collimation instruments.

However, in the case of a double crystal-based instrument with a simple flat single-bounce crystal, the rocking curve is rather broad and hence the q resolution is limited. Further, the

sensitivity of the instrument is poor at high q vis-à-vis a slit collimation instrument due to a background caused by diffuse scattering from the crystal surfaces. But with using the triple-bounce channel-cut crystals both as monochromator and analyzer, the rocking curve becomes much sharper, the resultant q-resolution is drastically improved, and the signal-to-noise ratio is also much better.

In this forum we will discuss the double crystal-based SANS activity at Trombay, India. The existing facility and some typical experimental investigations using this facility will be discussed first. The proposed facility and the progress towards its realization will be presented thereafter.

2. EXISTING SINGLE-BOUNCE FLAT CRYSTAL-BASED SANS FACILITY AT TROMBAY

The existing facility [2] is a double crystal-based moderate-resolution small angle neutron scattering (MSANS) facility. It consists of a non-dipersive (1-1) setting of a 111- reflection of a single-bounce flat silicon single crystal, with the sample placed between two crystals. The neutron wavelength used is 0.312 nm. The analyzer crystal rotates with a smallest step size of 0.0012^{o}. At 65 MW reactor power, the peak count rate of a blank rocking curve is about 55 counts per second at the detector position, and the signal-to-noise ratio is 450 for a typical experiment with sintered alumina. The accessible range of wave vector transfer q is 0.003-0.173 nm^{-1}. The instrument is calibrated with respect to the new high-resolution ultra-small angle neutron scattering instrument S 18 [3] at ILL. The important instrument parameters are listed in table 1. The schematic overview of the existing facility is depicted in Figure 1.

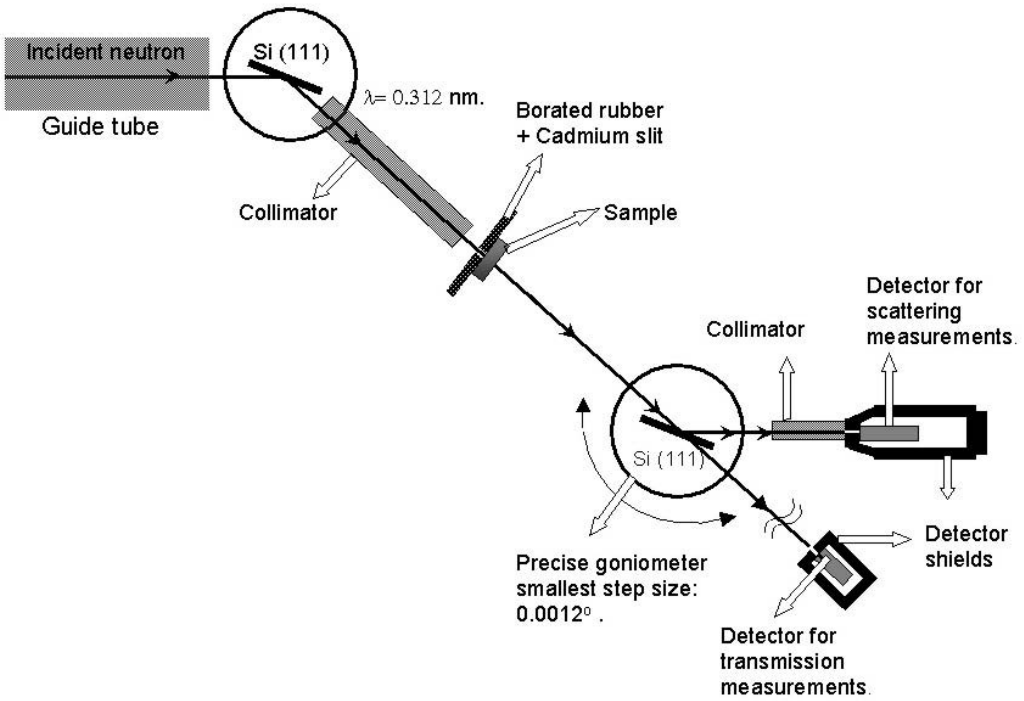

Fig. 1. Schematic overview of the present MSANS facility at Trombay [2].

Table 1. Instrument parameters of MSANS

Monochromator crystal	Si (111)
Analyzer crystal	Si (111)
Wave length (λ) used	0.312 nm.
$\Delta\lambda/\lambda$	1%.
Flux at sample position	~ 500 n /cm^2s^{-1}
Accessible q range	0.003-0.173 nm^-
Resolvable real space dimension	2000-40 nm.
Distance between monochromator and sample mount centre	128 cm.
Distance between sample and analyzer crystal	100 cm.
Distance between analyzer and detector	55 cm.
Smallest control step size of the analyzer crystal	0.0012^o
Detector	BF_3

3. MICRO-STRUCTURAL CHARACTERIZATION OF SOME ADVANCED MATERIALS BY USING THE EXISTING MSANS FACILITY

3.1. Pore morphology in sintered ZrO_2-8 mol % Y_2O_3 ceramics

Among the advanced ceramic materials, zirconia (ZrO_2) and zirconia-based ceramics have attracted a great deal of attention because of their tremendous technological applications. In particular, yttria-stabilized zirconia, a potential ceramic system for various structural and functional applications, exhibits many interesting characteristics. However, porosity, pore morphology and pore size distribution, etc., are also determining factors in the selection of these materials for a particular type of application.

Pore morphology and pore size distribution in yttria-stabilized zirconia (ZrO_2-8 mol % Y_2O_3) have been investigated [4] by using the existing MSANS facility. Figures 2 and 3 depict the SANS profiles for specimens sintered at 1200^oC (specimen 1) and 1270^oC (specimen 2) for different specimen thicknesses. Figure 4 represents the extracted single scattering profiles (SSP) for the above specimens, which exhibit nice shoulders. The appearance of such a shoulder [5] is indicative of the presence of two length scales in the system [4], as perceived by neutrons. In the present case, it is reasonable to assume that the larger length scale appears due to the agglomeration of the ceramic particles during compaction and heat treatments, while the lower length scale is due to the pores. The estimated pore size distributions are depicted in the inset of figure 4. The results indicate that the reduction in porosity at 1270^o C, as compared to that at 1200^o C, occurs through the elimination of the pores at the lower-end tail of the pore size distribution. In addition, the polydispersity is also narrowed down at 1270^o C and the nature of the distribution is altered significantly near the smaller radius side. The average pore size shifts towards the higher radius side. The specific surface area of the pores is also diminished at 1270^o C because of the elimination of the finer pores.

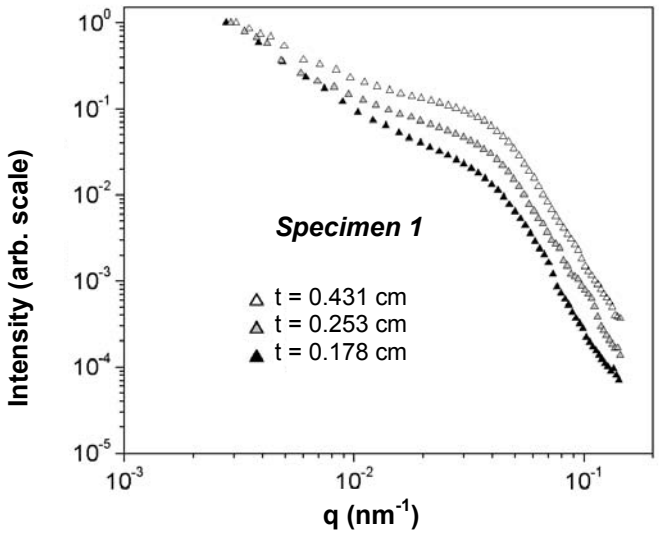

Fig. 2. SANS profiles of the ZrO_2-8 mol % Y_2O_3 ceramic sintered at 1200 ^{o} C (specimen 1) for different specimen thicknesses [4].

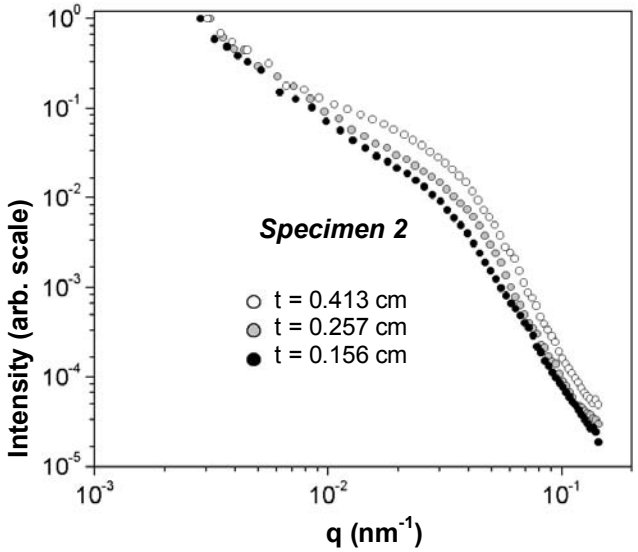

Fig. 3. SANS profiles of the ZrO_2-8 mol % Y_2O_3 sintered at 1270 ^{o} C for different specimen thicknesses [4].

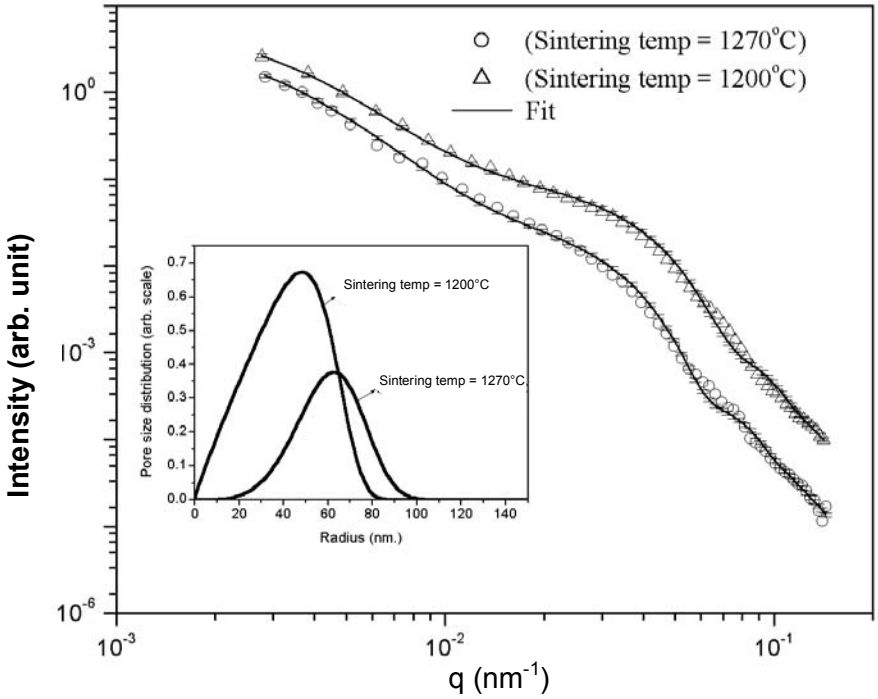

Fig. 4. Estimated single scattering profile for specimens 1 and 2. The inset shows the estimated pore size distribution.[4].

3.2. Pore growth during the initial and the intermediate stages of sintering in ZrO_2-3 mol % Y_2O_3 ceramics

MSANS has been employed to investigate [6] the evolution of pore morphology during the initial and the intermediate stage of sintering in ZrO_2-3 mol % Y_2O_3. The results indicate that, although there is a reduction in porosity due to the elimination of the pores, the average growth in pore size takes place during the sintering. This trend in the pore growth corroborates with the results of the computer simulation, based on Potts's model. The SANS data have been analyzed in the light of a polydisperse spherical pore model.

Powder prepared from zirconium yttrium hydroxide gel was wet-ground planetarily to form a sub-micron size [median diameter (D_{50}) of 0.7 μm] powder. Compacts were formed by uniaxial pressing at a pressure of 200 MPa and sintered at 1350^0 C for 15 min (specimen 1), 30 min (specimen 2) and 60 min (specimen 3) respectively in a superkanthal furnace. The density and open porosity of the pellets were determined by way of the Archimedes principle. Pellets with a density ~ 72 % (for specimen 1), 80 % (for specimen 2) and 93 % (for specimen 3) of the theoretical density (6.0 gm/cc.) value were formed. Figure 5 depicts the background transmission and resolution-corrected SANS profiles of specimens 1, 2 and 3 respectively for two different thicknesses of each specimen. Profiles are normalized at the minimum accessed q point. As the volume fraction of the pores is much less than 0.5, the small angle scattering can be attributed only to the pores. It is discernible from figure 5 that the SANS profiles are getting sharper, i.e., the radius of curvature of the profiles increases while moving from specimen 1 to specimen 3, and an identical trend is observed in the profiles of both thinner and thicker specimens. These observations clearly indicate, at this moment at least qualitatively, that the growth of pores takes place during sintering time. In order to

corroborate this observation, it is interesting to present the results of pore size evolution in ceramics during sintering, using computer simulation based on the Potts model [7] and the Monte Carlo method. The present simulation has been performed using the software SYNMIC [8]. A few snapshots of the simulated sintered structures at the initial stage are shown infigure 6. It was evident that, although the sintering process caused the reduction in the number of pores, it made the average pore size grow. The growth of pores, due to the coalescence of the finer pores, takes place as an indirect consequence of the reorientation and the mass transport of the grains during sintering, so they will attain morphological configurations with lower free energy. From the analysis of the SANS data it was found that the evolution of the mean radius of the distribution, as obtained from the SANS analysis, could be fitted with a temporal power law with exponent ~ 0.16. Investigations on other ceramic systems like ceria are also in progress to verify the trend of the pore growth [9,10].

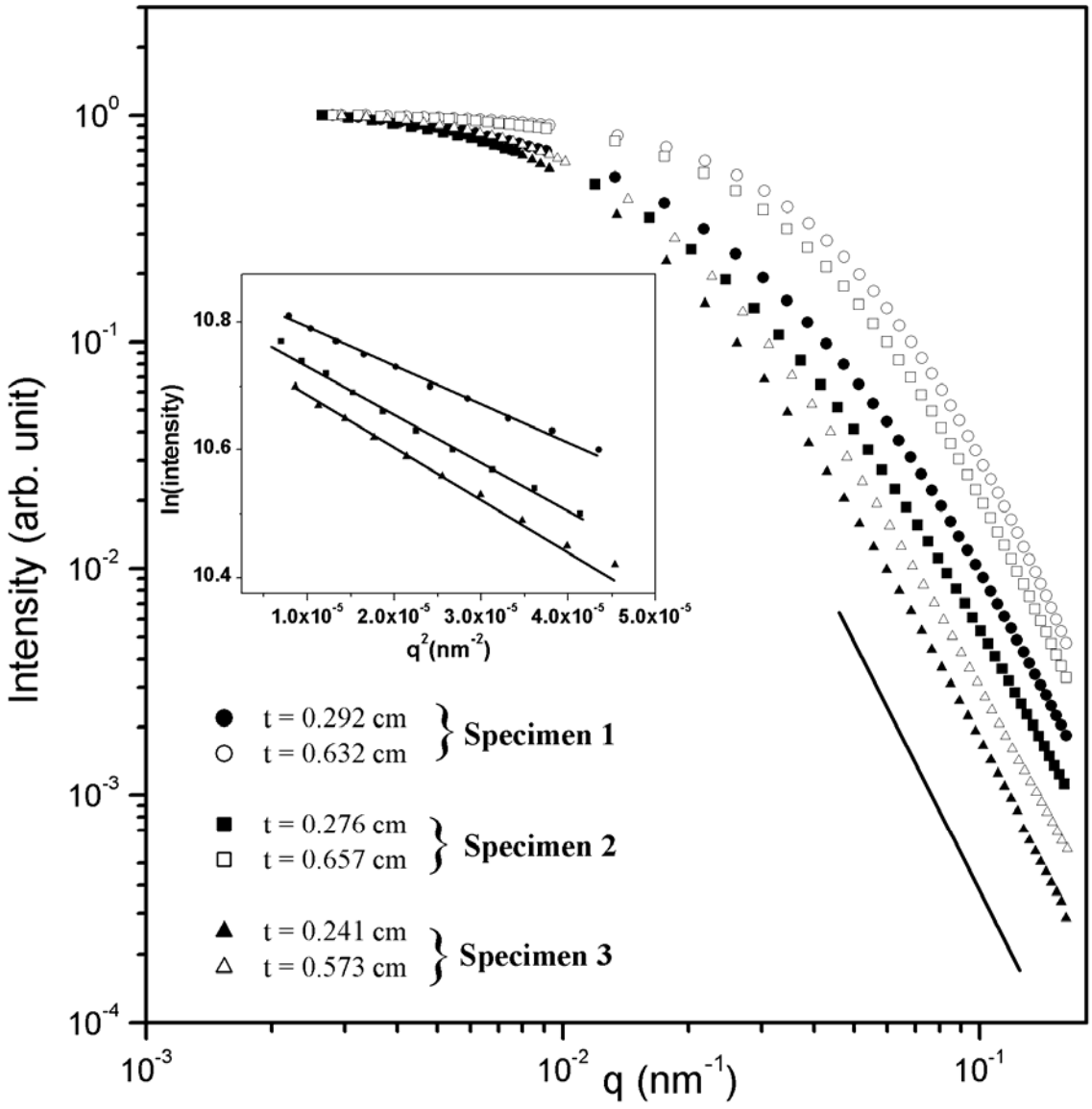

Fig. 5. Transmission, background and resolution-corrected SANS profiles for the ZrO_2-3 mol % Y_2O_3 specimens for three sintering times. The profiles are normalized at the minimum accessible q value. The solid line shows that linearity in the double logarithmic scale has been achieved for q>0.05 nm^{-1}. The inset shows the linearity of ln (Intensity) vs. the q^2 plot. This implies the completeness of the data at both extremes of the experimental q range [6].

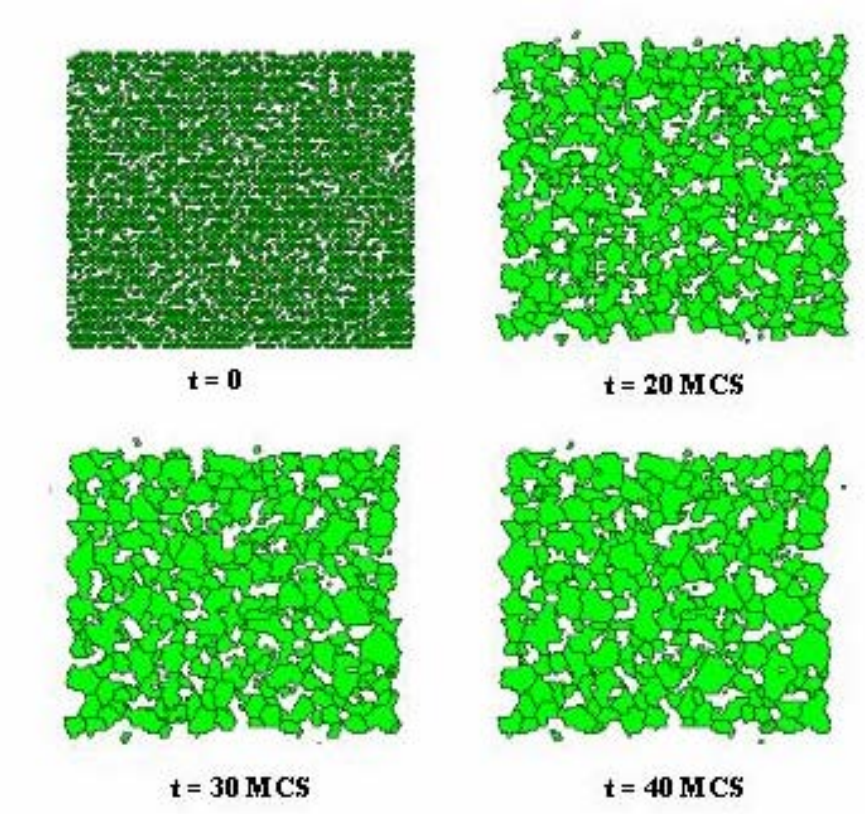

Fig. 6. The snapshots of the simulated microstructures of the ceramics for different Monte Carlo steps. White regions represent pore space. It is seen that the average size of the pores grows with the sintering time [6].

3.3. The effect of sintering temperature on the pore morphology in ZrO_2-8 mol % Y_2O_3 ceramics

A ZrO_2- 8 mol % Y_2O_3 powder compact prepared by way of a citric acid gel route has been sintered at different temperatures to achieve different porosity levels. Green pellets prepared by uniaxial pressing (200 Mpa) were sintered at 1200, 1250, 1300 and 1400^0 C for 3 hrs. The effect of sintering temperature on the pore morphology and pore size distribution in the same pellets has been investigated using MSANS. The results [11] indicate that the pores grow with the increase in the sintering temperature, although a reduction in the porosity occurs because of the elimination of the pores from the system. The quantitative analysis of the SANS data has been carried out in the light of a polydisperse globular pore model. The growth of the average size of the pores with increasing sintering temperature could be fitted to an Arrhenius-type growth. The necessity of considering a realistic model approximation in interpreting the data has also been dealt with. Figure 7 depicts the background, transmission and resolution-corrected SANS profiles for the specimens.

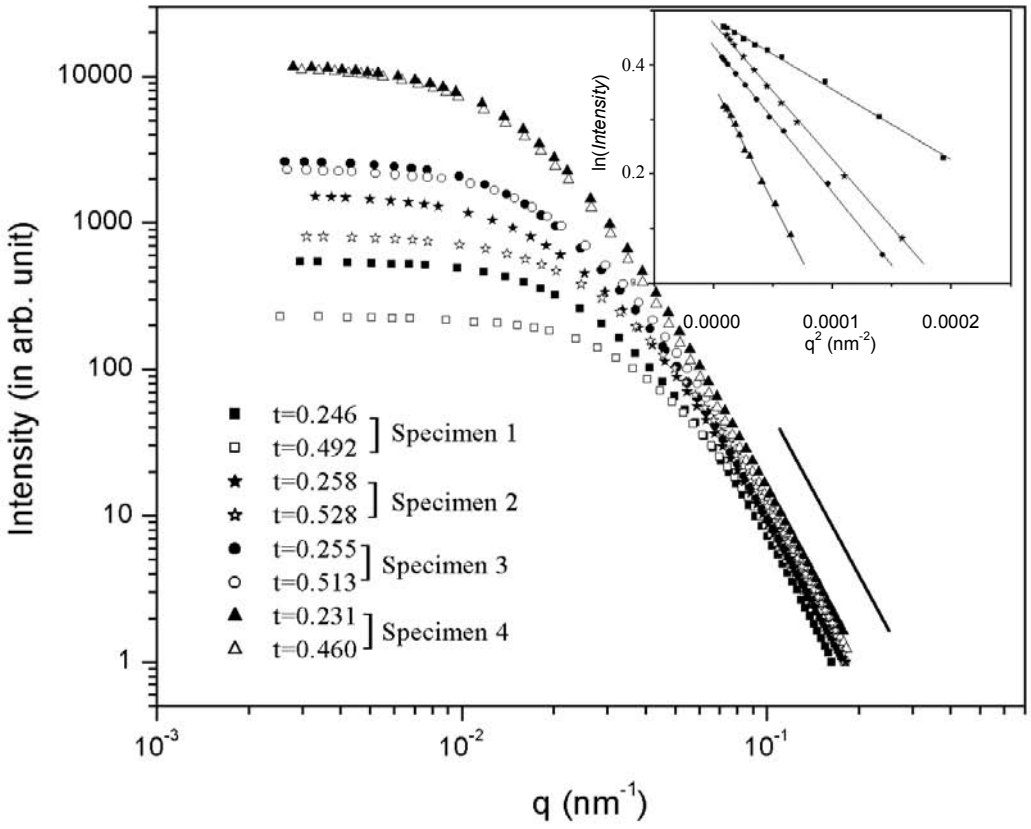

Fig. 7. SANS profiles (after transmission, background and resolution correction) of specimens ZrO_2-8 mol % Y_2O_3 for four sintering temperatures and two different thicknesses of each specimen [11].

3.3.1 Effect of pore morphology on low-frequency dielectric response in ZrO_2-8 mol % Y_2O_3 ceramics

MSANS has been employed to investigate [12] the pore morphology and pore size distribution in a sintered 8 mol % Y_2O_3-ZrO_2 ceramic in order to study the effect of pore morphology on the low-frequency dielectric response. Specimens with nearly identical porosity values (one set with a porosity of 28 % from finer and coarser grain and the other with a porosity of 39 % from finer and coarser grain) were synthesized from coarse and fine initial powder-particle size, with varying sintering times and temperatures. Figures 8 and 9 represent the corrected SANS profiles of the specimens. It is seen that the real and imaginary parts of the ac dielectric constant vary quite differently with the variation in porosity as well as with pore morphology and pore size. The frequency spectrum of the relative permitivity and the loss tangent have been measured in the range of ~ 0.01 –100 KHz. Unlike the simple Debye relaxation mechanism, where the loss tangent (vis-à-vis the imaginary part of the dielectric constant) shows a pronounced peak in frequency, in the present case the same increases are manifest in the lower frequency regime and a non-Debye type relaxation. The increase in the loss tangent in the vicinity of very low frequency can be attributed to the hopping and migration of oxygen ions, and it is significantly affected by the porosity, pore morphology and pore size

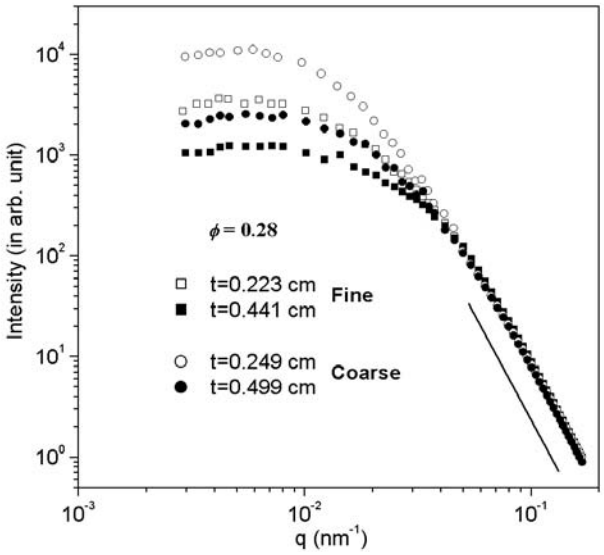

Fig. 8. SANS profiles of sintered ZrO_2-8 mol % Y_2O_3 ceramic compacts with a porosity of 28 %, prepared from fine and coarse particles. SANS profiles for specimens of two different thicknesses are also depicted.

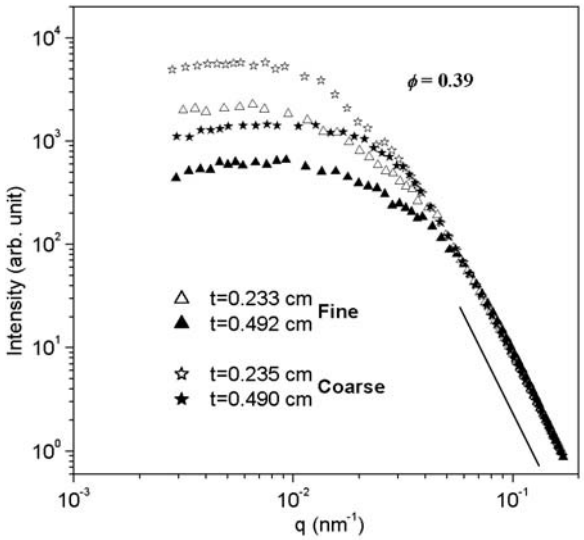

Fig. 9. SANS profiles of sintered ZrO_2-8 mol % Y_2O_3 ceramic compacts with a porosity of 39%, prepared from fine and coarse particles. SANS profiles for specimens of two different thicknesses are also depicted.

3.3.2 Pore surface roughening in rocks

The microstructure of rocks is a subject of practical importance and scientific interest from the petrologic point of view. Depending on the type of rock formation mechanisms, rocks can be mainly classified as (a) sedimentary, (b) igneous and (c) metamorphosed.

Pore-matrix interface roughening in some metamorphosed sedimentary rocks, sandstones and igneous rocks from different parts of India have been investigated [13,14] in the length scales of ~ 20-1000 nm using MSANS. The results revealed the fractal nature of the rock-pore interfaces. Figure 10 represents the profiles of the three specimens of metamorphosed rocks from Devoprayag, in the Himalayan region in India. A power law variation for a wide range

of q, a signature of fractal systems, is discernible from the figure. No signature of the upper cut-off in the accessible q range has been observed for these specimens.

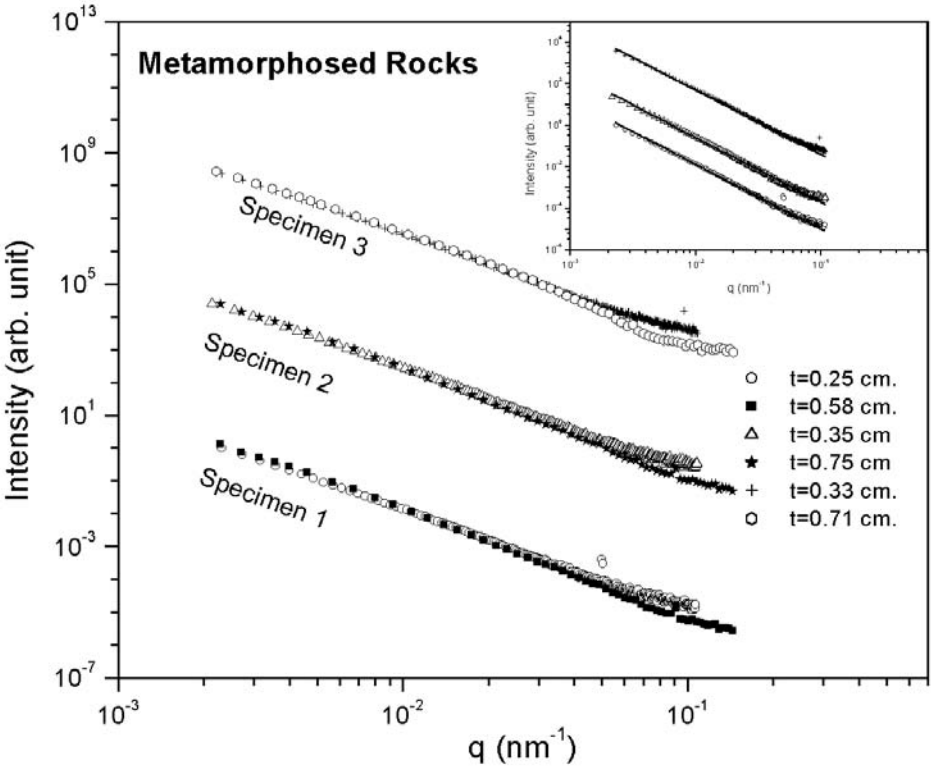

Fig. 10. SANS profiles of metamorphosed rocks. No upper cut-off has been observed in the accessible q range [13].

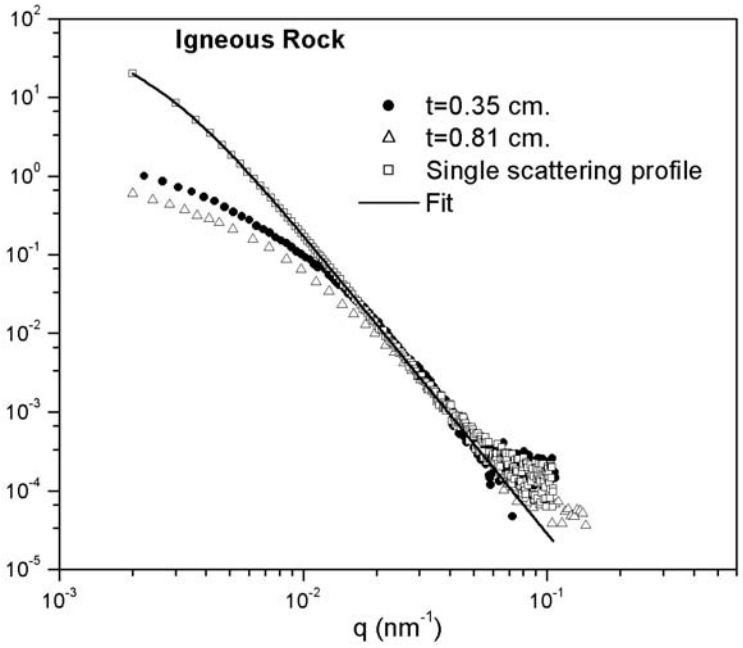

Fig. 11. SANS profiles of igneous rocks [13].

However, profiles of the igneous rock (from the Deccan basalt region) (figure 11) and the sedimentary sandstone rock specimens (from Barakar of the Singhbhum zone) [figure 12] indicate the presence of an upper cut-off of the surface fractal nature. The surface fractal dimension of the metamorphosed rocks and sandstones has been estimated to be ~2.8, while that for the igneous rocks has been found to be ~ 2.3. The relatively high surface fractal nature of the sandstones and metamorphosed rocks has been explained with the help of a computer simulation model based on the formation mechanisms (deposition and desolution mechanisms of the grains with a probability of P_+ and P_- respectively) of these rocks [6]. Figure 13 depicts the results of the simulation.

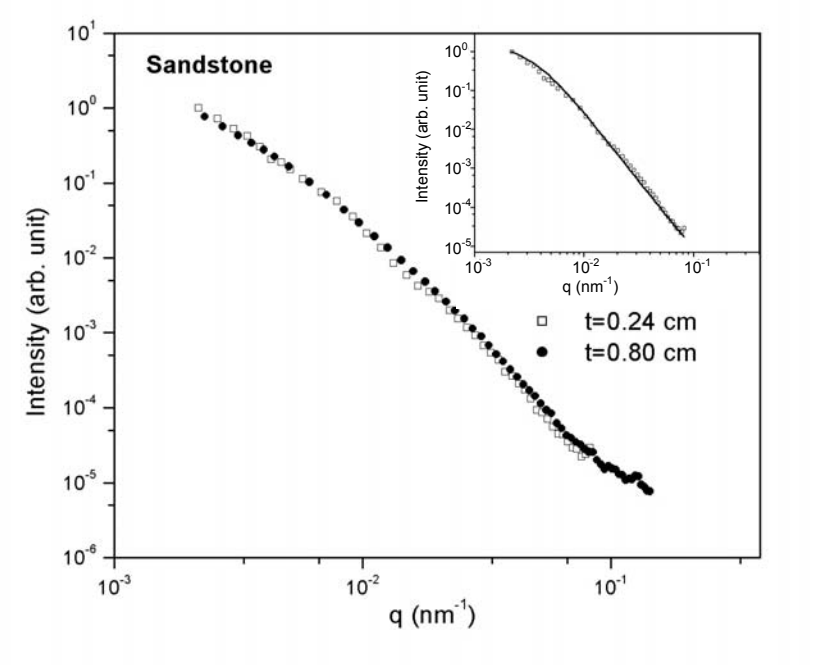

Fig. 12. SANS profiles of the sedimentary sandstone specimen [13].

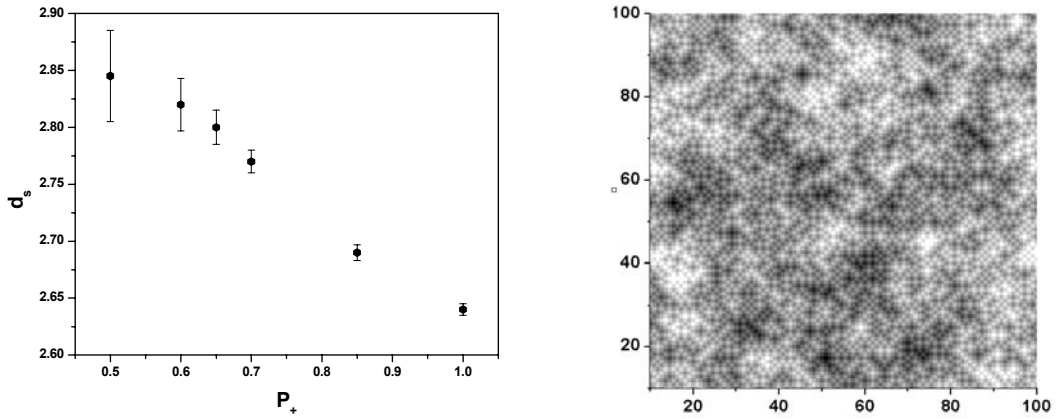

Fig. 13. Variation of the surface fractal dimension with a deposition probability (P_+) from the model and a typical computed surface with a fractal dimension of ~ 2.8 [13].

3.4. Carbide precipitates in solution-quenched PH13-8 Mo stainless steel

Precipitation in alloy systems is a subject of continued scientific and technological interest. PH 13-8 Mo steel is a precipitation-hardened steel which is capable of combining great

strength and hardness with good corrosion resistance properties. Hence, the steel is utilized in aircraft, nuclear reactors, petrochemical plants and many other industries. However, the presence of carbide formers such as Mo and Cr warrants the possible presence of carbides in the structure and in turn affects the mechanical properties.

SANS measurements on PH13-8Mo steel indicate [15-17] the strongly scattering nature of the system. The shape of the scattering profiles is dependent on the sample thickness. Figure 14 depicts the SANS profiles of these specimens. From the nature of variations in the functionality of the profiles with varying specimen thicknesses, as well as from transmission electron microscopy (TEM), it has been established that the small angle scattering signal predominantly originates from the metallic carbides in the specimen. The contribution due to Double Bragg Reflection is not significant in the present case. From two scattering profiles varying with sample thicknesses the true single scattering profile has been estimated. The single scattering profile has been analyzed with the help of a polydisperse cylindrical particle model with a fixed aspect ratio. The average length and diameter of the cylinders were estimated to be 248.7 and 72.6 nm respectively, and the aspect ratio was found to be 3.4. The standard deviations in length and radius distribution were found to be 44.1 and 6.3 nm, respectively.

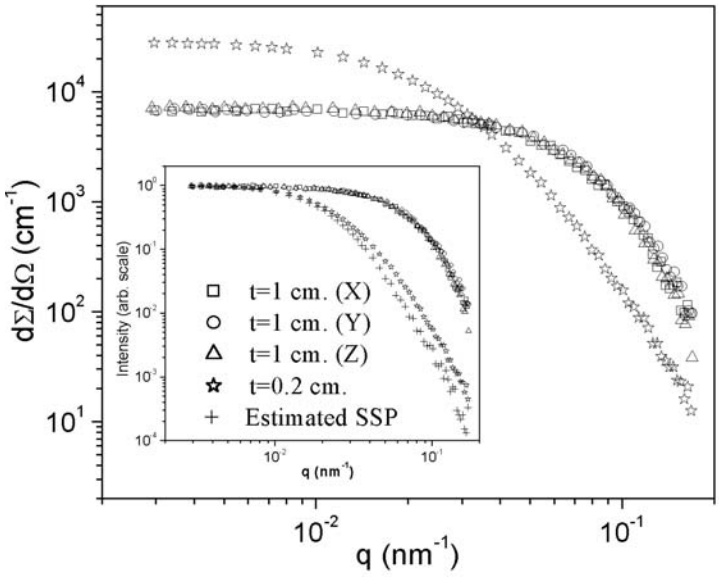

Fig. 14. Transmission, background and resolution-corrected SANS profiles for solution-quenched PH13-8 MO stainless steel. The SANS profile depends significantly on the specimen thickness. Profiles recorded with three perpendicular directions of a cubic specimen were found to be nearly similar [16].

3.5. Effect of titanium weight fraction on precipitate morphology in Fe-Ti alloy

Fe-Ti alloy has received wider attention in recent years primarily for two notable reasons: low cost and abundance of raw material. That is why this alloy is considered a prime candidate for the safe and economical storage of hydrogen. The hydriding property of FeTi is highly dependent on the exact titanium-to-iron ratio. This property is also influenced to a sizeable extent by the presence of certain impurity elements such as carbon, oxygen and nitrogen.

Fe-Ti alloy specimens (with 2, 4 &10 wt % of Ti) were prepared by mixing the constituent elements thoroughly in a non-consuming-type arc-melting furnace. To investigate the effect of weight fraction on the morphology of the precipitates, SANS experiments have been performed. It was observed [18] that with increasing weight fraction of titanium the average

size of the precipitates and the peak of precipitate size distribution shifted significantly towards the smaller radius side. This observation is in contrast to the normal precipitation behaviour of binary alloys. This trend in the formation of precipitates might be explained by the presence of impurity elements in the constituent elements. It is well known in metallurgy that the presence of certain elements in any metallic alloy system affects the grain growth kinetics. For example, in steel certain elements like Ti, V and Mo are deliberately added to prepare fine-grained steel. These impurity elements combine with non-metallic elements such as carbon, oxygen and nitrogen to form stable carbides, oxides and nitrides respectively. The impurity compounds sit on grain boundaries and thus inhibit grain growth, thereby reducing the coarsening of grains, which in turn reduces the size of precipitates.

4. INSTALLATION OF HIGH-RESOLUTION SANS AT TROMBAY

4.1. Proposed USANS facility

This project deals with the construction of an Ultra-Small angle Neutron Scattering (USANS) instrument at BARC. This is a Bonse-Hart-type double-crystal diffractometer (DCD), as the schematic diagram shown in Figure 15, in which a pair of triple-bounce channel-cut Si single crystals will be used as monochromator and analyzer. The (111) symmetric reflections will be used for both crystals. We have obtained these crystals from Prof. H. Rauch of Atom Institute, Vienna. In DCDs using single Bragg reflection at two perfect crystals in a nondispersive arrangement, the far-reaching tails of the single reflection rocking curves cause a rather high background within the accessible q-range. The use of channel-cut crystals does not modify the width of the reflection curve but greatly reduces its wings by successive Bragg reflections from the inner walls of the crystal. The q-resolution of the instrument depends on the neutron wavelength and is in the order of 10^{-5} Å^{-1}. This permits small angle scattering experiments to be carried out in the accessible q-range between 10^{-5} to 10^{-3} Å^{-1} to investigate relatively large-sized inhomogeneities and large-distance inter-particle correlations in materials. Thus, large inhomogeneities in materials, such as precipitates in alloys, pores in cements and ceramics, aggregates of macromolecules, magnetic domains, and many other objects, which are beyond the resolution limit of conventional pinhole SANS facilities can be investigated by way of this USANS instrument. A scattered neutron intensity profile at very low q values is recorded by an ultra-fine angular step ($< 0.0001^{o}$) scan through the analyzer crystal. During this period we were focusing most of our attention on the design and development of a high-resolution rotation stage for ultra-precision angular positioning of the analyzer crystal. The USANS experimental set-up will be mounted on a vibration-isolated platform to maintain angular stability of the settings within seconds of arc. A PC-based data acquisition and control system for our instrument is also in the process of procurement. The instrument is planned to be installed at one of the beam ports of the CIRUS reactor. This reactor was shut down in October 1997 for refurbishment work. It went critical on 30th October 2002. It was further shut down for ball tank repair and started again on 3rd October 2003. Right now it is operating at 12 MW power. According to plan the reactor will be operated at 40 MW power. At this power the neutron flux at the core of the reactor will be 0.6 x 10 ^{14} neutrons/cm^{2}.sec. In a short while we will be assigned a beam port for installing our instrument.

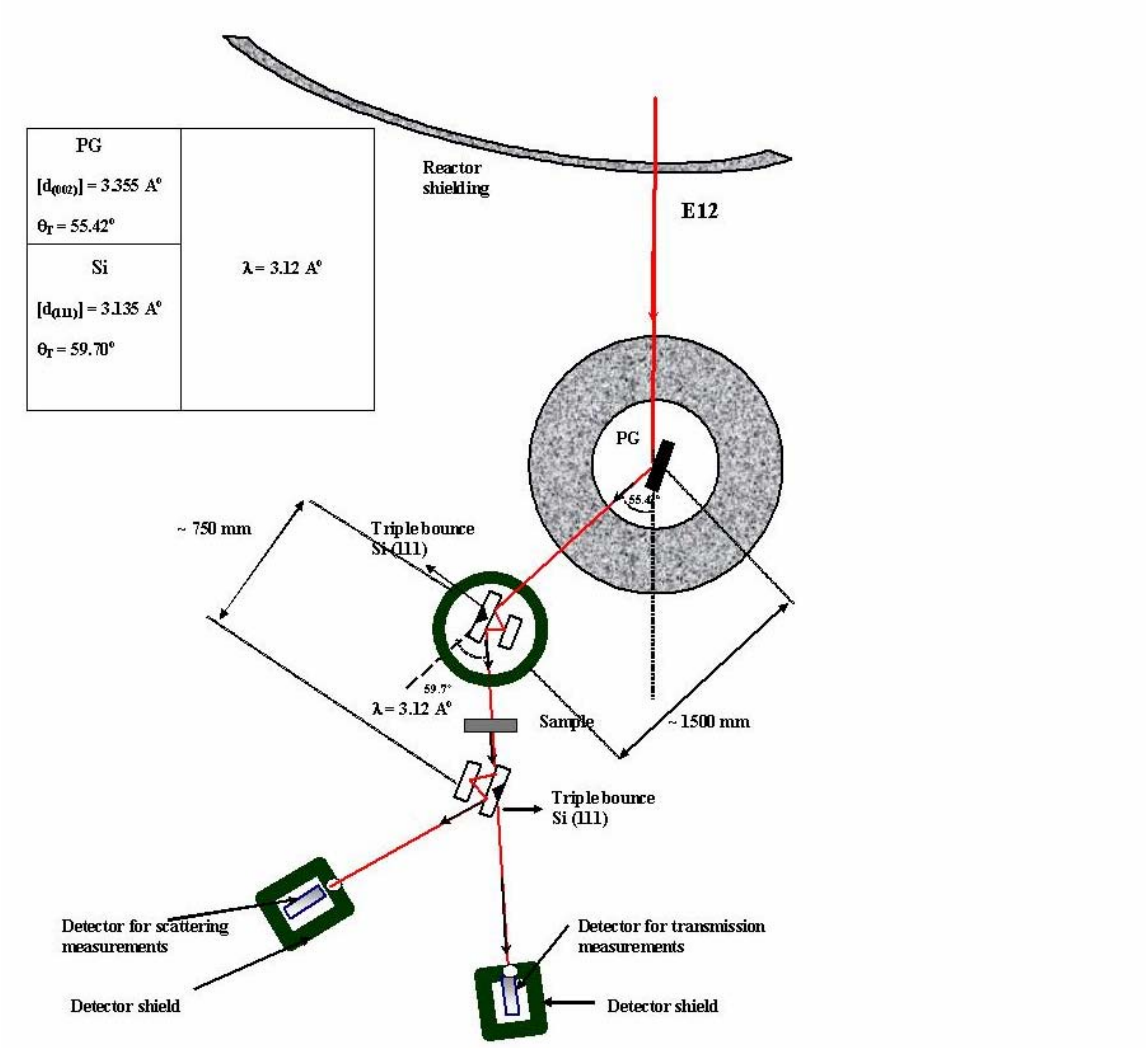

Fig. 15. The schematic layout of the proposed USANS facility

5. DESIGN AND FABRICATION OF THE ULTRA-PRECISION ROTATION STAGE

Scattered neutron intensity measurements were carried out in a USANS experiment by angular displacement of the analyzer crystal in two stages about an axis perpendicular to the scattering plane. The measurement of scattered intensity very near the direct beam was made in **ultra-fine** angular steps and at slightly higher angles in **fine** steps. For our instrument the fine angular positioning will be carried out in a step size of ~ 0.001^{o} through the tangential movement of a lever attached to the base supporting the analyzer. This will be done by pushing tangentially one end of a ~1/2-foot long lever arm whose other end is attached to the centre of the base supporting the analyzer. The lever arm is pushed by motorized movement of the lead screw of a micrometer head of graduation ~ 2.54 micrometer. The closed-loop optical encoder feedback controls the fine motor movement. Thus the linear movement of the lever arm causes the fine angular displacement of the analyzer crystal. However, ultra-fine angular positioning in steps below 0.001^{o} cannot be accomplished by a mechanism of rotation by motor. The mechanism used for ultra fine angular positioning is based on the principle of cantilever that makes use of the elastic property of materials, i.e., the lever arm bends on application of force and recovers upon release of force. A monolithic block of hard material having this elastic property generally referred to as flexure is used for this purpose. One end of this block is anchored rigidly to a base and the other end supports the analyzer crystal by a

rigid extension. Such a monolithic block (as shown in figure 16) has been designed at the Centre for Design and Manufacture, B.A.R.C. Figure 17 shows a three-dimensional picture of this block.

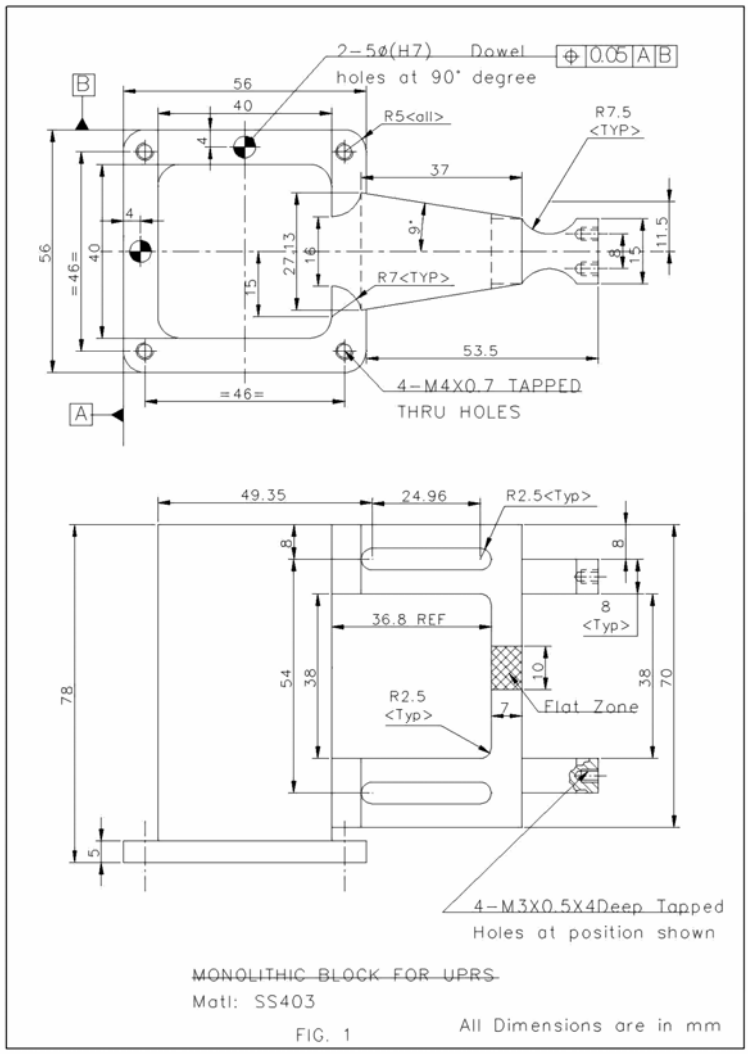

Fig. 16. Elevation of a monolithic block for the ultra-precision rotation stage.

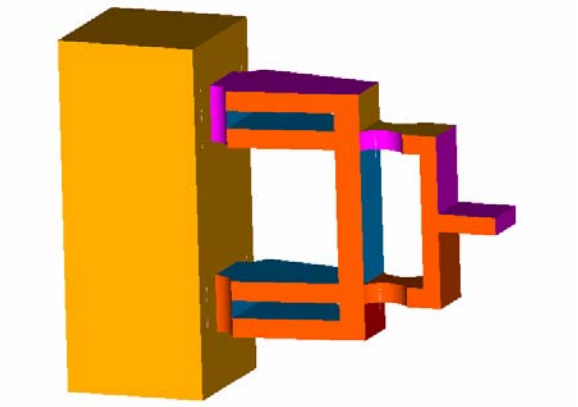

Fig. 17. 3-D view of a monolithic block for the ultra-precision rotation stage.

Calculations based on finite element method (FEM) analysis show that the application of a 1-kg force at the flat zone (as shown in figure 18) of the monolithic block shifts the centre of the analyzer by 2.4 x 10^{-4} mm in a tangential direction for a 75 mm radius of rotation. This displacement of the centre of the analyzer corresponds to an angular tilt of 0.00018^{o}. The deflection thus obtained in tangential direction is linearly proportional to the applied force. This would make possible the positioning of the analyzer crystal in increment of 0.00018^{o} for each incremental force of 1 kg to the monolithic block. The material of the monolithic block taken for analysis was SS 403 grade stainless steel. The effect of the weight of the analyzer crystal and the weight of the extension attached to the monolithic block to hold the crystal analyzer were taken into account for the FEM analysis (as shown in figure 18). Deflections in radial and axial directions were found to be 4x10^{-6} mm and 5x10^{-6} mm respectively. These deflections are 3% to 5 % of the deflection in the tangential direction of rotation of the analyzer. A prototype of the same is under fabrication at C.D.M. The piezo drive will be used to impart force on the flat zone of the flexure to obtain the required ultra-small angular positioning.

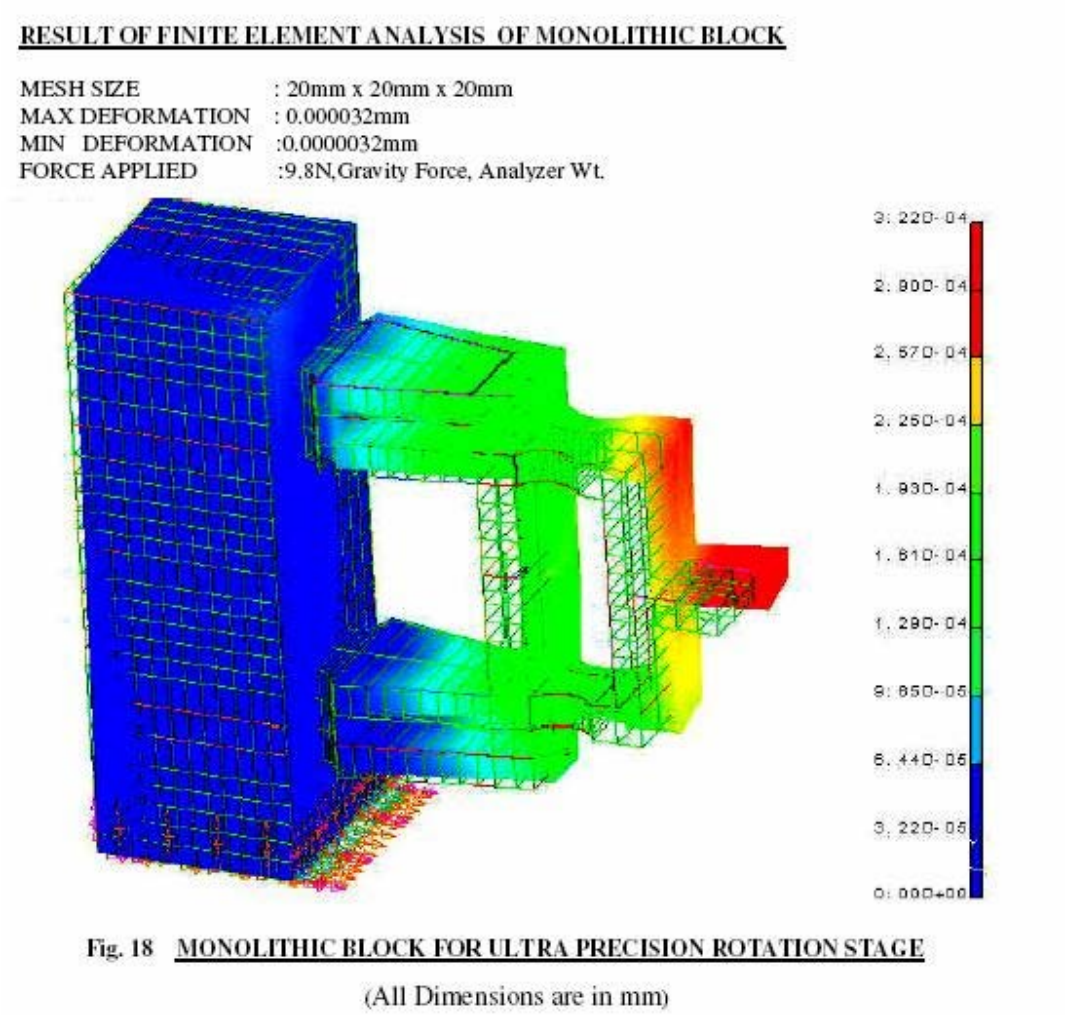

Fig. 18. Finite element analysis of a monolithic block for the ultra precision rotation stage.

On-line monitoring of ultra high precision rotation is necessary and the use of LVDT is being considered, although of a slightly lower precision. A base assembly (as shown in figure 19) for the ultra-precision rotation stage is under fabrication.

ULTRA PRECISION ROTATION STAGE BASE ASSEMBLY

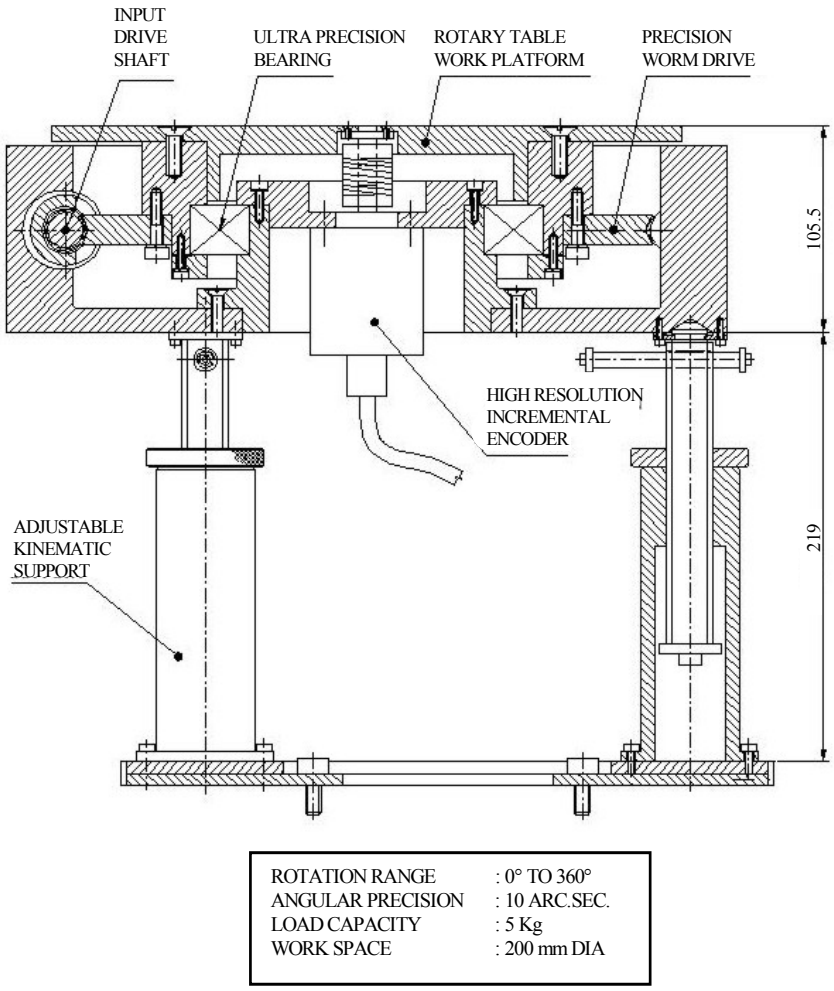

Fig. 19. Base assembly of ultra-precision rotation stage

This base assembly is equipped with precision worm and shaft drives to rotate the work platform by a DC motor from 0^o to 360^o with an angular precision of a 10 arc-second for coarse alignment of the analyzer crystal.

Two pieces of thickness-extension-type piezo-electric actuator were procured from a local manufacturer. Each actuator is composed of many thin piezo-electric ceramic (PZT) plates (dimension: 10 mm x 10 mm x 1 mm) bonded together. Their performance has been tested by optical interferometry and LVDT (Linear Voltage Differential Transformer). Both pieces have shown 20 microns displacement at 1000 Volt D.C. with good displacement characteristics.

6. FABRICATION OF VIBRATION ISOLATION TABLE

As scattered intensity measurements are carried out in ultra fine angular steps, it is essential that the angular stability of the monocromator, the sample platform and the analyzer be maintained within seconds of an arc. The vibrations from the floor or any other source at the instrument site should not perturb them. For this reason the monochromator, the sample platform and the actuator system holding the analyzer will be mounted on a vibration isolation table. Though thick and heavy granite-topped tables with a rugged structure are generally used for vibration isolation purposes, a table of a height greater than 700 mm was not

commercially available to suit our purpose. A vibration isolation table of a size of 1500 mm x 750 mm x 1400 mm (height) (as shown in figure 20) is under fabrication in our workshop.

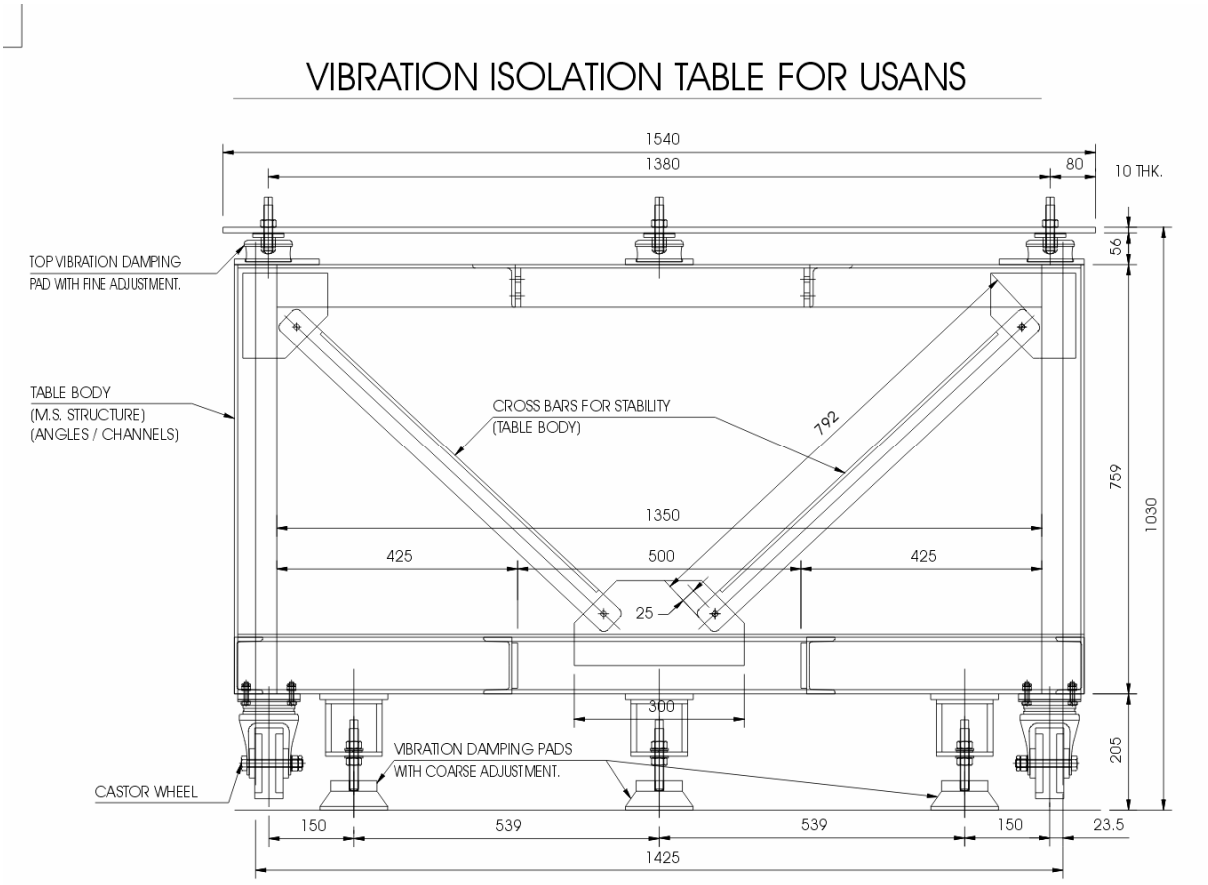

Fig. 20. Elevation of a vibration isolation table for a USANS diffractometer

Vibration damping tests have been carried out with commercially available vibration isolators made of various rubber materials for possible application in the construction of the table. Design corrections / improvements of the table are being tried out to achieve a vibration isolation which will meet our requirements.

We have also discussed our requirement for a vibration isolation table with reputed international manufacturers of such tables, like M/s Melles Griot BV, through their local agent in India. A table of the size that we require is not currently available from them, but they have agreed to fabricate one for us as per our requirements once the purchase order is placed. In case our own design fails to provide the required level of vibration isolation, we will arrange for funds to purchase the table from them.

6.1. Instrument Electronics

The electronics for our USANS instrument consist of two parts, i.e., a control system and a data acquisition system. The function of the control system is to set the spectrometer system at desired functional and operational settings by motor movement. These motor movements are controlled by motor drives through closed-loop optical encoder feedback. The function of the data acquisition system is to acquire data (counting neutron intensities) as required by a

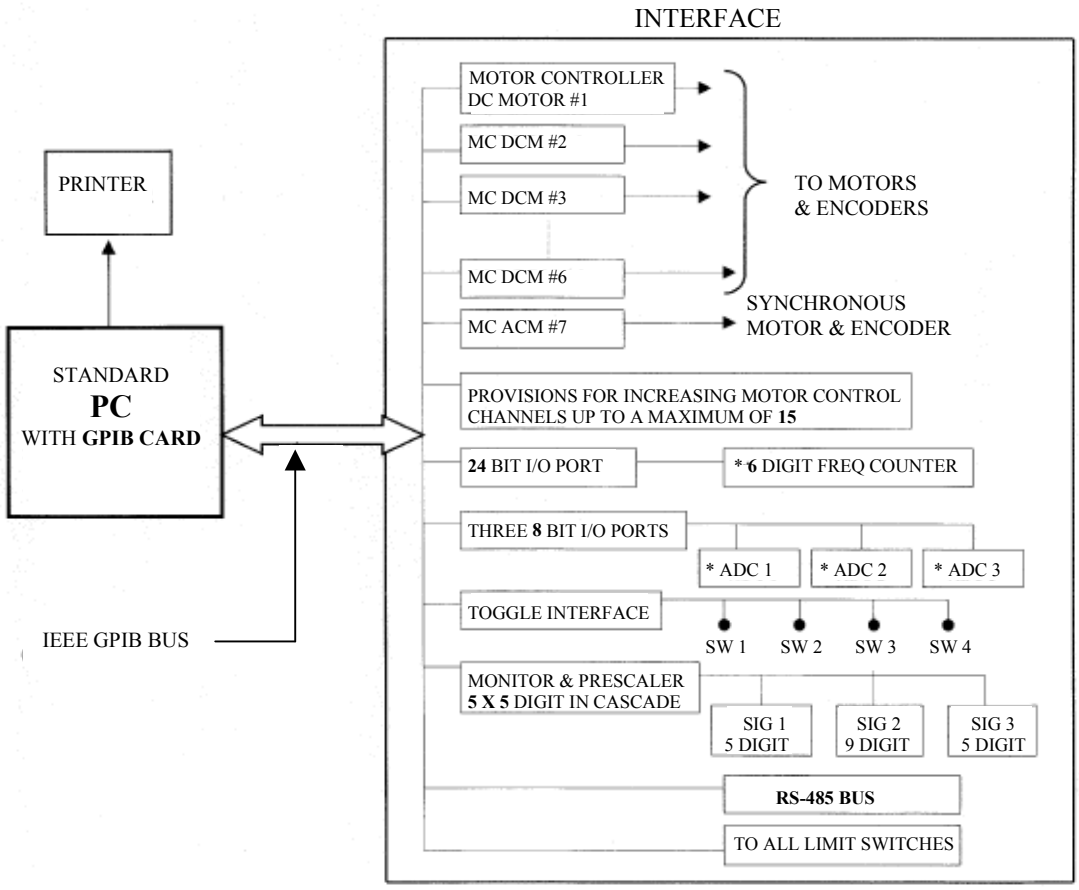

Fig. 21. Data acquisition system for USANS

programme. The design specifications of an automated control system and data acquisition system (as shown in figure 21) have been drawn up. We made a technical evaluation of the prospective manufacturers of the data acquisition and control systems. As there are no uncertainties in procuring the systems, once the hardware design and testing of the instrument are completed, procurement will be taken up.

7. CONCLUSIONS

An MSANS instrument with a pair of single-bounce flat crystals as monochromator and analyzer, has been successfully installed at Trombay, and has proven able to analyze and characterize various materials such as ceramics, alloys and rocks. The present instrument can access a q-range of about 0.003-0.173 nm^{-1}.

The USANS instrument currently under construction, making use of a pair of triple-bounce channel-cut crystals, will have a q-resolution in the range of 10^{-5} to 10^{-3} $Å^{-1}$ (depending on the neutron wavelength) and thus be able to investigate inhomogeneities of larger size.

For ultra precise rotation, the analyzer crystal will be mounted on a monolithic block of SS 403 grade stainless steel. A finite element analysis of the deflection in tangential direction on application of force for such an ultra-precision rotation stage has been thoroughly carried out. The results show that the deflection is proportional to the applied force in the desired range of angular displacement, and a prototype is currently under construction in our workshop. A vibration isolating table is also currently under construction in our workshop. A technical

evaluation of the prospective suppliers has furthermore been carried out regarding procurement of an electronic data aqcuisition system.

REFERENCES

[1] BONSE, U., HART, M., Tailless X ray single-crystal reflection curves obtained by multiple reflection,Appl. Phys. Lett. **7**, 238 (1965); BONSE, U., HART, M, Small angle x-ray scattering by spherical particles of polystyrene and polyvinyl toluene**,** Z. fur Phys. Lett. **189**, 151 (1966)

[2a] MAZUMDER, S., SEN, D., SARAVANAN, T., VIJAYARAGHAVAN, P.R., Performance and calibration of the newly installed medium resolution double crystal based small angle neutron scattering instrument at Trombay, J. Neutron Research; **9** 39 (2001)

[2b] MAZUMDER, S., SEN, D., SARAVANAN, T., VIJAYARAGHAVAN, P.R., Applied Physics A, **74,** S183 (2002)

[2c] MAZUMDER, S., SEN, D., SARAVANAN, T., VIJAYARAGHAVAN, P.R. Current Science, **81**, 257 (2001)

[2d] MAZUMDER, S., SEN, D., SARAVANAN, T., VIJAYARAGHAVAN, P.R., Neutron News, **13**, 26 (2002).

[3] HAINBUCHNER, M., VILLA, M., KROUPA, G. BRUCKNER, G., BARON, M., AMENITSCH, H., SEIDL, E., RAUCH, H., The new high resolution ultra small angle neutron scattering instrument at High Flux Reactor in Grenoble**,** J. Appl. Cryst., **33**, 851 (2000).

[4] SEN, D.,PATRA, A.K., MAZUMDER, S., RAMANATHAN; S., Pore morphology in sintered ZrO_2-8 mol%Y_2O_3: A Small angle neutron scattering investigation, J. Alloys and compounds **340,** 236 (2002)

[5] MAZUMDER, S., SEN, D., SASTRY, P.U.M., CHITRA, R., SEQUEIRA, A., CHANDRASEKARAN, K.S., Small angle x-ray scattering of porous silicon at two different wavelengths, J. Phys: Condens Matter **10,** 962 (1998)

[6] SEN, D.,PATRA, A.K., MAZUMDER, S., RAMANATHAN; S; Pore growth during initial and intermediate stage of sintering in ZrO_2-3 mol % Y_2O_3: A small angle neutron scattering investigation**,** J. Alloys and Compounds*,* **361** 270 (2003).

[7] HASSOLD, G.N., HOLM; E.A., An efficient finite temperature algorithm for the advanced Potts model*, Computers in Phys.* **7**(1) 97 (1993)

[8] MATSUBARA, H., FURUKAWA, K., BROOK, R.J., Computer simulation of sintering process of solid particles, Proc. Euro Ceram, **IV, 3** 597 (1995).

[9] PATRA, A.K., RAMANATHAN, S., SEN, D., MAZUMDER; S., SANS investigation on pore morphology in Ceria, DAE Solid State Physics Symposium, India (2003), **46**, 359 (2003)

[10] PATRA, A.K., RAMANATHAN, S., SEN, D., MAZUMDER, S., SANS investigation on evolution of pore morphology and pore size distribution for varying sintering time in porous Ceria Pramana: J. Physics, **63**, 327 (2004)

[11] SEN, D., MAHATA, T., PATRA, A.K., MAZUMDER, S., SHARMA, B.P., Effect of sintering temperature on the pore growth in ZrO_2-8 mol % Y_2O_3 ceramic compact prepared via citric acid gel route: A small angle neutron scattering investigation, J. Alloys and Compounds **364**, 304 (2004).

[12] SEN, D., MAHATA, T., PATRA, A.K., MAZUMDER, S., SHARMA; B.P., Effect of pore morphology and porosity on low frequency dielectric response in sintered 8 mol % Y_2O_3 - ZrO_2 ceramic, J. Physics: Condensed Matter, **16**, 6229 (2004).

[13] SEN, D., MAZUMDER, S., TARAFDAR., S**.,** Pore morphology and pore surface roughening in rocks: A small angle neutron scattering investigation J. Mat. Sci **37** (2002) 941
[14] SEN, D., MAZUMDER, S., TARAFDAR, S., SANS investigation on the pore surface roughening in rocks, Appl. Phys (A), **74**, S1049-1051 (2002).
[15] MITRA, J., DEY, G.K., SEN, D., PATRA, A.K., MAZUMDER, S., DE; P.K., Solution quenched structure of wrought PH 13-8 Mo stainless steel, Scripta Materilia, **51**, 349 (2004)
[16] MAZUMDER, S., SEN, D., PATRA, A.K., MITRA, J., DEY, A.K. DE; P.K., A Small angle neutron scattering investigation on solution quenched PH13-8 Mo stainless steel, DAE Solid State Physics Symposium, India, **46**, 345 (2003)
[17] SEN, D., PATRA, A.K., MAZUMDER, S. MITRA, J., DEY, G.K., DE; P.K., Carbide precipitates in solution quenched PH13-8 Mo stainless steel: A small angle neutron scattering investigation, Materials Science and Engineering A **397**, 370 (2005).
[18] PATRA, A.K. TRIPATHY, P.K., SEN, D. MAZUMDER, S. NAIK, S., GAONKAR, V.G., KOTWAL. I., Effect of titanium volume fraction on precipitate morphology in Fe-Ti alloy: A SANS investigation, DAE Solid State Physics Symposium, India, **45**, 37 (2002)

STUDY AND DESIGN OF A NEW GENERATION OF SANS INSTRUMENTS: SMALLER, MODULAR, WITH ENHANCED CAPABILITIES AND LOW SERVICING REQUIREMENTS

F.G. Carvalho

Physics Department, Condensed Matter Physics Group,
Nuclear and Technological Institute, Sacavém, Portugal

Abstract. Small Angle Neutron Scattering (SANS) is a powerful tool for the investigation of the sub-micrometer structure of condensed matter with important applications in various fields (Materials Science and Engineering, Soft Condensed Matter, Geology, etc.). SANS facilities are currently in heavy demand. The upgrading of existing facilities and the development of new concepts for optimizd performance is therefore of the greatest importance.

1. INTRODUCTION

The ITN team has been working on the problem of design optimization of SANS instruments. The mathematical solution of the problem is well known [1-5], consisting of a set of relations involving the geometrical parameters of the instrument and defining the so-called "matched instrument". For a fixed total length of the instrument, the count-rate is optimized for equal flight paths (symmetrical arrangement) [1-3]. The ITN group has addressed the choice of the best-performing arrangement for an actual SANS instrument, taking into account the actual physical limitations of various geometrical parameters involved [4]. The solution of the problem with constraints other than setting a fixed value for the total length of the instrument, in general, takes the form of an asymmetrical arrangement and leads to a higher count-rate with unchanged resolution, compared to the symmetrical arrangement with the same sample-to-detector length. This has been confirmed by experiment [5].

Single-channel collimation has been considered in all studies referred to above, although certain advantages to be gained by using two-dimensional converging collimators were reported more than twenty years ago [6]. A decade later such collimators were introduced into SANS facilities operating at pulsed neutron sources [7-8]. However, few studies were published concerning the optimized use of converging 2-D collimators, and then only particular aspects of the multi-channel collimating arrangement were dealt with, e.g., the bearing on the instrument resolution of the distance between the collimator exit plane and the sample [9]. In a recent paper [10] the ITN team came up with an expression for the detector count-rate at constant resolution to allow the comparison between SANS instruments equipped with different collimator types (single-channel and multi-channel). The paper shows that the use of converging multi-channel collimation (CMC), giving multiple independent incoming beam channels that converge at the detector, leads to significantly higher count-rates. In fact, count-rate gains of one order of magnitude can be achieved, as compared to those obtained with a single-channel collimator. Since the collimator geometry must be changed accordingly whenever the detector position is changed, an additional advantage will be gained by using a variable-geometry CMC unit.

Multi-channel collimation, on the other hand, follows the trend of new developments in neutron area position sensitive detectors, which goes towards the design and construction of small detector units with very small elementary detecting elements (pixels). Large active areas would be obtained in a flexible way by assembling several detector modules. The successful development of such modular small-pixel detectors together with that of variable-geometry multi-channel collimators would provide the means to realize SANS instrument miniaturization, with considerable improvement in performance over SANS facilities of

conventional design, as currently in use. This will be particularly interesting for work at low-flux research reactors.

At present, 2D-converging multi-channel collimators with fixed geometry equip a few SANS instruments installed at pulsed neutron sources for which the detector-to-sample distance remains fixed. However, most existing SANS facilities are installed at steady-state reactors, and for these the coverage of a large region of reciprocal space, as required in standard SANS experiments, implies a variation in the sample-to-detector distance. This is an incentive for the development of a 2D-converging multi-channel collimator with adjustable geometry.

2. PARTICIPATION IN THE CRP AND SCOPE OF THE WORK

Participation in the Agency's Co-ordinated Research Project entitled "Development and Practical Utilization of Small Angle Neutron Scattering Applications" was in tune with current interests of the ITN team. In fact, the listing of potential outcomes from the CRP included under the heading "Hardware-related outcomes" the "optimization of SANS devices according to the physical layout of the facilities". Thus participation followed naturally from the work already performed or in progress at ITN on the development of the SANS technique by the time the application was written. The main results obtained so far were of a theoretical nature pertaining to the problem of SANS instrument optimization. These results have consequences on practically all aspects of the geometry or configuration of a SANS facility, including specifications of collimator assemblies, detectors and neutron optical components, such as beam guides and neutron wavelength selection devices. Last but not least the team was engaged in the implementation of a SANS facility at the local research reactor [11, 17].

It was foreseen from the beginning that the ITN team would focus its efforts on the development of a prototype of a variable-geometry CMC that appeared to be a promising step on the road towards a new generation of SANS instruments with higher performance. Bilateral collaboration within the framework of the CRP with the Hungarian partner KFKI, who was also taking part in the CRP, was a natural consequence of their experience in the design and construction of 2D-position sensitive neutron detectors and of the expectation of improved performances by associating the converging multi-channel collimator and detectors with smaller pixel sizes. It was known that the Hungarian group had developed a PSD detector with a 1 mm^2 pixel.

On the other hand, the experience of the Hungarian partner in the construction of neutron guides could help in the design of the beam line for the Portuguese SANS instrument with respect to improving the signal-to-noise ratio of the facility.

Finally it was understood by the parties that the ITN 1 MW swimming-pool research reactor would offer good conditions for in-beam testing of the detector prototypes as well as of other components that would be produced in the course of the project work.

A detailed work plan for the Project was first drafted and agreed upon during the First Research Co-ordination Meeting, held at the IAEA Headquarters. It was specified that the Project's activities would be developed in partnership between KFKI-BNC, Hungary, and ITN, Portugal and that there would be three main components of the work, identified below, covering a period of three years:

2.1. Converging multi-channel collimator

Develop a 2-D converging multi-channel collimator (CMC) and evaluate its effectiveness. The ITN team will perform the development of the prototype and tests will be carried out at BNC.

2.2. Neutron guides

Evaluate the feasibility of installing a neutron beam guide at the SANS facility of ITN (KFKI/ITN). If the feasibility study is positive a preliminary design of the neutron guide installation will be carried out (KFKI).

3. POSITION-SENSITIVE DETECTORS

Develop a lower-cost, small, two-dimensional position-sensitive detector which can potentially be used as part of a larger array.

The ITN and BNC teams are prepared to co-operate generally in the field of 2-D PSD detectors, in particular in the development of a lower-cost, small PSD detector (200 × 200 mm^2 active area and a 1 × 1 mm^2 pixel). This will be of such a design as to also constitute an element of a large-area modular detector system. For this it will be essential to maximize the ratio of active-to-total area.

The Hungarian partner is also interested in developing a large-area detector, and ITN will contribute by helping to solve specific problems related to the charge collection process.

It is foreseen that the BNC team will perform the development of the detector prototypes, and the testing will be carried out at ITN.

4. DESCRIPTION OF THE WORK CARRIED OUT AND RESULTS OBTAINED

4.1. Converging multi-channel collimator

The main CMC parameters for the first prototype were selected (entrance and exit window sides; number of channels). A computer simulation was performed in order to model the device and to establish the collimator performance (channel cross-talk) as a function of the relevant geometrical and neutron parameters (absorption and scattering cross-sections, size and spacing of the neutron absorbing elements that make up the collimating channel walls) [12].

The material selection for and mechanical design of a 40 cm-long 100-channel CMC was successfully undertaken. The design principle is such that the geometry or channel configuration of the prototype can easily be modified between fixed settings. The collimator walls are discontinuous and may be described as curtains of parallel strips of a convenient absorbing material separated by empty intervals of the same width as the strips.

In our view the progress towards the proposed objective was satisfactory notwithstanding the departures from the proposed work plan. In fact, the design of the first prototype turned out to be considerably more complicated than had been anticipated. The main problems have been: (a) selecting the shape and material of the neutron-absorbing elements that form the collimator curtain walls; (b) establishing the fabrication process of the absorbing elements; and (c) mechanically designing the frames that support the vertical and horizontal arrays of the absorbing elements, particularly, developing adequate mechanical solutions to implement the degrees of freedom corresponding to the translation and rotational movements of the collimating planes associated with the variation of the collimator geometry.

These problems were solved satisfactorily and progress was made in a manner that justified the abandonment of the first step as initially programmed, i.e., the construction of a static or rigid CMC. The design of the variable-geometry model (manually controlled) was completed and the construction of the first prototype in our workshop is well advanced, although it could not yet be completed.

Particular attention has been paid to the physical and nuclear properties of the composite material to be used in the production of the absorbing strips that make up the curtain walls of

the collimator [15]. The computer simulation that guided the initial design of the CMC device was upgraded to account for the total reflection processes occurring at the surface of the absorbing strips. Results show that when the critical angle for total reflection exceeds a few mrad, there will be some contamination of the direct beam, affecting negatively the resolution function. Mixtures of an epoxy resin with Gd_2O_3 and Ti powders in different concentrations were prepared and investigated. Preliminary test measurements with neutrons were carried out at Saclay in collaboration with a French team from LLB. The results indicate that the strips can be produced with adequate mechanical and neutron-absorbing properties. It was shown that the quality of the surface of the absorbing strips largely determines the angular spread of the reflection, and that the addition of Ti considerably reduces the probability of total reflection. A more thorough examination by means of neutron scattering and reflection on the surface of the strip material was programmed for early 2004.

Presently, a decision concerning the possible development of a remotely controlled CMC unit (design, construction and test of a remote-control driving system for the variable geometry CMC) that was originally contemplated is not confirmed pending the reassessment of the matter from the point of view of the effective usefulness of remotely controlling the CMC and considering the technical complexity of implementing the control.

Besides the design and construction work of a first CMC prototype, consideration was given on the theoretical side to the development of the concept of converging multi-channel collimation applied to SANS instruments.

In this respect it was possible to establish guidelines for the implementation of the concept in a specific SANS facility by carrying out a detailed study of the instrument performance when a CMC or an assembly of CMC units were installed in the beam line [16]. The study explored the possibility of using an association of variable fixed-length 2-D CMC units to cover the required range of sample-to-detector distances. The study showed that the overall instrument performance obtained in this way, although deviating from the optimum, may still offer a considerable improvement over the conventional SANS experimental arrangement with single-channel collimation.

Concerning the performance of a CMC device, a detailed analysis of the contribution of the individual channels to the operation of the device was carried out by means of a Monte Carlo computer simulation [14]. The simulation showed that the coupling between the divergence of the incident neutron beam and the inclination of the individual CMC channel axis relative to the beam direction modulate the channel performance as far as intensity and resolution of the transmitted neutrons are concerned. While this does not impair in any significant way the usefulness of the device, the results are helpful to the designer.

Since the construction of the prototype could not be completed, the tests foreseen in collaboration with the Hungarian partner at the Budapest reactor did not take place. The main cause of delay was shortage of skilled manpower, resulting in inadequate technical support to research groups. It was expected to complete the prototype during the first half of 2004 and to carry out the foreseen in-beam tests of the device during the second half of the year.

In conclusion, it is fair to say that progress towards the proposed goal of developing a 2-D converging multi-channel collimator for SANS was significant, although not all the objectives of the work plan could be attained. It should be noted in particular that relevant theoretical contributions were made to the development of the concept of converging multi-channel collimation applied to SANS instruments.

4.2. Neutron guides

Major steps towards the installation of the ITN SANS facility were undertaken during the period of the present CRP.

1. The instrument was installed at the exit of a 4 inch transverse beam tube of the reactor to avoid direct sight of the reactor core. No cold source was available, and the instrument was fed by the neutron flux scattered by a 2 mm thick and 75 mm diameter disk-shaped volume of demineralized light water inserted into a continuous-flow circuit. This scatterer was, placed inside the transverse beam tube in front of the reactor core. Preliminary tests performed after installation of the in-pile components showed that, although the beam tube had no direct sight of the reactor core, the level of unwanted background was considerably high, requiring adequate filtering. One of the possibilities to filter the beam would have been the installation of a curved neutron guide. Due to the local space constraints and the absence of a cold neutron source, the use of neutron guides required proper evaluation, and this was done in collaboration with KFKI. The Hungarian partner was carrying out a Monte-Carlo simulation study that tested different guide arrangements. The following general conclusions were reached after discussions between the partners:
2. The level of the background can be drastically diminished;
3. If single-channel collimation is used, an adequate neutron guide arrangement would consist of a short bender followed by a straight guide section – in this case, the signal at sample would be only slightly lower than that expected without guides (but with a much higher signal-to-background ratio);
4. If a CMC were used, the net signal at sample would also be improved.

Altogether the installation of a neutron guide appears more promising than the use of filtering crystals, particularly in case (iii) above.

However, the results obtained from the simulation study point to a major change in the original layout of the small angle scattering instrument, including the replacement of all in-pile components already installed. This would require the allocation of considerable resources to the project (both financial and human), which, at present, is unfortunately not possible. A decision was made to proceed with the current installation work-plan. If and when an opportunity window opens, the upgrading of the facility will be considered. Then, further work will have to be performed to refine details of the final design, requiring further interaction with the Hungarian partner. The interaction between the partners and the work done so far established a good basis for the success of future work.

4.3. Position-sensitive detectors

As indicated above, the overall objective with respect to detector development under the contract was to develop a lower-cost, small-sized, two-dimensional position sensitive detector which could potentially be used as part of a larger detector array. During the November 2000 RCM Meeting in Vienna, a small-pixel (1 mm by 1 mm) 200 by 200 mm square PSD was agreed upon as a reference design target, drawing on the Hungarian experience.

The Hungarian partner also confirmed their interest in developing a large-area detector, and ITN proposed to contribute by helping to solve specific problems related to the charge collection process which would require precise identification through discussion and exchange of information.

Apart from details, the division of work would be for the BNC team to perform the development of the detector prototypes, and for ITN to contribute with tests and calculations.

A first step towards the necessary problem definition (Action (1) in the First RCM Report) was taken during the December 2000 visit of Dr. László Cser to Sacavém. It appeared that there were a certain number of aspects concerning the discharge processes in the neutron gas-filled proportional detectors, including the characteristics of the charge collection in relation to the spatial and time resolution of the counting that one could attempt to model usefully. For that purpose the specialized experience existing at ITN could be drawn upon. A first discussion during Dr. László's visit supported this view and indicated that Monte Carlo techniques could be used advantageously.

Since the detector prototypes could not be made available for testing, there has been no further progress from the side of ITN. In this context it should be said that the installation work of the SANS facility at Sacavém also experienced delays due mainly to problems of technical support.

Also, the Hungarian partner could not complete the definition of the modelling exercise to be dealt with by Monte Carlo techniques.

This is thus the one area of work where progress has been unsatisfactory and more efforts are needed for implementation of the planned cooperation. As far as the ITN team is concerned, the principal obstacle to the normal progress of work is the shortage of manpower, mainly skilled technicians, but also the long delays in purchasing parts and components. The situation has become worse in recent years. On the other hand, the case for the proposed detector development remains strong, and efforts to develop cooperation along this line should be continued.

5. CONCLUSIONS: THE RELEVANCE OF PARTICIPATING IN THE CRP

From the point of view of the ITN group, participation in the CRP was beneficial insofar as it has helped to establish new links of cooperation and to strengthen already existing links between scientists and groups from laboratories in different countries. These laboratories have different levels of expertise and resources, which fact presents an opportunity for the cross-fertilization of ideas. On the other hand, channels are opened through which groups and centres less experienced and suffering from a shortage of resources - human, material and financial -can access up-to-date know-how and facilities that help their own development efforts. The CRP as an organized effort to bring together people and ideas under the aegis of the IAEA to foster bilateral and multilateral cooperation between research groups and institutions is a commendable initiative. One should, however, be aware of the difficulties that such work inevitably encounters, originating in the constraints on the less developed centres. These constraints often penalize the pace of progress of the work programmed and lead to discrepancies between programme and execution.

This has happened in our case as pointed out in Section 3.

A Partnership was established between Hungarian and Portuguese groups laying the foundation for mutual continued collaboration. A Seminar organized jointly by ITN and the Physics Department of the Faculty of Sciences of the Lisbon Classical University provided an opportunity for an exchange of information on the respective facilities and activities of the two groups and a discussion on the division of work related to the CRP. However, due to constraints from both sides the assigned tasks could not be completed as planned.

The intention of performing in-beam tests of the CMC prototype under construction at Sacavém at the Budapest Neutron Centre and of the Hungarian PSD detector prototypes at the ITN reactor still stands.

The CRP Research Co-ordination Meetings were a valuable opportunity to develop contacts with colleagues from the participating centres. In the case of Brazil, Greece, Austria,

Germany and France these contacts were particularly interesting insofar as doors were opened for future collaboration based on improved mutual acquaintance of the parties. In the case of LLB cooperation had been well established for a long time, but new information of interest from the point of view of ITN's own work on the development of the CMC concept was gained on work developed there.

Last but not least, the financial side. The scarcity of research funds is especially critical in most developing countries. It happens that even money for travelling is hard to obtain. This is obviously an obstacle to developing cooperation between centres geographically far apart. It is also important to analyze what motives may bring the more developed partners to participate in a CRP, since their participation is indispensable for the success of the CRP. One motive may be the exchange of information exactly between the more developed partners, in which case an equilibrium must be reached between participants from both developed and developing countries. Portugal, being probably at an intermediate level, in our opinion is in a particularly good position to profit from the cooperation sponsored by the IAEA, as shown by our experience of many years of participation in IAEA programmes.

REFERENCES

[1] SCHMATZ, W., SPRINGER, T., SCHELTEN, J., IBEL, K., Neutron Small angle Scattering: Experimental Techniques and Applications, J. Appl. Cryst. **7** 96 (1974)

[2] SEEGER, P.A., Optimisation of Geometric Resolution in Small angle Scattering, Nucl. Instrum. Meth., **178** 157 (1980) .

[3] MILDNER, D.F.R., CARPENTER, J.M., Optimisation of the Experimental Resolution for Small angle Scattering, J. Appl. Cryst., **17** 249 (1984).

[4] F.M.A. MARGACA, E.M.A., FALCAO, A.N., SALGADO, F.J., CARVALHO, F.G., Solving the Problem of SANS Instrument Optimisation, J. Appl. Cryst. **24** 994 (1991) .

[5] FALCAO, A.N., PEDERSEN, J.S., MORTENSEN, K.,Optimum Intensity in Small Angle Neutron Scattering. An Experimental Comparison between Symmetric and Asymmetric Geometries, J. Appl. Cryst. **27** 333 (1994) .

[6] NUNES, A.C., A Focussing Low-Angle Neutron Diffractometer, Nucl. Instrum. Meth. **119** 291 (1974) .

[7] ISHIKAWA, Y., FURUSAKA, M., NIIMURA, N., ARAI, M., HASEGAWA, K., The Time-of-Flight Small angle Scattering Spectrometer SAN at KENS Pulsed Cold Neutron Source, J. Appl. Cryst. **19** 229. (1986)

[8] NIIMURA, N., HIRAI, M., ISHIDA, A., AIZAWA, K., YAMADA, K., UENO, M., Thermal Neutron Small angle Scattering Spectrometer (WIT) Using a 2D Converging Slit and Annular Glass Scintillator Detectors at KENS, Physica B, **156&157** 611.(1989)

[9] MILDNER, D.F.R., CARPENTER, J.M., Resolution of Small angle Scattering with Soller Collimation, J.App.Crys. **20** 419 (1987) .

[10] MARGACA, F.M.A., FALCAO, A.N., SALGADO, J.F., CARVALHO, F.G., Multichannel Collimation for SANS Instruments, Physica B, **276-278** 189-191 (2000).

[11] FALCÃO. A.N., MARGAÇA, F.M.A., SALGADO, J.F., CARVALHO, F.G., "A Contribution to the Development and Practical Utilisation of the Small Angle Neutron Scattering Technique (I)", in "Development and Practical Utilisation of Small Angle Neutron Scattering (SANS) Applications (F1.20.13)", Summary Report, First Research Co-ordination Meeting (F1-RC-830), 13-16 November 2000, IAEA Headquarters, Vienna.

[12] FALCÃO, A.N., MARGAÇA, F.M.A., CARVALHO, F.G., "The Use of Multichannel Collimation in Small Angle Neutron Scattering: A Computer Simulation Study", Appl. Phys. A **74** (Suppl.), S1462 (2002).
[13] FALCÃO, A.N., MARGAÇA, F.M.A., SALGADO, J.F., CARVALHO, F.G., ”A Contribution to the Development and Practical Utilisation of the Small Angle Neutron Scattering Technique (II)", 2d Research Co-ordination Meeting of the IAEA CRP "Development and Practical Utilisation of Small Angle Neutron Scattering Applications", IAEA Headquarters, Vienna, Aug. 20-23, 2002.
[14] FALCÃO, A.N., MARGAÇA, F.M.A., CARVALHO, F.G., ”Intensity and Resolution Effects in Converging Multichannel Collimators for SANS by Monte Carlo Simulation", J. Appl. Cryst., , **36**, 1262 (2003).
[15] FALCÃO, A.N., MARGAÇA, F.M.A., CARVALHO, F.G., ”A Contribution to the Practical Implementation of a Variable Geometry Converging Multichannel Collimator for SANS", J. Appl. Cryst., **36**, 1266-1269 (2003).
[16] MARGAÇA, F.M.A., FALCÃO, A.N., CARVALHO, F.G., "Guidelines for the Implementation of Converging Multichannel Collimation in a Specific SANS Facility", J. Appl. Cryst. (2004) (*in press*)
[17] MARGAÇA, F.M.A., FALCÃO, A.N., SALGADO, J.F., CARVALHO, F.G., "Wavelength Dependence of the Performance of a SANS Instrument Installed at a Steady Source" (2003) (*to be submitted)*

OPTIMIZATION OF VELOCITY MONOCHROMATORS FOR LOW-POWER RESEARCH REACTORS

A.V. Poutchkov

Institute for Physics and Power Engineering, Obninsk, Kaluga Reg, Russian Federation

Abstract. Investigations have been made for different solutions to mechanical monochromators for low-power research reactors, optimized with respect to neutron beam intensity and cost. Choosing the best design and materials has proven to be of great importance. It was found that aluminium, being light and convenient, is a good choice for low and medium rotation speeds, and can become an excellent neutron absorbant when added only a few percent of rare-earth material.

1. INTRODUCTION

Due to the large scattering cross-sections at low angles, SANS can be used at many lower-flux neutron sources. Nevertheless, one of the main problems of SANS at low-power research reactors is the intensity of useful neutrons. A partial solution to this problem is the use of a high-transmission mechanical velocity monochromator. Thus it is very important to design an effective neutron monochromator. In this context, it is necessary to optimize the ratio of the intensity to the resolution by means of the geometrical parameters and the construction of the monochromator.

2. THE RESULTS OF THE FIRST-YEAR WORKING PLAN

The mechanical monochromator is the integral part of the small angle neutron scattering devices (SANS) placed at the steady-state reactors. The parameters of the mechanical monochromator determine the general parameters and quality of the SANS as a whole. Therefore the choice of design and optimization of the monochromator's parameters is an important stage in the designing and manufacturing of the SANS.

2.1. General relations of the mechanical monochromator parameters

There are two basic types of mechanical monochromators. Let us arbitrarily call the first one the "disc type" [1,2]. This mechanical monochromator looks like a set of neutron-absorbing discs placed along an axis. The discs have special holes (slits) which form a helical-shaped channel for the neutrons.

The second group is arbitrarily called the "cylindrical type" [3,4]. The design of this type in general is a cylinder. On the surface of the cylinder, neutron-absorbing helical lamellas are placed. The space between the lamellas serves as the passage for the neutrons. The lamellas and the cylinder can be made of plastic [3] or metal [4]. In any case the lamella materials contain neutron-absorbing dopants. The quantity of the dopant should be enough for the absorption of neutrons in the operating energy range.

The main objective, as applied to SANS at low-power reactors, is to obtain a maximum of useful monochromatic neutrons at moderate resolution. From the experience of recent years "moderate resolution" can be taken as the value of 10-15%.

According to the first-year working plan the transmission and resolution functions of the mechanical monochromator for SANS would provide estimates for the typical parameters of the neutron beam and geometrical parameters of the rotor slit.

The above estimates provide some insight into the choice of, and the general relations between the parameters of the mechanical monochromator of SANS devices in low-power reactors.

These estimates are a basis for the general considerations to allow for the agreement of the parameters of the collimating system of the primary neutron beam and the mechanical monochromator respectively. In this case the horizontal divergence of the beam has an intimate connection with the slit parameters of the mechanical monochromator, while the vertical divergence has a wide range of permissible values.

As for the static transmission function of the mechanical monochromator, the metal variant of the lamellas (for example an aluminium "alloy" with rare-earth elements) provides a better static transmission of up to 95%.

2.2. The choice of material for the absorption plates of the rotor of mechanical monochromators

It is obvious to us that for the creation of velocity monochromators that will be used for low and middle-speed rotation, the alloys based on aluminium, as a light and convenient material, are very attractive. The experience of designing the velocity monochromator for the Algerian reactor shows that the speed of rotation is not higher than 6000-8000 rpm [4]. It is very important that on this basis we can create materials able to absorb neutrons with a high cross-section, as needed for the velocity monochromator absorbing plates. It is efficient to dope the aluminium alloy with rare-earth elements, first of all gadolinium, an element with a high absorption cross-section for thermal neutrons (see Table 1).

Table 1. Absorption cross-sections for thermal neutrons for rare earth elements

Element	$_{62}$Sm	$_{63}$Eu	$_{64}$Gd	$_{66}$Dy
Absorption cross-section at neutron energy E=10meV, barns	$6.7*10^3$	$9.5*10^3$	$70*10^3$	$1.7*10^3$

3. THE RESULTS OF THE SECOND-YEAR WORKING PLAN

3.1. Formulation of the predesign of the mechanical monochromator (MM)

The velocity monochromator is designed to transmit cold neutrons with a definite wavelength (energy). The main parameters of the monochromator are as follows:

a) L=625 mm; r=200 mm; h=60 mm; Θ=17°

b) Rotational speed of 1500-4500 rpm, neutron wavelength 4-10 Å

c) Transmission ~0,85

d) Resolution ~14 %

The thickness of the neutron absorbing sheets, which are made of special alloy (Al-90%, Gd-10%), is equal to 0.5 mm. The attenuation factor for neutrons with an energy <100 meV is exp (-60).

The monochromator operates in a vacuum. The preliminary evacuation runs by a portable mechanical vacuum pump Model BH-461. A special motor drives the monochromator. The

rotational speed is controlled by an electronic system (CAMAC) which incorporates the quartz-stabilized generator. The layout of the monochromator control system is shown in figure 1.

Rotor 1 of the monochromator is driven by a DC electric motor Model 4MI-12F with a power of 1 kW. The control system includes AC/DC rectifiers for power supply of excitation winding and armature winding, a stabilization system for rotational speed (stability is 2%), and a measurement system to monitor the rotation speed. The rotational speed sensor of a magnetic type consists of the fixed inductance coil and a permanent magnet incorporated into the rotation disc.

The control system blocks the neutron measurements if a rotation speed differs by ≥2% from the specified value.

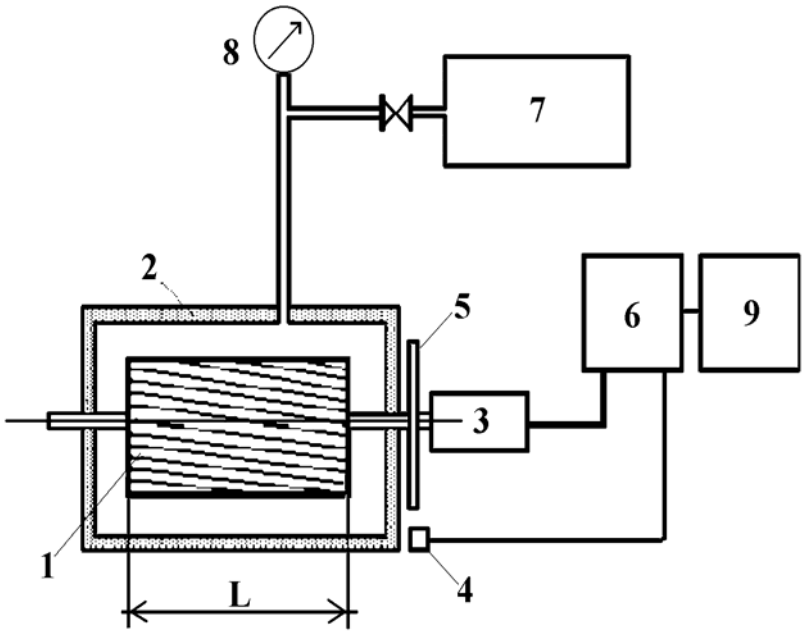

Fig. 1. Layout of the monochromator system.

1-Rotor; 2-Body; 3-Electric motor 4MI-12F; 4-Magnetic sensor; 5-Disc with magnetic mark; 6-Power supply and stabilization of rotational speed; 7-Vacuum mechanical pump; 8-Vacuum manometer; 9-Control system

The design provides high transmission (more than 90%) and a wavelength resolution of $\Delta\lambda/\lambda$ ~14%, allowing neutron wavelengths to be selected between 4 Å and 10 Å. The rotor is an aluminium cylinder rotating in a vacuum jacket around the horizontal axis. The rotor slits of helical shape are formed by absorbing plates with a thickness of 0.5 mm, made of Gd (10%)-Al alloy. The bearing adjacent to the motor is cooled by airflow from its ventilator. The possibility of bearing temperature control is foreseen, but long term tests have shown that its temperature does not exceed ~ 30–40°C. As to vibration control, in the construction used the vibrations are not estimated to be a remarkable threat.

The system of velocity stabilization is based on the comparison between a pre-assigned frequency and one generated by the magnetic head. As established in long term tests, the deviation of rotation frequency from the preset one in the working interval (1000 - 4500 rpm) is about ± 3 - 5 rpm.

The wavelength calibration of the monochromator and assessment of its resolution can be performed by the time-of-flight method. For this purpose, the end face of the rotor is covered by a disc made of adsorbing material. The disc has two slits to generate pulses of monochromatic neutrons. For a start signal the magnetic head is used.

3.2. Formulation of the construction of the absorbing plates of the MM rotor (Figure 2)

Only a small quantity of gadolinium is needed for the preparation of highly efficient neutron-absorbing alloy. This fact is very important for the manufacturing of the alloys because of the small influence of the dopant on the mechanical properties of the material.

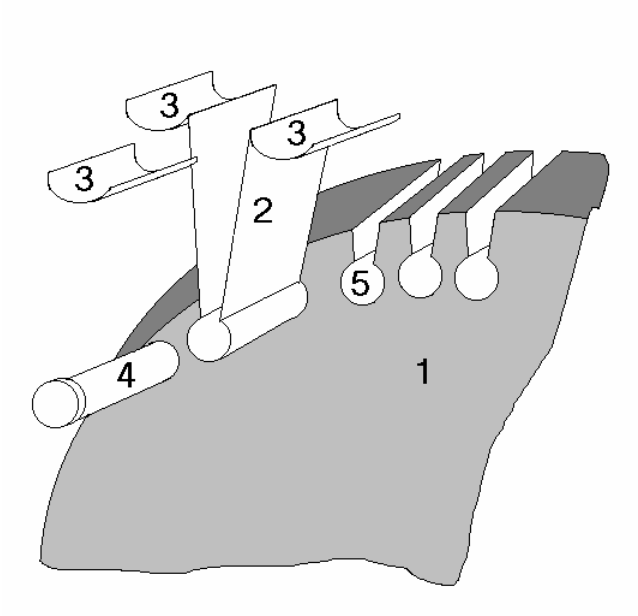

Fig. 2. Scheme of the lamellas adjusting themselves with the central part of the rotor disk: 1-Central part of rotor disk; 2-Lamella (Al+Gd alloy); 3-Inter lamella part (Al+Cg alloy); 4-Needle; 5-Position of the lamella in the central part.

3.3. Properties of the pilot lot of the absorbing plates with the optimum content of rare-earth elements

We investigated three types of neutron-absorbing materials, proposed for using in the designing of the mechanical monochromator: two aluminium-gadolinium alloys (7% and 10% of Gd) and a titanium-gadolinium alloy with 10% of Gd. The latter alloy has better mechanical properties than the aluminium ones and is interesting in connection with the future design of high-speed rotation velocity monochromators. The above-mentioned materials were delivered by the manufacturer in the form of bars of 50 x 100 x 200 mm^3 dimensions. These bars were rolled for the manufacturing of sheets of 0.5-1 mm thickness. The rolling consists of few steps. After each step a vacuum annealing was performed. Figure 3. shows the typical microstructure of the final samples of the aluminium-gadolinium and titanium-gadolinium alloys (the microscope magnification being ~ 500).

Fig. 3. Typical microphotograph of the Al+10 % Gd sample

The structure of the samples was a uniform mixture of particles with a calibre of 5-20 μm and some metal phase particles with a calibre of~30-60 μm.

The results of the measurements of the sample transmission are shown in figure 4. The results of the calculation of the transmission of the different contents of gadolinium are presented in the figure, together with the experimental data. One can see that the real content of gadolinium in the alloys is slightly less than that declared by the manufacturer . Nevertheless, this content suffices for the production of the absorbing plates for the rotor of our velocity monochromator.

In spite of our demand that the content of the alloy was known well, which was certified by the manufacturer, we decided that a control examination of the neutron absorption properties of the actual material was needed, namely the determination of the transmission of thermal neutrons. An experiment was performed on a DIN-2PI spectrometer [6]. For our experiment we used the method of determining the total neutron cross-section based on the standard vanadium sample neutron scattering [7]. The real content of gadolinium in the alloys was found to be slightly less than the manufacturer had declared. Nevertheless, this content was high enough for the production of the absorbing plates for the rotor of the velocity monochromator. Let us illustrate this in the example of the mechanical monochromator for the SANS on the Algerian reactor in Draria [4]. The angle of the absorbing plates (lamellas) at the neutron beam exit is $\theta \sim 5^{o}$, and hence, for the 0.5 mm thickness of the plate neutron path inside the lamella material is $\Delta l \sim 0.5/\sin 5^{o} \sim 5$ mm of aluminium-gadolinium alloy. If the content of gadolinium is ~ 5 %, the transmission of the plate for the 5 meV neutrons (this is a upper limit of the neutron energy after the cold beryllium filter) will be less than $T \sim 10^{-14}$. It is obvious that this lamella is absolutely “dark” for the neutrons ~20 meV, so the transmission of this plate will be $T \sim \exp(-15) \sim 3*10^{-7}$.

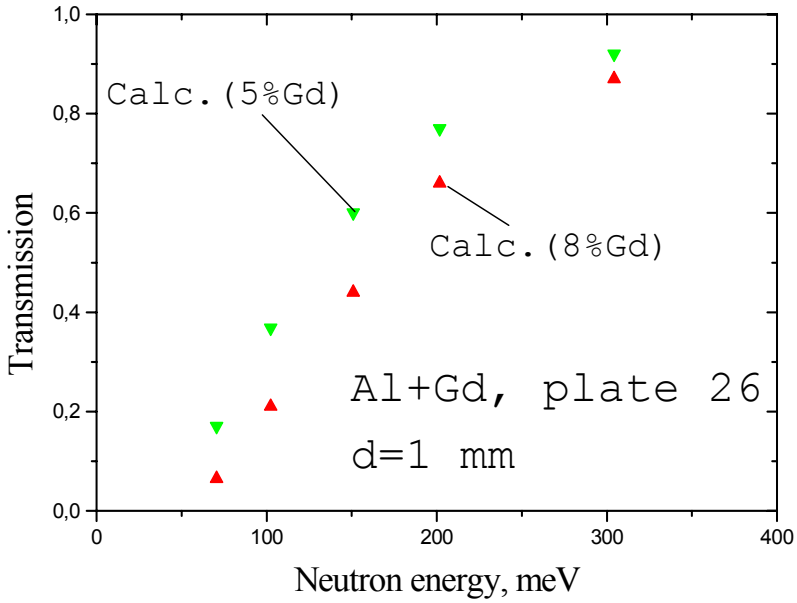

Fig. 4. Energy dependence of the transmission of the aluminium-gadolinium plate (Al+8 % Gd). Dark squares are the experimental data. The upper curve – (Al+5 % Gd) sample. Triangles - the results of calculations for the different contents of gadolinium.

3.4. Estimation of the radiation effects on the absorbing plates of the MM rotor during operation in low-power reactors

Concerning mechanical monochromators (MM), we have discussed in our previous reports how the process of monochromatization and removal from the neutron beam of unwanted neutrons (neutrons of unuseful energies) is achieved through the absorption of the neutrons by the absorption materials of the rotor monochromator. In this case, the important question emerges as to radiation effects after the neutron absorption: is the induced activity dangerous for the operating personnel or for the users of these instruments?

In this connection, we consider it necessary to conclude our two previously presented reports concerning the design and details of the mechanical monochromator construction by the estimation of the radiation situation due to induced radiation in the neutron absorption materials of the MM parts. We will discuss these effects for the MM reported above containing the absorbing plates manufactured from the (Al+10 wt % Gd) alloy. The detailed discussion of the physical properties of this alloy has been presented above and in the previous reports.

It is apparent that the SANS also has other sources of radiation background (γ-rays and neutron background), considering that, for example, the beryllium filter requires very efficient shielding. Such sources might be non-vacuum parts of the neutron beam, etc. Here we restrict our task to estimating the effects of the activation of the MM only. Nevertheless, we hope that these estimates help to understand the radiation situation of the instrument and to plan the radioactive protection in accordance with the real conditions of the experiment, the characteristics of the reactor, and the rules and regulations of the country.

4. THE RESULTS OF THE THIRD YEAR OF THE PROJECT

4.1. Design of the rotor monochromator

The estimates and experimental studies of the second year of the project provided real parameters for the mechanical monochromator (MM) design and improvements of the MM rotor (figure 5).

One of the important problems in designing the metal sectional mechanical monochromator is the choice of the optimal shape of the central part of a section. The shape should minimize the weight of the construction and have good strength properties.

The construction of the cylindrical-type MM for SANS installations has been done.

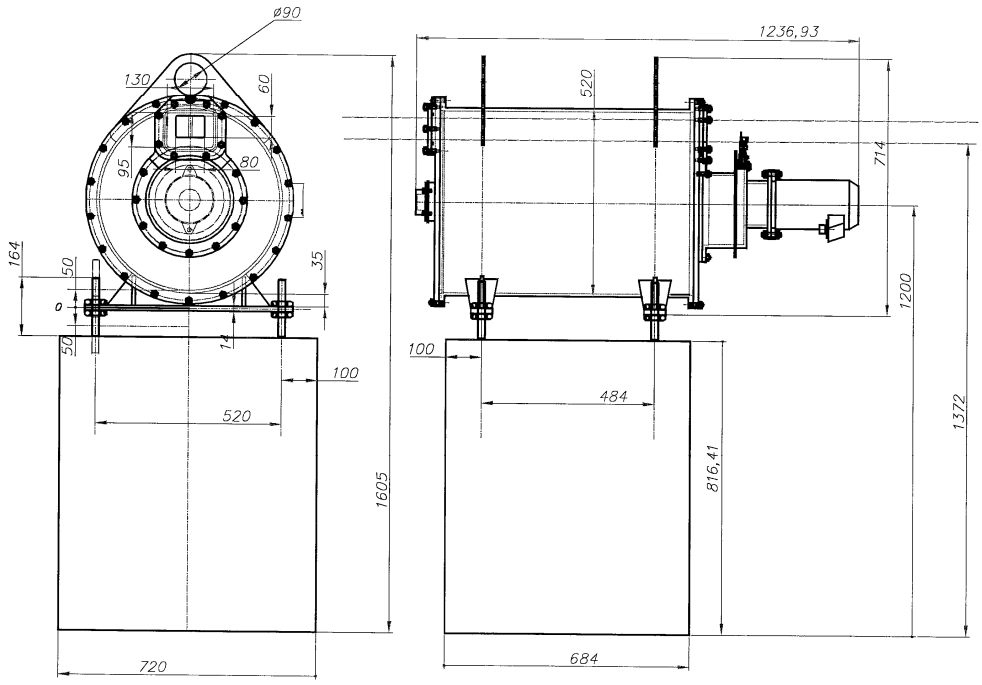

Fig. 5. General view of the mechanical monochromator

The design proposed has two particular constructional features. First, the project opens the way to minimize the amount of the expensive adsorbing material (Al-Gd alloy) used to manufacture the rotor lamellas. This will be achieved by the special location (arrangement) of the lamellas along the central cylindrical rotor body.

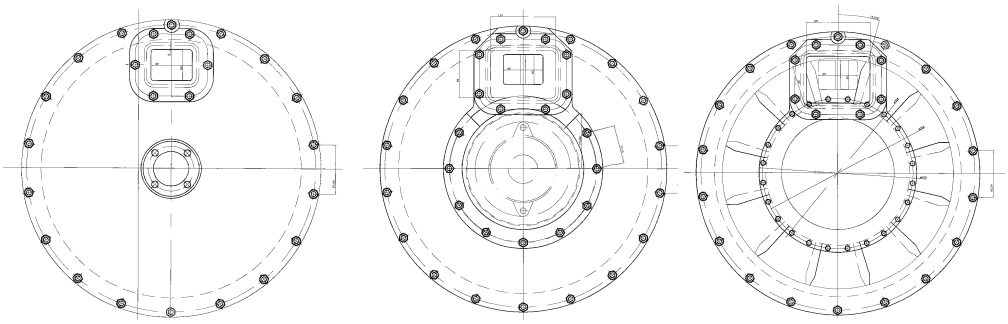

Fig. 6. View of the flanges of the monochromator body

Second, the central carrying part of the rotor has a special lightweight construction. Ultimately, the consideration suggested can be considered to be the decisive step towards the general optimization of the metal rotor construction for MM of this (cylindrical) type.

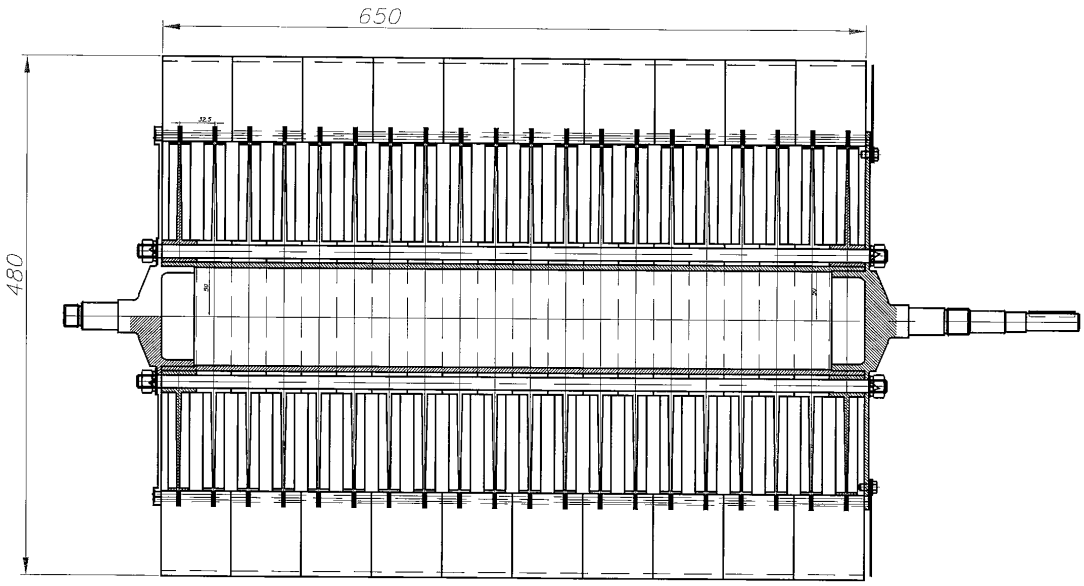

Fig. 7. General view of the rotor of the monochromator.

The rotor looks like a cylinder, rotating around the horizontal axis (figure 7). It is constructed as a set of cylindrical aluminium sections, pivoted on the common aluminium tube of a diameter ~100 mm with steel butt ends. On the periphery of these sections the thin adsorbing plates (δ = 0.5 mm), made of Gd (8%) – Al alloy, are fastened. The plates are inclined relative to the axis, and their set forms a common helical slit along the cylindrical surface. The rotor is confined to a vacuum housing with thin aluminium windows ($\delta \sim$ 0.5 mm) for the in-and-out transmission of the neutron beam.

4.2. Main parameters of the velocity monochromator

4.2.1 Motor

DC brush motor (4MI12S, routine operation speed 6000 rpm) of 1 kW power, air-cooled, connected to the rotor by a metal-rubber coupling of special construction, tested in long- term operations. The weight of the motor is ~ 3 kG.

The tentative characteristics of the rotor are given in Table 2:

Table 2: Characteristics of rotor

Working length	650 mm
Diameter, corresponding to the half-width of the slit	420 mm
Height of slit	60 mm
Width of slit for half-height	5.5 mm
Thickness of adsorbing plates	0.5 mm
Helical angle on the working length	0.21 rad
Working interval of rotation speed	(1000 – 4000) rpm
Range of neutron wavelength selected	(3 – 10) Å
Resolution for neutron wavelength	~ 15 %
Weight of rotor	~ 50 kG

4.2.2 Trip control

Computer controlled automatic system of rotation speed stabilization, including: the visualized speed control (in rpm, speed constancy ~ 0.2 %); visualized control of the current and tension of the motor supply; visualized control of the bearing temperature; alarm systems switching off the motor supply if the controlled parameters are outside the prescribed limits.

4.2.3 The effective transmission of the rotor

The rotor is constructed as a set of 10 sections. So, the real slit consists of 10 flat pieces, and in general it does not correspond to the natural helical shape. The flatness of single sections (l = 65 mm) causes the effective slit width for neutrons to be about 4% less compared to its geometrical value. Thus the effective transmission of the rotor will be $T_{eff} \approx 5.5*0.96/6 \approx 0.88$.

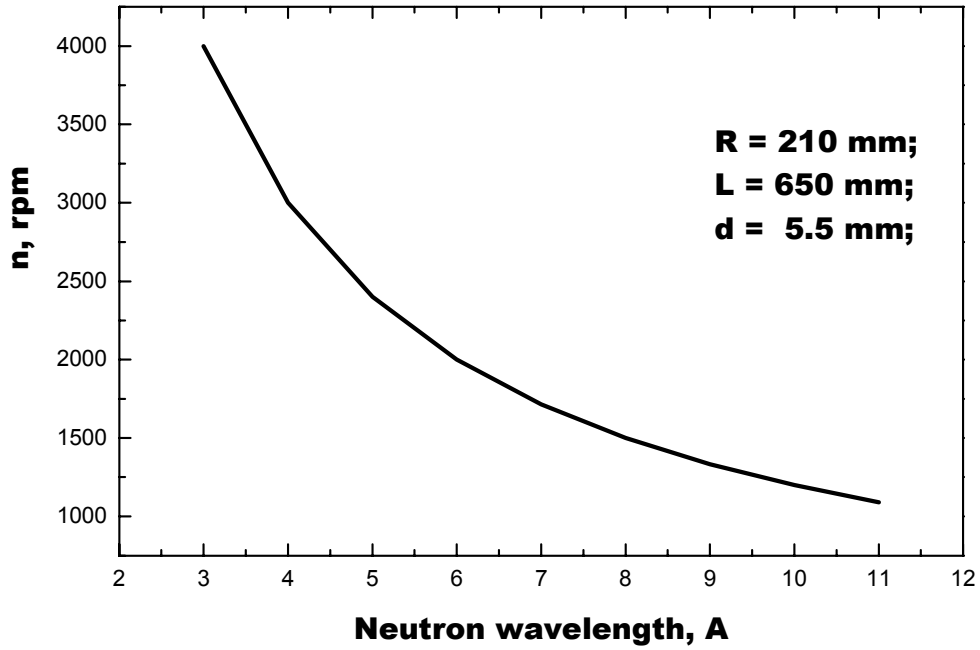

Fig. 8. The neutron wavelength, selected by rotor, as the function of its rotation speed

5. CONCLUSIONS AND GENERAL REMARKS

1. When designing the specific mechanical monochromator of cylindrical type, various options are possible:
    a) The coreless cylinder has the lamellas on the surface. In this case the motor can be placed inside the cylinder and the size of the whole device can be greatly reduced;
    b) The sectional cylindrical variant of the monochromator (for example [4]), where the helical slit is formed by separate lamellas placed in such a way that they form a true-shape helical slit;
    c) The sectional cylindrical variant of the monochromator, where the sections have different lengths and parts of the sections have no lamellas, as in the case of a disc-type mechanical monochromator [1]. This variant will avoid the expensive absorbing material of lamellas.
2. The sectional variant of a mechanical monochromator offers, after some design improvements, a chance to create the device with a changeable angle slit. This variant considerably increases the range of the useful neutron wavelength of a mechanical monochromator.
3. The light and convenient aluminium alloys are good materials for designing a mechanical monochromator, as part of a SANS instrument, if the speed of rotation of the rotor monochromator is not too high (up to 6000-10000 rpm for the typical diameter of the rotor). Only a few percent of rare earth elements, for example gadolinium, are enough to attain an excellent material for use in absorbing plates in monochromator manufacturing. These lamellas are absolutely “dark” for the neutrons after the beryllium filter. One of the important advantages of metal monochromators in comparison to plastic ones is their high radiation resistance.
4. The estimation of radiation effects in the absorbing lamellas of the MM during operation leads to the following conclusions:

- The γ-ray background has a momentary character, and thus the activation of the metallic part of the MM is absent;
- The γ-ray background is small and can be suppressed efficiently if required;

5. The optimization of the rotor design and the judicious selection of the material enabled us to reduce the rotor weight by three times in comparison with the prototype, allowing us to decrease the power of the electromotor and thus to achieve the project purpose.

REFERENCES

[1] ROSTA, L., Neutron physical properties of a multidisc velocity selector, Physica **B156-157,** 615 (1989).

[2] HAMMOUDA, B., Multidisk neutron velocity selectors, Nucl. Instr. and Methods **A321,** 275 (1992).

[3] FRIEDRICH, H., WAGNER, V., WILLE, P., A high-performance neutron velocity selector, Physica **B156-157,** 547 (1989).

[4] DANILKIN, S., KONSTANTINOV, V, NOVIKOV, A. PUCHKOV, A, SOLOVJEV, B., ZEINALOV, SH., AND WIEDENMANN, A, SANS Spectrometer for 1MW NUR reactor at URGN, Algeria, Physica **B276-278,** 100 (2000).

[5] DASH, J., SOMMERS, H.S., Jr., A High Transmission Slow Neutron Velocity Selector, Rev.Sci.Instr. **24,** 91 (1953).

[6] Yu. TARAN (Ed) User Guide, Neutron Experimental Facilities at JINR. JINR Press, Dubna, 1992.

[7] LIFOROV , V.G.,*et al*. Preprint IPPE-1112, 1980.

[8] DANILKIN,S.A.,. NOVIKOV, A.G., PUCHKOV, A.V., Mechanical monochromator for cold neutrons. Proceedings of the European Spallation Source Conference, 16-17 May 2002, Bonn, Germany.

NEUTRON DETECTOR AND SANS DEVELOPMENT AT SAFARI-1

J.B. Keshaw, C.B. Franklyn

Radiation Utilisation, NECSA, Pretoria, South Africa

Abstract. Position sensitive neutron detectors are an essential part of neutron scattering instruments, hence the development of one-dimensional position sensitive detectors (PSD) for use in small angle neutron scattering (SANS) instruments was carried out as part of an IAEA sponsored collaborative research project. The result was the fabrication and testing of several prototype, 12cm active length, ^{3}He 1-D position sensitive proportional counters with a position resolution and count-rate capability well suited for use in SANS applications.

1. INTRODUCTION

As part of the regeneration of a science and technology base around the SANS facility being constructed at the SAFARI-1 research reactor, it was considered relevant to develop an in-house understanding of neutron detector technology by developing and constructing our own detectors, rather than acquiring appropriate detectors "off the shelf".

A review of several articles on neutron detectors and their applications [1] revealed that the optimum approach at constructing a position sensitive neutron detector for use in the SAFARI-1 small angle neutron scattering facility and possibly also in neutron diffraction facilities, was the route of a 1-D ^{3}He proportional counter employing the resistive wire technique. It must be emphasized that with the recent rapid improvements in computing technology, optical devices (e.g., CCD camera systems) and several other factors, this may not always be the optimum approach in future SANS instrument design. However, bearing in mind the limited resources available, the chosen option was felt to be justified [1].

2. DETECTOR DEVELOPMENT

The development of the detector took place in several chronological steps, starting with modelling, design, and finally construction and testing of several prototypes.

2.1. Modelling of the charge division

In order to better understand, appreciate, and anticipate the performance of the resistive wire-type detector, an electronic model of its operation principles was studied by reviewing several articles [1] and collating those important outputs relevant to the requirements of this work. Equations describing the time evolution of signal outputs from either end of the 1-D resistive wire detector (for a Dirac-delta function-type event pulse at some position along the detector) were derived, and agreed with those presented in previous work from other researchers. Numerical and mathematical analysis of these equations showed how the algorithm of charge division (i.e. that of dividing the pulse height from one end of the detector by the sum of the pulse heights from both ends) gives a signal pulse height in direct proportion to the position of the detected event along the detector.

This derivation was taken a step further to include the effect of a non Dirac-delta-type detection event, i.e., an event described by some arbitrary charge distribution function of position along the wire, which is more typical of the physical reality of the detection process, where the avalanche spread may take up as much as 10% of the active length of the detector. Results of this model indicated that the charge division signal obtained was actually in direct proportion to the "centre of charge", better known as the charge centroid, of the detected event. An application of how this model may be used for improving the position sensitivity of the detector by using various gas mixtures (affecting the avalanche charge distribution along the length of the detector) was looked into and further analyzed [1].

After the initial introductory and theoretical work was done, the actual experimental work on constructing a detector began.

2.2. Construction of a gamma-ray proportional counter

As a first step, a ~20cm long gamma-ray sensitive, proportional counter filled with P-10 (10% methane in Argon => gamma- and X-Ray sensitive) gas was constructed. This detector had a tungsten wire electrode of ~5μm diameter and was not tested as a position sensitive device. The aims of this experiment were to determine whether the construction, sealing, electrical and gas-filling systems of the detector were adequate for the next step in the development of a position sensitive proportional counter. This task was completed successfully with the gamma-sensitive detector tested for stability over more than 100 hours.

2.3. Modification to a position-sensitive proportional counter

In order to make the counter position sensitive, the tungsten central wire was replaced with a 7μm diameter carbon-fibre wire. According to the literature surveyed, this had never been done on a neutron detector before [1], but carbon fibres had been used for charged-particle detectors in high-energy physics applications. The insertion of the carbon fibre required a slight modification of the assembly process as the carbon fibre is delicate and brittle compared to the tungsten wire. Once assembled and filled with P-10 gas, this detector demonstrated a position resolution of ~ 13.4 mm. This resolution was not good, and was attributed to the bad divergence of the gamma-ray source used in the test, low P-10 gas pressure, and scattering from the stainless-steel detector window rather than the electronics. However, the results indicated good position linearity and a uniform efficiency (within 7 %) across the length of the detector. A study of the poor position resolution was not considered necessary at this stage of work because the factors suspected of causing the bad resolution would not necessarily be present when the detector would be operated as a neutron detector.

2.4. Modification to a neutron sensitive detector

The first attempt at testing the detector filled with a neutron-sensitive gas (261kPa ^{3}He and 27kPa CF_4) failed because the gas broke down (at 600 V) well below the targeted operating voltage of >1000 V.

Experimental investigations (using ^{4}He for this purpose) into breakdown voltage as a function of pressure (0.0195-644kPa) for a fixed-ratio gas mixture (7% CF_4 in ^{4}He) filled detector revealed a Paschen's Law-type relationship. However, the maximum breakdown voltage of 700 V at 644kPa was not satisfactory for the PSD application intended, so further investigations were necessary. A further study, whereby the CF_4 component was varied (0-60%) revealed that breakdown voltages in excess of 1200 V could be obtained for a CF_4 component of ~30%.

An equivalent ^{3}He-CH_4 mixture exhibited similar behaviour, with operating voltages in excess of 1000 V attainable without breakdown problems. The next step was to test the detector with a neutron source in order to determine its performance characteristics, such as efficiency, position resolution and stability.

2.5. Neutron tests of the ^{3}He 1-D PSD

Initial tests of position resolution and efficiency were carried out on a beam-line at the SAFARI-1 research reactor. These tests revealed a position resolution of less than ~ 3.2 mm, and a straight line fit of peak position vs. beam position gave an R^2 of 0.9998, indicating good position linearity over the ~130 mm active length [1], [2].

Due to beam divergence on the SAFARI-beam line further tests of the detector at the HMI SANS V4 (August 2001) beam-line gave the following important results relating to the performance of the detector [1], [3]:

- A "best" position resolution (at a reduced efficiency of ~80%) was found to be ~ 1.16 mm over the 120 mm useful active length.
- Efficiency of >81.6 % for 6Å neutrons.
- Efficiency uniformity within 20 % over the active length of the detector; however, this non-uniform efficiency was mainly due to an electronics problem related to the ADC, and could be corrected.
- Count rates in excess of 37 kHz over ~6 mm length indicated dead time losses of less than 1 %.

These tests at HMI also included using the detector in the study of diffraction from a silver behenate sample, and revealed results in good agreement with previous experiments [1]. It was due to these tests that state-of-the-art data acquisition electronics supplied by Mesytec, Gmbr, was identified as the most suitable for our charge division-type position sensitive detectors.

Another test of the prototype detector as well as of two other detectors (constructed based on this prototype) involved the investigation of shielding materials using the direct neutron beam of the SAFARI-1 Neutron Radiography beam-line. Here count rates in excess of 40 kHz per detector were observed with negligible dead time [1].

3. FUTURE INVESTIGATIONS INTO NEUTRON DETECTORS

Throughout the course of developing the position sensitive neutron detector, many interesting phenomena, as well as associated problems and solutions thereof, were stumbled upon. Unfortunately, the scope of this project did not allow for much further investigations into all of these, and a continuation of this work would involve investigations into design aspects discussed below.

3.1. Gas breakdown

It would be most interesting to investigate the influence of factors such as electrode sizes, materials and purity of the gas mixtures on the breakdown voltage more thoroughly in the future. This may at least allow for the development of a more efficient gas mixture and/or electrode that could increase the breakdown voltage well beyond what was achieved in these experiments.

3.2. Pulse height distribution

A qualitative discussion of the effects of efficiency of the stopping gas, detector geometry, and ^{3}He partial pressure on the shape of the pulse height distribution from a ^{3}He gas neutron detector was given [1]. This information was found to be missing in nearly all the articles on ^{3}He neutron detectors reviewed in this work.

Monte-Carlo simulations of the neutron capture spectra for different detector configurations would also be highly informative, especially with today's much improved computing technology and wider databases on gas properties. Clearly, such studies would be invaluable for any future work on ^{3}He detector development.

3.3. Stopping gas

As has already been pointed out [1], the purity of the gas is of high importance as it strongly affects the pulse height distribution. Further investigations into this effect would be most useful, especially if the effect of impurities could be quantified, as this could help determine the useful lifetime of the detector based on out-gassing rates of the chamber material, etc.

Although our investigations made extensive use of CH_4 as the stopping gas, mainly due to its lower gamma sensitivity, CF_4 has been chosen as stopping gas by others [1] because of its much greater stopping power. However, as discussed [1], greater stopping power gas fillings may not necessarily improve the position resolution of the detector.

It must be emphasized that the increased gamma-sensitivity posed by CF_4 could have a further negative effect on the performance of the detector, because the gamma-ray events would take up electronic processing time and hence increase the dead-time of the detector system, thereby reducing its efficiency at high count rates.

4. OUTCOMES OF DETECTOR DEVELOPMENT

Although neutron position sensitive detectors are commercially available, gaining an understanding and appreciation of how such detectors function is an essential prerequisite to operating a neutron scattering facility. An important outcome of this research has been the development of a prototype 1-D position-sensitive neutron detector, which is to be modified for use in a star-like or stacked 2-D configuration to meet the needs of a future small angle neutron scattering facility to be based at the SAFARI-1 research reactor beam-line.

The IAEA Coordinated Research Project on detector development for SANS applications played an important role in the project of developing the SANS facility at SAFARI-1 [4]. It encouraged cooperation between NECSA and the HMI to the extent that training, experiments and lab visits could be carried out by NECSA personnel at the HMI SANS beam-line [3], [5], [6]. This communication allowed for an expert mission (Feb. 2002) to South Africa by Dr. A. Wiedenmann (HMI) to evaluate the feasibility of setting up a SANS facility at SAFARI-1 and make recommendations [7].

CRP RCM meetings held in 2002 and 2003 were most valuable, as issues regarding SANS instrument configurations and development could be discussed with experts from many facilities [8], [9]. It was there that information regarding the MEET velocity selector was obtained from a CRP member, Dr. A. Putchkov. Consequently, it was decided to use this selector for the SAFARI SANS instrument because of its easier maintenance and sufficient resolution (15 %) and wavelength range (at least 4-10Å) capabilities.

Contact with researchers at operational SANS facilities were also established at the RCM meetings. Discussions with Jose Texiera (LLB) and Laslo Cser (KFKI) stimulated the idea of scientific visits (via IAEA TC) resulting in hands-on training at these respective facilities.

5. CONCLUSIONS

Position sensitive neutron detectors have always played an essential role in the SANS instrument, however, there exists no single “best” choice on which detector system is suited for SANS in general. The choice of which detection system to employ requires a study of the capabilities and resources available for the instrument development, and this relies heavily on information only available through extensive collaboration and cooperation with other laboratories.

Continued future research on developing better neutron detectors will certainly improve the performance of SANS instruments worldwide, as has already been seen in the case of HMI and ILL modifying and replacing detector components in recent years.

However, detectors are not the only components of a SANS instrument, and hence the development of such an instrument required extensive investigations into possible SANS beam-line scenarios and options, which was one of the most important outcomes of the IAEA CRP that led to the TC project of establishing a Southern African SANS facility at SAFARI 1.

REFERENCES

[1] KESHAW, J., Design, construction and testing of a one-dimensional 3He neutron detector, M.Sc Dissertation, University of Witwatersrand, South Africa. Available from J. Keshaw

[2] KESHAW, J., FRANKLYN, C., Design, construction and testing of a 1-D position-sensitive neutron detector, poster presented at International Conference on Neutron Scattering, 2001.

[3] KESHAW, J., WIEDENMANN, A., MONTERMANN, G., Tests of RUDETEC detector, BENSC experimental reports 2001. Available from HMI.

[4] KESHAW, J., FRANKLYN, C., Development of a Southern African SANS facility, poster presented at European Conference on Neutron Scattering, September 2003. Attached in annex.

[5] KESHAW, J., WIEDENMANN, A., FRANKLYN, C., SANDERSON, R., SANS Measurements on polymer samples, BENSC experimental reports 2002. Available from *HMI*.

[6] KESHAW, J., Report on HMI training and ICNS Conference, 2 September to 29 November 2001. NECSA Internal Doc. No. RT-VLG-0309, May 2003. Available from J. Keshaw, (2001visitNECSA.doc - 550Kb).

[7] KESHAW, J., Report of Expert Mission for SANS, 10-21 February 2002, NECSA Internal Doc. No. RT-VLG-0207, May 2002. Available from J. Keshaw (expertmission.doc - 309Kb).

[8] KESHAW, J., Report on SAS2002 Conference and HMI SANS Experiments during September 2002. NECSA Internal Doc. Pending. Available from J. Keshaw.

[9] CRP Report for 2001 SANS RCM.

LIST OF PUBLICATIONS BY THE PARTICIPANTS UNDER THE CRP

[1] FALCÃO, A.N., MARGAÇA, F.M.A., and CARVALHO, F.G., "The Use of Multichannel Collimation in Small Angle Neutron Scattering: A Computer Simulation Study", Appl. Phys. A **74** (Suppl.), S1462-S1464 (2002)

[2] FALCÃO, A.N., MARGAÇA, F.M.A., CARVALHO, F.G., "Intensity and Resolution Effects in Converging Multichannel Collimators for SANS by Monte Carlo Simulation", J. Appl. Cryst., , **36** 1262 (2003)

[3] FALCÃO, A.N., MARGAÇA, F.M.A., CARVALHO, F.G., "A Contribution to the Practical Implementation of a Variable Geometry Converging Multichannel Collimator for SANS", J. Appl. Cryst., **36** 1266 (2003)

[4] MARGAÇA, F.M.A., FALCÃO, A. N., CARVALHO, F.G., "Guidelines for the Implementation of Converging Multichannel Collimation in a Specific SANS Facility", J. Appl. Cryst. (2004) (in press)

[5] MARGAÇA, F.M.A., FALCÃO, A.N., SALGADO, J.F., CARVALHO, F.G., "Wavelength Dependence of the Performance of a SANS Instrument Installed at a Steady Source" (2003) (to be submitted)

[6] MAZUMDER, S., SEN, D., PATRA, A.K., KHADILKER, S.A., CURSETJI, R.M., LOIDL, R., BARON, M., and RAUCH, H., Dynamical scaling of structure factor for some non-Eucledian systems Phys. Rev. Lett. **93**, 255704 (2004):

[7] MAZUMDER, S., SEN, D., ROY, S.K., HAINBUCHNER, M., BARON, M., and . RAUCH, H., Manifestation of the statistical nature of a medium in multiple Small angle scattering , J. Phys.: Condens. Matter, **13** 5089 (2001).

[8] SEN, D., PATRA, A.K., MAZUMDER, S., and RAMANATHAN, S., Pore morphology in sintered ZrO2-8 mol%Y2O3: A Small angle neutron scattering investigation, J. Alloys and compounds, **340** 236 (2002).

[9] ROSTA,L.CSER, L., Zs.RÉVAY, Gain factors with the new supermirror guide system at the Budapest Neutron Centre, Appl. Phys A **74** S292 (2002)

[10] ALMÁSY, L., JANCSÓ, G., CSER, L., Application of SANS to the determination of Kirkwood-Buff integrals in liquid mixtures, Appl. Phys. A **74** S1376 (2002)

[11] CSER, L., FÜZI, J., RIECSÁNSZKY, L., Gy.TÖRÖK, Polarized neutron reflectometer at the Budapest Research Reactor Appl. Phys. A **74** (Suppl.) S213 (2002)

[12] FÜZI J, TÖRÖK Gy, ROSTA L, Neutron focusing with permanent magnet hexapole lenses; Physica B **350** 169 (2004)

[13] LEN A, PÉPY G, ROSTA L, Multibeam focussing in SANS technique; Physica B; 350, E771-E773, 2004 Conference Proceedings

[14] FÜZI J; Magnetic Lenses for Neutron Beams; In: Proceedings CD of the 11th IGTE Symposium on Numerical Field Calculation in Electrical Engineering, 13-15 September, Graz; Ed: Bíró O, pp. 371 (2004)

Book Chapter

[15] CSER, L., Salma, I., MOLNÁR, G., Anyagvizsgálatok Neutronokkal(Matreials Studies by Neutrons, in Hungarian), Nukleáris tudomány és a 20. Század: Muhelytanulmányok sorozat (Strategic Research at the Hungarian Academy of Sciences), (Eds Glatz F, Vértes A MTA ISSN 1419-1822, pp75-90 (2002)

[16] Report of second RCM F1-RC-830 (Working Material) Reproduced by the IAEA, 2003

LIST OF PARTICIPANTS

Carvalho, F.G.	Head, Condense Matter Physics Group ITN-Nuclear and Technological Institute Physics Department 2686-953 Sacavam, Portugal Tel: +351 21 994 6075/57 Fax: +351 21 994 1525 E-mail: fredc@itn1.Itn.pt
Cser, L.	KFKI Research Institute for Solid State Physics and Optics of the Hungarian Academy of Science H-1525 Budapest 114 P.O. Box 49, Hungary Tel: +36 1 392 2222 xt 1526 Fax: +36 1 392 2501 E-mail: cser@sunserv.kfki.hu
Filho, J.M.	Commissao Nacional de Energia Nuclear do Brasil, Instituto de Pesquisas Energeticas e Nucleares P.O. Box 11049 Sao Paulo, Brazil Tel: +55 11 3816 9291 Fax: +55 11 3816 9188 E-mail: jmestnik@net.ipen.br
Franklyn, C.B.	Pelindaba Nuclear Institute NECSA Nuclear Technology Department P.O. Box 582 Pretoria 0001, South Africa Tel: +27 12 305 5848 Fax: +27 12 305 5851 E-mail: franklyn@aec.co.za
Lee, C.H.	KAERI Neutron Beam Application Department Taejon Korea Rep of Tel: +82 42 868 8443 Fax: +82 42 868 8448 E-mail: leech@kaeri.re.kr
Mazumder, S.	Solid State Physics Division Bhabha Atomic Research Centre Trombay, Mumbai 400085, India Tel: +91 22 559 4644 Fax: +91 22 550 5151/551 9613 E-mail: smazu@apsara.barc.ernet.in

Messoloras, S.	N.C.S.R. “Demokritos” Institute of Nuclear Technology Radiation Protection Aghia Paraskevi, Attiki, Greece Tel: +301 650 3732 Fax: +301 653 3431 E-mail: spyros@ipta.demokritos.gr
Pepy, G.R.	Centre National De La Recherche Scientifique Commissariat A L’Energie Atomique Laboratoire Leon Brillouin CEA Saclay – 91191 Gif-Sur-Yvette Cedex Tel: +33 1 6908 3449 Fax: +33 1 6908 8261 E-mail: pepy@llb.saclay.cea.fr
Poutchkov, A.	Institute for Physics and Power Engineering Bondarenko sq. 1 Obninsk 249020 Kaluga Region, Russian Federation Tel: +7 08439 983 68 E-mail: puchkov@ippe.obninsk.ru
Rauch, H.	Atominstitut der Oesterreichichen Universitaeten Stadionalle 2 A-1020, Vienna. Austria Tel: +43 1 58801 14101 Fax: +43 1 58801 14199 E-mail: rauch@ati.ac.at
Teixeira, J.	Centre National De La Recherche Scientifique Commissariat A L’Energie Atomique Laboratoire Leon Brillouin CEA Saclay – 91191 Gif-Sur-Yvette Cedex, france Tel: +33 1 6908 6650 Fax: +33 1 6908 8261 E-mail: teix@llb.saclay.cea.fr
Wiedenmann, W.	Hahn Meitner Institut Berlin Glienicker Strasse 100 14109 Berlin, Germany Tel: +49 30 8062 2283 Fax: +49 30 8062 3059 Email: wiedenmann@hmi.de

No. 20, August 2005

IAEA
International Atomic Energy Agency

Where to order IAEA publications

In the following countries IAEA publications may be purchased from the sources listed below, or from major local booksellers. Payment may be made in local currency or with UNESCO coupons.

Australia
DA Information Services, 648 Whitehorse Road, MITCHAM 3132
Telephone: +61 3 9210 7777 • Fax: +61 3 9210 7788
Email: service@dadirect.com.au • Web site: http://www.dadirect.com.au

Belgium
Jean de Lannoy, avenue du Roi 202, B-1190 Brussels
Telephone: +32 2 538 43 08 • Fax: +32 2 538 08 41
Email: jean.de.lannoy@infoboard.be • Web site: http://www.jean-de-lannoy.be

Canada
Bernan Associates, 4611-F Assembly Drive, Lanham, MD 20706-4391, USA
Telephone: 1-800-865-3457 • Fax: 1-800-865-3450
Email: order@bernan.com • Web site: http://www.bernan.com

Renouf Publishing Company Ltd., 1-5369 Canotek Rd., Ottawa, Ontario, K1J 9J3
Telephone: +613 745 2665 • Fax: +613 745 7660
Email: order.dept@renoufbooks.com • Web site: http://www.renoufbooks.com

China
IAEA Publications in Chinese: China Nuclear Energy Industry Corporation, Translation Section, P.O. Box 2103, Beijing

Czech Republic
Suweco CZ, S.R.O. Klecakova 347, 180 21 Praha 9
Telephone: +420 26603 5364 • Fax: +420 28482 1646
Email: nakup@suweco.cz • Web site: http://www.suweco.cz

Finland
Akateeminen Kirjakauppa, PL 128 (Keskuskatu 1), FIN-00101 Helsinki
Telephone: +358 9 121 41 • Fax: +358 9 121 4450
Email: akatilaus@akateeminen.com • Web site: http://www.akateeminen.com

France
Form-Edit, 5, rue Janssen, P.O. Box 25, F-75921 Paris Cedex 19
Telephone: +33 1 42 01 49 49 • Fax: +33 1 42 01 90 90 • Email: formedit@formedit.fr

Lavoisier SAS, 145 rue de Provigny, 94236 Cachan Cedex
Telephone: + 33 1 47 40 67 02 • Fax +33 1 47 40 67 02
Email: romuald.verrier@lavoisier.fr • Web site: http://www.lavoisier.fr

Germany
UNO-Verlag, Vertriebs- und Verlags GmbH, Am Hofgarten 10, D-53113 Bonn
Telephone: + 49 228 94 90 20 • Fax: +49 228 94 90 20 or +49 228 94 90 222
Email: bestellung@uno-verlag.de • Web site: http://www.uno-verlag.de

Hungary
Librotrade Ltd., Book Import, P.O. Box 126, H-1656 Budapest
Telephone: +36 1 257 7777 • Fax: +36 1 257 7472 • Email: books@librotrade.hu

India
Allied Publishers Group, 1st Floor, Dubash House, 15, J. N. Heredia Marg, Ballard Estate, Mumbai 400 001,
Telephone: +91 22 22617926/27 • Fax: +91 22 22617928
Email: alliedpl@vsnl.com • Web site: http://www.alliedpublishers.com

Bookwell, 2/72, Nirankari Colony, Delhi 110009
Telephone: +91 11 23268786, +91 11 23257264 • Fax: +91 11 23281315
Email: bookwell@vsnl.net

Italy
Libreria Scientifica Dott. Lucio di Biasio “AEIOU”, Via Coronelli 6, I-20146 Milan
Telephone: +39 02 48 95 45 52 or 48 95 45 62 • Fax: +39 02 48 95 45 48

Japan
Maruzen Company, Ltd., 13-6 Nihonbashi, 3 chome, Chuo-ku, Tokyo 103-0027
Telephone: +81 3 3275 8582 • Fax: +81 3 3275 9072
Email: journal@maruzen.co.jp • Web site: http://www.maruzen.co.jp

Korea, Republic of
KINS Inc., Information Business Dept. Samho Bldg. 2nd Floor, 275-1 Yang Jae-dong SeoCho-G, Seoul 137-130
Telephone: +02 589 1740 • Fax: +02 589 1746
Email: sj8142@kins.co.kr • Web site: http://www.kins.co.kr

Netherlands
De Lindeboom Internationale Publicaties B.V., M.A. de Ruyterstraat 20A, NL-7482 BZ Haaksbergen
Telephone: +31 (0) 53 5740004 • Fax: +31 (0) 53 5729296
Email: books@delindeboom.com • Web site: http://www.delindeboom.com

Martinus Nijhoff International, Koraalrood 50, P.O. Box 1853, 2700 CZ Zoetermeer
Telephone: +31 793 684 400 • Fax: +31 793 615 698 • Email: info@nijhoff.nl • Web site: http://www.nijhoff.nl

Swets and Zeitlinger b.v., P.O. Box 830, 2160 SZ Lisse
Telephone: +31 252 435 111 • Fax: +31 252 415 888 • Email: infoho@swets.nl • Web site: http://www.swets.nl

New Zealand
DA Information Services, 648 Whitehorse Road, MITCHAM 3132, Australia
Telephone: +61 3 9210 7777 • Fax: +61 3 9210 7788
Email: service@dadirect.com.au • Web site: http://www.dadirect.com.au

Slovenia
Cankarjeva Zalozba d.d., Kopitarjeva 2, SI-1512 Ljubljana
Telephone: +386 1 432 31 44 • Fax: +386 1 230 14 35
Email: import.books@cankarjeva-z.si • Web site: http://www.cankarjeva-z.si/uvoz

Spain
Díaz de Santos, S.A., c/ Juan Bravo, 3A, E-28006 Madrid
Telephone: +34 91 781 94 80 • Fax: +34 91 575 55 63 • Email: compras@diazdesantos.es
carmela@diazdesantos.es • barcelona@diazdesantos.es • julio@diazdesantos.es
Web site: http://www.diazdesantos.es

United Kingdom
The Stationery Office Ltd, International Sales Agency, PO Box 29, Norwich, NR3 1 GN
Telephone (orders): +44 870 600 5552 • (enquiries): +44 207 873 8372 • Fax: +44 207 873 8203
Email (orders): book.orders@tso.co.uk • (enquiries): book.enquiries@tso.co.uk • Web site: http://www.tso.co.uk

On-line orders:
DELTA Int. Book Wholesalers Ltd., 39 Alexandra Road, Addlestone, Surrey, KT15 2PQ
Email: info@profbooks.com • Web site: http://www.profbooks.com

Books on the Environment:
Earthprint Ltd., P.O. Box 119, Stevenage SG1 4TP
Telephone: +44 1438748111 • Fax: +44 1438748844
Email: orders@earthprint.com • Web site: http://www.earthprint.com

United Nations (UN)
Dept. I004, Room DC2-0853, First Avenue at 46th Street, New York, N.Y. 10017, USA
Telephone: +800 253-9646 or +212 963-8302 • Fax: +212 963-3489
Email: publications@un.org • Web site: http://www.un.org

United States of America
Bernan Associates, 4611-F Assembly Drive, Lanham, MD 20706-4391
Telephone: 1-800-865-3457 • Fax: 1-800-865-3450
Email: order@bernan.com • Web site: http://www.bernan.com

Renouf Publishing Company Ltd., 812 Proctor Ave., Ogdensburg, NY, 13669
Telephone: +888 551 7470 (toll-free) • Fax: +888 568 8546 (toll-free)
Email: order.dept@renoufbooks.com • Web site: http://www.renoufbooks.com

Orders and requests for information may also be addressed directly to:

Sales and Promotion Unit, International Atomic Energy Agency
Wagramer Strasse 5, P.O. Box 100, A-1400 Vienna, Austria
Telephone: +43 1 2600 22529 (or 22530) • Fax: +43 1 2600 29302
Email: sales.publications@iaea.org • Web site: http://www.iaea.org/books

06-07091